UNIVERSITY OF OKLAHOMA

GRADUATE COLLEGE

DROP PENETRATION MEASUREMENT OF ZnO AND TiO_2 NANOPARTICLES FOR POTENTIAL ANTIBACTERIAL APPLICATIONS IN DENTAL ADHESIVES

A THESIS

SUBMITTED TO THE GRADUATE FACULTY

in partial fulfillment of the requirements for the

Degree of

MASTER OF SCIENCE

By

SABRINA GARNER
Norman, Oklahoma
2020

DROP PENETRATION MEASUREMENT OF ZnO AND TiO_2 NANOPARTICLES FOR POTENTIAL ANTIBACTERIAL APPLICATIONS IN DENTAL ADHESIVES

A THESIS APPROVED FOR THE
STEPHENSON SCHOOL OF BIOMEDICAL ENGINEERING

BY THE COMMITTEE CONSISTING OF

Dr. Edgar A. O'Rear

Dr. Fernando Luis Esteban Florez

Dr. Vassilios Sikavitsas

Dr. Rong Gan

Table of Contents

Table of Figure

Abstract

Despite all efforts carious lesions continues to be a significant problem in dentistry. Secondary caries is a biofilm-originated disease that typically occurs at the tooth-adhesive resin interface. According to previous studies, secondary caries is the most common cause of failure of polymer-based bonded restorations. To help reduce the formation of secondary caries, the biofilm forming between the tooth structure (enamel and dentin) and the adhesive resin needs to be prevented. Some studies have shown the ability of metal oxides to have antimicrobial properties. Amine oxides have also shown antibacterial characteristics. Based on this context, the effectiveness of zinc oxide nanoparticles and amine oxides in dental adhesive resins as non-leaching long-term antibacterial agents to prevent biofilm formation is examined in this study.

When altering the composition of commercially available dental adhesive resins either by incorporating antibacterial agents (e.g., chlorhexidine, antibiotics, fluoride) or nanoparticles, it is important to extensively characterize the mechanical, chemical, and biological properties of experimental materials to determine their potential clinical utilization. In addition, it is important to fully characterize the nanoparticles of choice to tailor the interfacial chemistry between nanoparticles and the polymer and functionalize the nanoparticles to achieve optimum biological performance. In the present study, the wettability of different solvents (distilled water, diiodomethane, bromonaphthalene, formamide, ethanol and ethylene glycol) on zinc oxide nanoparticles (Nanogard^{TM} and NanoTek^{TM}) and that of water on experimental dental adhesive resins was investigated to determine the surface properties of

nanoparticles and experimental dental adhesive resins. Results reported in the present study may help to determine the effects of the incorporation of nanoparticles and surfactants on the ability of OptiBond Solo Plus (Kerr Corp. USA), which is a fifth generation dental adhesive resins, to efficiently establish the hybrid layer between the tooth structure and the composite resin.

In Chapter 2, a modified drop penetration method is described and was employed to reveal some surface properties of nanoparticles investigated, such as wettability and surface energy components of nanoparticles before their incorporation into dental adhesive resins. Six solvents (water, diiodomethane, bromonaphthalene, formamide, ethanol and ethylene glycol) were examined for two nanoparticle substrates, zinc oxide and titanium dioxide, with the goal of assessing the suitability of a modified drop penetration method (DPM) for orders of magnitude smaller particles. Specimens composed solely of nanoparticles (either zinc oxide or titanium dioxide) were compressed into flat discs using a manual press. Solvents were then individually dispensed, using a computer-controlled syringe, onto the surfaces of individual specimens (3 drops/specimen) while the shape and volume of droplets were recorded using digital images (at 25 frames/second) for 1 minute in the experimental chamber of a contact goniometer (at room temperature). Contact angles were then calculated (ranges between 20–80°) and were demonstrated to be in reasonable agreement with previous reports in the literature, but failed to provide acceptable results for surface energy components. Because of that, it was necessary to eliminate

certain solvents and substrates that did not meet the inclusion criteria described in Chapter 2.

In Chapter 3, the nanoparticles and amine oxide surfactant were incorporated into commercially available dental adhesive resins. A series of tests are described to determine water wettability properties of experimental materials and their antibacterial properties against *Streptococcus mutans*, which is a well-known caries-producing microorganisms and has been used as a model organism in numerous studies. The contact angles (initial and final) of adhesives with and without the incorporation of nanoparticles and surfactants was determined using the Laplace-Young equation to reveal the effects of nanoparticles and surfactants on their surface properties. Results reported are anticipated to positively influence subsequent studies in the field of dental biomaterials and materials sciences because it provides fundamental information regarding how surface properties may impact the service lives of materials investigated. The incorporation of nanoparticles and surfactants were shown to alter the typical wettability behavior of commercially available dental adhesive resins and experimental materials were observed to display higher contact angles (both initial and final) and therefore were considered more hydrophobic. A similar behavior could not be observed when the commercial adhesive resins was altered by the incorporation of investigated surfactants. In this instance, experimental materials were observed to display lower contact angles when compared to their commercially available counter parts and, therefore, were considered more hydrophilic. A minimally invasive and real-time bioluminescence assay was employed to determine the metabolic status of *S.*

mutans to determine the antibacterial properties of experimental materials following previously published protocols. Results attained demonstrated that experimental materials investigated (containing either nanoparticles or surfactants) did not decrease the metabolic activity of *S. mutans* when compared to the metabolic status observed in biofilms grown against commercially available dental adhesive resins. Because of that, it was decided to conduct a minimum bactericidal concentration test (MBC) where nanoparticles investigated (either zinc oxide or titanium dioxide) were suspended directly in planktonic cultures of *S. mutans*. The objective of this experiment was to increase the exposure of microorganisms to nanoparticles investigated and to demonstrate any potential antibacterial effect from the nanoparticles against *S. mutans*. After being exposed to nanoparticles, the viability of *S. mutans* was determined using the colony forming unit assay (CFU/mL) by plating the microorganisms into agar plates supplemented with yeast extract and spectinomycin. Results reported have indicated that zinc oxide nanoparticles (either coated or uncoated) were not capable of inhibiting *S. mutans* in the conditions tested as denoted by agar plates displaying viable colonies in all dilutions (10^0 to 10^{-9}). An opposite behavior was observed when microorganisms were exposed to the surfactant. In this case, *S. mutans* were shown to be inhibited in all dilutions investigated, thereby displaying a strong antibacterial effect. Taken together, results reported indicate that nanoparticles did not show any type of antibacterial behavior when in suspension or when immobilized in a commercially available dental adhesive resin.

Chapter 1 – Introduction

Oral hygiene is an important aspect of everyday life. Brushing teeth with fluoride-containing toothpastes and flossing has been demonstrated to diminish the incidence of biofilm-originated oral diseases such as dental caries, gingivitis and periodontitis. The use of fluoride in toothpaste and the addition of fluoride to water sources in the United States of America have been described as successful strategies to improve oral health. Despite these efforts, dental caries continue to plague children and adults and which is a significant problem in modern dentistry. While dental caries are one of the most prevalent and preventable diseases, caries affect nearly 91 percent of the United States population aged 20 to 64[1]. Dental caries are characterized by an irreversible process by which the hard tissues of teeth (enamel and dentin) are slowly and progressively dissolved by lactic acid formed from the bacterial metabolization of complex carbohydrates and sugars from dietary habits[2]. If left untreated, it results in partial or complete destruction of the clinical crown and may lead to tooth loss, which is a common problem in the world. In fact, approximately 52% of the United States population aged 20 to 64 have experienced the loss of at least one tooth.[3]

It has been of interest to incorporate antibacterial agents into coatings, composite resins or implants (dental and orthopedic). In the medical field, nanoparticles are typically used for the fabrication of antibacterial coatings, nanostructured composite materials and implants[4,5]. Incorporation of micro- or nanopowders would influence the surface wettability of the coating, resin, or implant and may affect their mechanical integrity and function once placed in the body.

In dentistry, nanoparticles (Ag, ZnO, TiO_2, N_TiO_2, NF_TiO_2 and NAg_TiO_2) have been incorporated into commercially available polymer-based materials (adhesive resins, composite resins, dental cements) to exert antibacterial properties against a multitude of pathogenic oral bacteria. In the present study, metal oxide nanoparticles and surfactants were incorporated into a commercial dental adhesive resin. Since it is well-known that the incorporation of antibacterial agents (such as nanoparticles and surfactants) into dental polymers may change the properties (surface, mechanical, chemical and biological) of the parental material. It becomes of fundamental importance to characterize the properties of the resulting experimental materials. Nanoparticles' surface properties was determined using wettability approached to give insight regarding possible applications such as coatings, dispersions, or powder processing. The water wettability of experimental adhesive resins containing nanoparticles and surfactants was also investigated. The surface properties relate to the mechanical integrity and function of the adhesive. The two surface wettability measurements (nanoparticles, adhesive, and a mixture of both with and without surfactant) can be used to determine the influence the incorporated materials have on the overall surface properties of the adhesive.

Formation of Dental Caries

The acquired pellicle is a thin film mainly composed of salivary glycoproteins that is formed on the surface of enamel immediately after teeth have been cleaned (either by prophylaxis or daily oral hygiene techniques). Such pellicle allows for the attachment and growth of Gram-positive aerobic cocci (such as *Streptococcus*

sanguinis). After that, glucosyltransferase-producing bacteria attach to the newly-formed pellicle and initiate the precipitation of exopolysaccharides, thereby starting the formation of the dental plaque. Such anaerobic environment allows for Gram-negative cocci, rods and filaments to colonize the dental plaque. These bacteria will then metabolize sugars and complex carbohydrates, through fermentation pathways, into extracellular polymeric substance (EPS; exopolysaccharides) and lactic acid. A biofilm is a highly organized and sessile multilayered community of commensal bacteria that encompasses around 700 different types of bacteria and are capable of colonizing the surfaces of teeth (pit, fissure and smooth).

Depending on their anatomical characteristics and localization in the oral cavity, mineralized surfaces are more prone for bacterial accumulation and biofilm growth, which has been demonstrated to significantly increase risk of caries. Pit and fissures are typically localized at the occlusal region of molars and pre-molars and not only are very hard to clean using traditional oral hygiene techniques, but also, may be associated with areas of enamel malformation, which further exacerbates the chances for the development of dental caries. Over time, mineralized surfaces (pit, fissure and smooth) colonized by oral biofilms will then be irreversibly and progressively demineralized, which is clinically known as dental caries.

If untreated, carious lesions will progress from the enamel to the dentin and from there to the pulp complex, which can be a very painful problem. The evolution of the carious lesion can give rise to the infection and subsequent necrosis of the pulp complex, which can spread to periodontal tissues (soft and hard),[6] and ultimately lead

to the loss of the affected tooth. The loss of one tooth may lead to tooth movement, parafunctional occlusion and temporo-mandibular disorders, which will consequently, result in more inflammation and pain.

Dental caries are thought to form due to different factors including natural tooth characteristics and environmental factors, that combined, change the ecology of biofilms from a state of health into a disease associated state[7]. The oral environment is probably the most complex and important factor when determining the primary cause of caries. Dietary habits based on the consumption of complex carbohydrates and refined sugars (base of Western diet) has been shown to be a significant contributing factor for the development of dental caries. Sucrose is the most cariogenic dietary sugar because pathogenic bacteria can metabolize it to lactic acid, which decreases the local pH to values lower than 5.0. These acid-producing bacteria are able to thrive in acidic conditions, which favors the multiplication of caries-producing bacteria, such as *Streptococcus mutans*, lactobacilli, and bifidobacteria[8]. The low pH kills the once thriving commensal bacteria and allows the pathogenic bacteria to survive and take the place of the commensal bacteria. Using fluoride toothpaste not only helps to return the pH to neutral, but also has been shown to be antibacterial against bacteria present in the oral microcosm. These factors on their own may not cause caries, but a combination of the factors may result in the formation of caries.

Dental Restoration Techniques

Caries can be diagnosed in different ways. Sometimes a carious lesion is visible under visual clinical examination. In areas that are less accessible to the naked eye,

other types of diagnosis can be used including tactile (probing with a clinical explorer), laser- or image-assisted (X-rays or cone-beam computer tomography) to determine the presence and the extension of the lesion. Based on the severity of the lesion and the age of the patient, the lesion can be treated using atraumatic procedures including silver diamine fluoride application, step-wise excavation, removal of disorganized tissues using rotary instruments (at low and high speeds) followed by the placement of a restorative material such as composite resins, glass ionomer cements, porcelains, ceramics or metals. Some of these methods can also employed when the tooth structure is damaged due to trauma leading to chipping or fracturing.

Silver diamine fluoride application is the least invasive method of carious lesion treatment. Silver diamine fluoride is a liquid clinically applied to the cavitated lesion in dentin. The sealant is applied to the tooth and light cured. It halts the progression of the disease and increases the potential of remineralization of the tooth. One side effect from this treatment is the infected tooth will be stained brown; however, only the treated portion of the tooth will be stained permanently.

The removal of the carious lesions using rotary instruments is the most common approach used in dentistry followed by the placement of a restorative material (metal, polymer or ceramic) to restore the function and the esthetics of the tissue lost to the lesion. Composite resin restorations are mercury-free materials that are used in minimally invasive and ultraconservative treatments (Figure 1). These types of materials do not require extensive removal of sound tissues and are typically bonded to the tooth structure using a dental adhesive resin that is micromechanically attached

to the tooth structure. Ideally, the adhesive resin should completely fill the crevices in the tooth to prevent future bacterial infiltration. If the adhesive from the filling fails to completely adhere to the tooth structure due to polymerization shrinkage, incomplete enveloping of exposed collagen fibrils and phase separation of hydrophilic and hydrophobic components, bacteria are allowed to penetrate the adhesive interface, form biofilms and produce secondary caries.

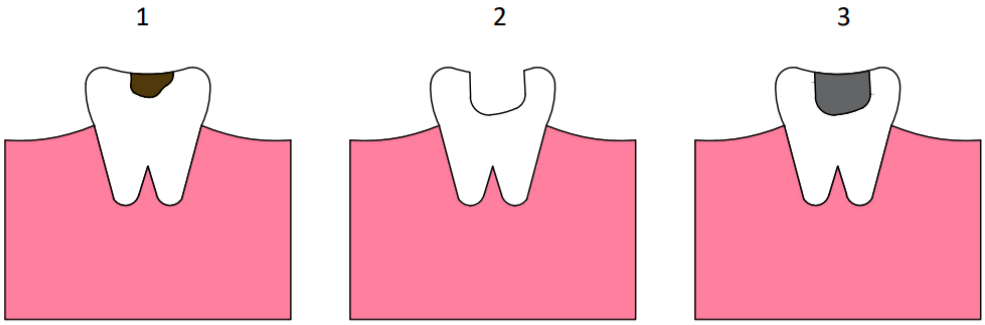

Figure 1 – Diagram of tooth with dental caries

1) Decayed tooth with cavity. 2) Tooth with decayed area removed. 3) Tooth with adhesive and filling to replace the decayed tooth.

Crowns are used if the carious lesion is more severe and involves the removal or one or more cusps. An onlay or a full crown is then fabricated and cemented in place to restore the function and esthetics of the affected portions of the tooth. A simple filling cannot be used on these because the tooth remnant will not be able to withstand masticatory forces (Figure 2). Crowns are available in various materials including: stainless metals, composite resin, metal-ceramics and porcelain.

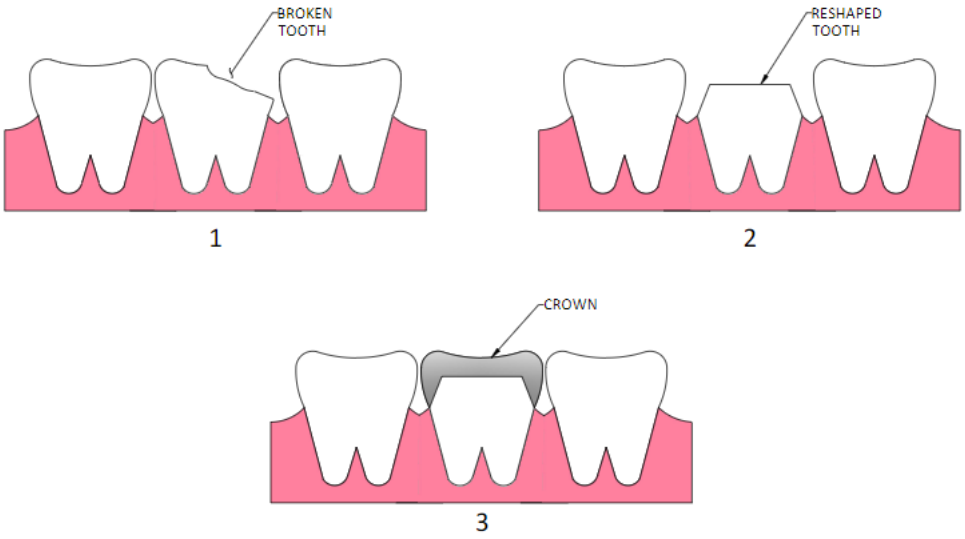

Figure 2 – Diagram of crown

1) Tooth is chipped, damaged or broken. 2) Tooth is reshaped to accept the crown. 3) The crown is cemented into place on reshaped tooth.

Radical endodontic treatments are performed if the carious lesion has infected the pulp complex. In more serious cases, necrotic pulp is associated with the formation of a periapical abscess. The objective of the radical endodontic treatment is to remove the infected pulp and open a channel of communication to deliver treatment to periapical regions where abscesses might be present (Figure 3). After the infection has been successfully treated, a permanent obturation material (gutta percha) in place to obliterate the entire root canal space. The clinical crown of the tooth is then filled with a direct or indirect restorative material with or without the utilization of an intracanal post used for structural support. Then a crown is cemented onto the core fabricated and the anatomy and esthetics of the rebuilt tooth. Adhesive is used to fill the gaps to prevent bacteria from infiltration the tooth again.

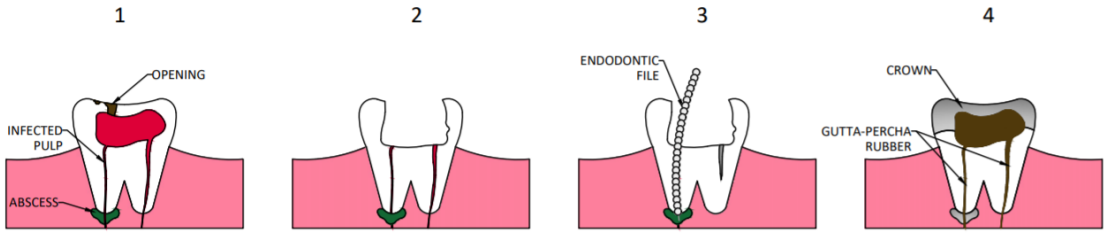

Figure 3 – Diagram of root canal

1) Decayed tooth with opening experiencing infected pulp and abscess. 2) Opening is drilled in tooth. 3) A file is used to remove infected pulp and clean the tooth. 4) The open cavity from the removed infected pulp is filled with gutta-percha rubber and a crown is cemented over the opening.

The treatment for the most severe case of carious lesion is extraction of the complete tooth. In these cases, a dental implant or a partial prosthesis (removable or fixed) is then fabricated to restore the function of the lost tooth while maintaining the horizontal and vertical relationships between teeth and arches. A fixed partial prosthesis can be used to restore one or more missing teeth (known as pontics). To that end, the abutment teeth adjacent to the space left by the lost tooth (or teeth) are then prepared using high-speed turbines and different types of diamond burs under copious air/water irrigation to prevent any iatrogenic injuries. The treatment-planned preparations are designed specifically to meet the requirements of the restorative material of choice (metal, metal-ceramic or full-ceramic). After that, the extra-orally fabricated crowns and attached pontics are then cemented onto the abutment teeth using an appropriate dental cement (glass ionomer, zinc oxide and eugenol, etc.) to fully restore the function and esthetics of the tissues lost to caries (Figure 4).

Endosteal dental implants are one of the most efficient and functional methods to restore teeth because they are capable to fully restore the masticatory function of

the lost teeth and have been demonstrated to have long-term service lives and high levels of clinical success. The implant fixture made of a commercially pure titanium alloys in placed (friction fit or screwed in) the maxillary or mandibular bones. Despite favorable clinical reports and wide spread acceptance by clinicians and patients, recent studies have demonstrated that titanium alloys tend to release ions of vanadium and aluminum that have been correlated with local and systemic inflammation, Alzheimer disease and dementia. In addition, the mismatch between the Young's modulus of bone (~70 MPa) and the implant fixture (~110 MPa) promotes the death of periphery cells by a stress-shielding mechanism, which impacts implants' primary stability and leads to the critical failure of the placed implants.[9,10].

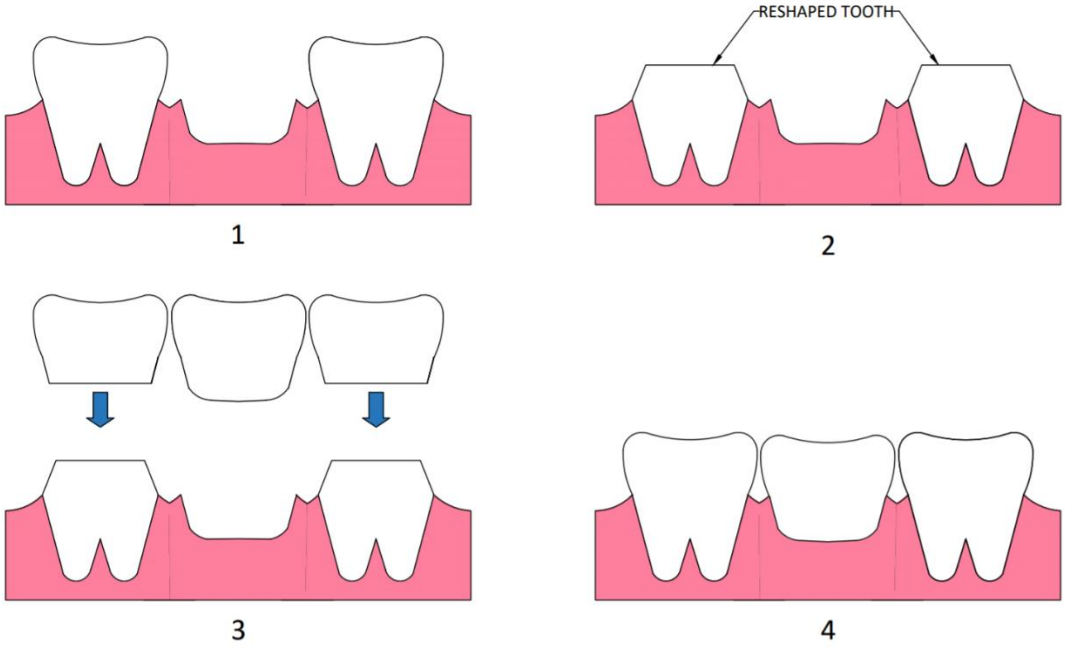

Figure 4 – Diagram of bridge restoration

1) A tooth is missing. 2) The adjacent teeth are sawed down. 3) A bridge is created to be inserted over sawed teeth and to replace the missing tooth. 4) The bridge is placed over the two shaved teeth and cemented in place.

Antibacterial Adhesives

Dental adhesive resins are an integral part of modern esthetic restorative techniques. These polymer-based materials are capable to establish the bond between the tooth structure (hydrophilic) and the composite resin (hydrophobic). Several reports have indicated that the major common cause of failure of these types of restorations is secondary caries between the adhesive resin and the tooth structure (either enamel or dentin). Therefore, the development of novel dental adhesive resins with non-leaching and long-term properties are very relevant for the field of dental biomaterials.

Ideally, these novel materials would not only display strong antibacterial properties, but also, would be capable to precipitate hydroxyapatite in areas of incomplete enveloping of exposed collagen fibrils to deter the growth of pathogenic bacteria and fill any gaps present in the adhesive layer. In addition, these materials should display adequate surface, mechanical and biological properties. The present thesis describes research on the incorporation of nanoparticles and surfactants with well-known antibacterial properties into commercially available dental adhesive resins to result in experimental materials with antibacterial functionalities[11]. The present thesis also investigated the potential synergistic effect between nanoparticles and surfactants against *S. mutans* (planktonic suspensions and non-disrupted biofilms). Nanoparticles' surface properties were investigated, using a modified drop penetration method and surface energy components to allow for their functionalization in

multifunctional methacrylates as demonstrated in Chapter 2. In Chapter 3, the antibacterial properties of nanoparticles and surfactants are examined against *S. mutans* (planktonic suspensions and non-disrupted biofilms) using the CFU/mL and a recently developed and validated bioluminescence assay[12].

Metal oxides have shown antibacterial properties when used in biological studies[13–17]. The incorporation of metal oxides into dental adhesive resins were demonstrated to result in experimental materials displaying promising antibacterial properties against important microorganisms present in dental caries, thereby indicating the utility to arrest the development of secondary caries[18]. Metallic nanoparticles can be easily dispersed into other materials while retaining their antibacterial properties. Even though the antibacterial mechanism of metal oxide nanoparticles has not been fully discovered, it is believed that their major mechanism of action is based on the generation of reactive oxygen species (ROS) and due to lipid peroxidation[19]. These short-lived and high reactive molecules are capable of oxidizing numerous organic components such as the bacterial membrane, DNA damage, and inhibition of certain intracellular enzyme activities that are vital for the viability and growth of cells[20].

Zinc Oxide Nanoparticles

Zinc oxide nanoparticles are studied and used for many different purposes including their potential for bacterial inhibition. Many studies have reported incorporation of zinc oxide nanoparticles into materials for antibacterial purposes. A study conducted by Kasraei et al. found that zinc oxide nanoparticles exhibited

antibacterial properties. The control blood agar plate showed a mean number of 126 ± 29.47 *Streptococcus mutans* colonies on the surface while the blood agar plate with composite zinc oxide at 1% concentration resulted in a mean number of 0.93 ± 1.53 Streptococcus mutans conlonies[18]. Zinc oxide has shown antibacterial properties against both gram-positive and gram-negative bacteria[4,18,21,22]. Zinc oxide has been incorporated into many dental applications which is why this study is interested in utilizing zinc oxide nanoparticles to inhibit the growth of bacteria on teeth that may lead to carious lesions. One immediate concern associated with certain metal oxides, specifically zinc oxide, when being introduced to the oral cavity is toxicity. In some studies, it was found that when nanoparticles are ingested into the body, they can be dispersed easier to different regions because of their small size which can induce oxidative stress and cause overall damage to liver and kidney cells[23,24]. The same mechanism that could prove harmful to healthy cells is used to kill the harmful bacteria that comes in contact with the metal oxide[19]. It can be noted that low concentration of metal oxides have been found to not exhibit detrimental toxicity to humans[21,22,25].

Titanium Dioxide Nanoparticles

The metal titanium has been used for many years in the medical and dental fields for implants due to its antibacterial properties and high biocompatibility[26]. Incorporating titanium dioxide particles into dental applications is of interest due to its antibacterial abilities. It has been found that titanium dioxide nanoparticles like zinc oxide nanoparticles have antibacterial properties and are effective against gram positive and negative bacteria[14]. The antimicrobial properties of titanium dioxide are

linked to its crystal structure, shape, and size[27]. Due to the photocatalytic properties of titanium dioxide nanoparticles, they efficiently eradicate the bacteria[28–30].

While titanium, the metal, has proven to be a reliable antibacterial implant, a major concern when using titanium dioxide nanoparticles for its antimicrobial properties is the reactive oxygen species produced under UV light. Reactive oxygen species are known to cause damage to DNA[31]. One interest for titanium dioxide nanoparticles in this study is its incorporation into dental adhesive resins to prevent bacteria growth. When curing dental adhesive resins, UV light is used which would result in activating the reactive oxygen species. One solution to this problem is to dope the titanium dioxide nanoparticles with metal ions which helps reduce reactive oxygen species. Doping the nanoparticles also enhances the antibacterial and photocatalytic properties[32,33]. The antibacterial characteristics of titanium dioxide in the adhesive was examined in another study. It was found that specimens fabricated with experimental dental adhesive resins containing 50, 67 or 80% (v/v) of nitrogen doped titanium dioxide nanoparticles were shown to have strong antibacterial behavior when compared to the antibacterial behavior of unaltered dental adhesive resins[15]. Plain TiO_2 nanoparticles were not as effective at preventing bacteria growth as the metal doped TiO_2 nanoparticles[14].

Surfactant: Dimethyldodecylamine oxide

Surfactants are amphipathic structures which allow these compounds to alter the surface and interfacial properties of solutions[34,35]. Dimethyldodecylamine oxide (DDAO) is the surfactant evaluated in this study. DDAO is one of the surfactants in

the amine oxides group and are surfactants that are amphoteric. DDAO is a surfactant that possess zwitterionic properties due to its positive and negative charges present on the structure (Figure 5). Zwitterionic surfactants are known to have antimicrobial properties even at low concentrations[34] which is one of the reasons this is the surfactant chosen for this study. A study conducted by Subik et al concluded that DDAO among other amine oxide surfactants such as 4-Dodecylmorpholine-N-oxide, 1-dodecylperhydroasepine-N-oxide, and 4-alkylmorpholine-N-oxides disorganizes the membrane of different bacteria which is the primary source of the antimicrobial activity exhibited in these surfactants[36].

Figure 5 – Dimethyldodecylamine oxide

It is expected that the zinc oxide particles working in conjunction with the dimethyldodecylamine oxide will have a synergistic property and create an antibacterial material that could help eliminate secondary cavities caused from microbial invasion. Zinc oxide and DDAO have shown high antibacterial characteristics and will allow the dental resin to maintain its white color and be more aesthetically pleasing for patients. It is hypothesized that by combining these two materials known for their antibacterial properties, they will synergize and work even more affectively together to inhibit growth of S. mutans than they would alone.

The interest in antibacterial adhesives has led to the investigation of the surface properties of the zinc oxide and titanium dioxide nanoparticles. Studying the contact angles of the nanoparticles will allow for surface characterization with potential determination of the surface energy components. This will provide further insight on the possible effects of the nanoparticles on the adhesive and the impact the nanoparticles may have on the mechanical properties and bonding abilities. The interest in antimicrobials also warrants the testing of the antibacterial properties of the nanoparticles and surfactant against bacterium commonly associated with dental caries. This will give insight to the likelihood of these materials to prevent bacterial growth in dental restorative techniques requiring adhesives.

Chapter 2 –Drop Penetration Method to Study Surface Properties on Nanoparticles*

*Portions of this material has appeared as an article in Nanomaterials, "https://www.mdpi.com/2079-4991/10/6/1099/pdf".

Introduction

Nanoparticles (NP), which are discrete structures displaying high surface area-to-volume ratios, have a wide variety of applications in several segments of industry, engineering and health-care including paints, coatings, catalysts, cosmetics and pharmaceuticals [37–44]. In the medical field, NP are typically used for the fabrication of antibacterial coatings, nanostructured composite materials and implants[4,5] with metal oxides of silver, zinc and titanium[4,15,45,46] being the most commonly used due to their proven antibacterial and biocompatibility properties. Because metal oxides are known for their antibacterial properties, their incorporation into a dental adhesive is of interest for this research on surface properties. Surface character of the nanoparticles is important to ensure good wetting and integration of the nanoparticles into the adhesive without compromising bonding function. In general, NP are mechanically dispersed by various methods (e.g., orbital planetary mixer, spatulation and ultrasonication) within the matrix of different types of materials (e.g., metals, ceramics and polymers), and their functionalization levels may be adversely impacted by agglomeration phenomena and strong interfacial effects. Therefore, understanding the surface properties of nanostructured powders may facilitate the development of novel nano-filled materials displaying improved properties (e.g., chemical, mechanical, and biological) and may even help to predict their performance during service.

Properties such as roughness, hardness, bond polarity and electronegativity typically dictate how materials interact with organic and inorganic molecules, water, human tissues (both hard and soft) and cells (eukaryotic and prokaryotic), thereby directly influencing the biological and fouling properties of nano filled materials. Several studies have shown that the interaction between different types of solvents (such as water, alcohol, acetone) and solid surfaces, measured by contact angle measurement, and the work of van Oss-Chaudhury-Good (vOCG)[47–49] to determine the surface free energies of a different surface.

Measurement of the contact angle of a powder is known to have its challenges. To date, there have been a number of ways developed to determine the wettability of powders[50] with much of the work being reported by the pharmaceutical industry. The Washburn capillary rise (WCR) method illustrated in Figure 6A uses a glass tube or column packed with powder to correlate the rate of liquid uptake (in terms of mass) to contact angle measurements[50,51]. There also exists a variation on WCR known as thin layer wicking with the powder deposited on a substrate[52]. Due to its simplicity and low cost, WCR stands out as the most commonly used method to determine the contact angles of powders. Despite such popularity and wide spread use, the WCR method has been demonstrated to be restricted in regards to the types of systems that can be measured; therefore, researchers have investigated the possibility to adapt the Washburn, static contact angle, and Wilhelmy plate techniques[50] (Figure 6) for accurate determination of contact angles of powders in WCR-restricted systems.

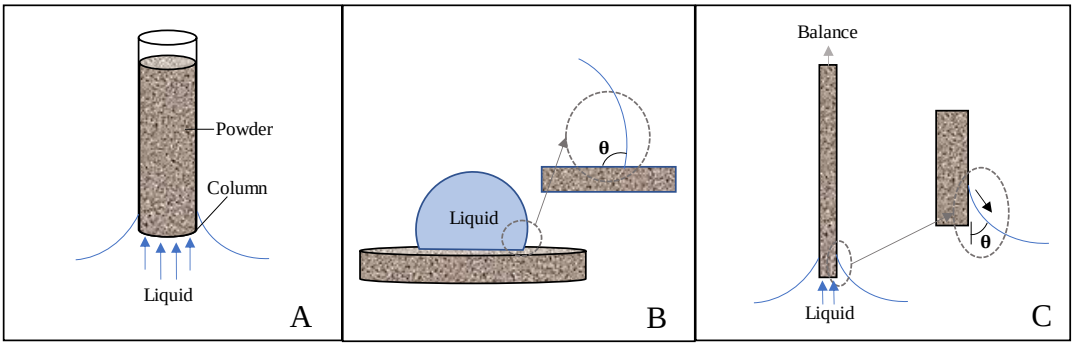

Figure 6 – Contact angle determination methods

Three common methods for determining a contact angle of a liquid on a solid. A) Washburn capillary rise, where a capillary tube is packed with a solid and the liquid taken up is related to the wettability of the powder. B) static contact angle, where a liquid droplet is placed on a solid and the contact angle is determined from the liquid's point of contact. C) Wilhelmy plate, where a plate is inserted into a liquid and removed, the surface tension force is balanced by the force needed to pull or push the solid into or out of the liquid.

When reviewing the various methods for contact angle determination on compact powders, there are some key advantages and disadvantages to consider for each (such as cost, time, reliability, and accuracy). For example, WCR is not appropriate for determining the wettability of hydrophobic particles using water as capillary forces will not allow the fluid to advance [53]. In addition, WCR method is also not suitable for particles that swell or packings that collapse during testing. According to Ramirez-Flores, the packing procedure is a critical determinant of reproducibility [54] with channeling and wall effects being well-known problems that further impact the ability of WCR to be used effectively. Notwithstanding these concerns, the WCR method represents a convenient method for determining the contact angles of powders. Moreover, it should be appreciated that particulate substrates complicate the use of the

SCA and Wilhelmy plate methods which are generally employed for finding the wettability of monolithic materials with flat surfaces.

The static contact angle (SCA) technique depicted in Figure 6B, is typically carried out in a goniometer by dispensing a liquid droplet onto a solid surface, followed by the analysis of the drop profiles and the determination of wettability (in terms of contact angles) using the Laplace-Young equation. In comparison to other available methodologies, the static contact angle is one of the most efficient when cost and time are considered; however, its major disadvantage is associated with its limited accuracy in determining contact angles that are smaller than 20° [50]. These problems are further exacerbated by surface roughness, whether it is a loose layer of powder or a pressed disc. It has been demonstrated that variations in these surface properties can cause the Laplace-Young contact angle to more closely resemble the apparent contact angle, thereby adversely impacting the ability to measure the wettability of a powder[43,54].

The Wilhelmy plate (WP) method is an interfacial tension analysis that is calculated based on the observation of advancing and receding contact angles as the substrate (nonporous, thin, rectangular and flat) is immersed into a liquid and then pulled back out into the position where the substrate (plate) first makes contact with the liquid. During this process, the advancing and receding contact angle are obtained from measurements of force after taking the surface tension into consideration. Even though WP is more expensive due to the requirement for the utilization of a precision microbalance, this method has the advantage of being capable to precisely measure small contact angles[55]. Based on these properties, researchers have adapted the WP

method for powder-based specimens deposited onto the surfaces of wafer or glass slides and fixed using an adhesive[50]. Potential sources of error are related to the uncertainties associated with values of the wetted perimeter as directly influenced by surface roughness[50] and the possibility of added weight through the absorption of liquid into the porous substrate.

Recently, Liu et al. introduced a modified approach to the Drop Penetration Method (DPM) and applied it to determine the wettability of powders displaying particle size-distributions between 10-100 μm [56]. This method has been proven to work effectively in measuring the contact angles of solvents on micron sized particles; however, it would be beneficial if this method could also be used on nanoparticles. The Washburn method has been used for determining the contact angle of nanoparticles; however, this method, as noted above, is associated with issues such as channeling. The modified DPM is a promising technique that will not have wall effects that contribute to channeling issues. DPM as introduced by Liu is a technique where digital images are captured to provide a time-dependent assessment of the penetration of the liquids (reference solvent and investigated solvent) into wafer specimens fabricated from compressed powders. This approach combines elements of the SCA and WCR methods, wherein a droplet is dispensed onto a solid surface of interest and advancing contact angles can be observed while the liquid is drawn into the porous material by capillary action. Despite these similarities, DPM differs from the SCA and WCR methods when it comes to data processing and experimental output (in terms of contact angles' numerical values). A significant difference between the WCR and

DPM methods is that the former investigates liquid penetration opposed by gravitational forces while the latter works with gravity. The Bond number, which is defined as the ratio of the gravity to capillary forces[57] (Equation 1).

Equation 1 $$B_o = \frac{\Delta \rho g R l}{\sigma}$$

Where Δρ is the difference in densities, g is the gravitational constant, l is the core length, R is a typical size of a pore, and σ is the interfacial tension.

Based on this critical scenario, the purpose of the present study was to examine the applicability of the DPM method reported by Liu et al. for the measurement of contact angles of powders composed of nanoparticles with dimensions that are 2-3 orders of magnitude smaller than those investigated by Liu et al. A wide range of solvents was employed in the present study to allow the determination of their contact angles on powders of nanoparticles of zinc oxide and titanium dioxide. Contact angle results obtained in the present study (modified-DPM) were compared to contact angle values previously reported in the literature for particles of similar compositions and size-distributions as determined using a variety of methodologies.

Theory

The derivation of the Drop Penetration Method and equations involved are explained in details by Liu et al.[56]. Scaling and nondimensionalization of the governing equations led to a relationship for the contact angle, as demonstrated below by the final derived equation for contact angle determination:

Equation 2 $$\cos(\theta_T) = \frac{\tau_{\alpha R}}{\tau_{\alpha T}} \frac{\mu_T}{\mu_R} \left(\frac{r_{cT}}{r_{cR}}\right)^2 \frac{\gamma_R}{\gamma_T}$$

where τ_α represents the penetration times, μ represents viscosity, r_c represents the contact radius, γ represents surface tension, and subscripts R and T represent the reference liquid and test liquid, respectively[56]. Subscript α indicates the particular fraction of the droplet volume that has penetrated into the disk for the value of τ. The reference liquid must have a zero-contact angle with the powder under consideration, that is, complete wetting $\cos(\theta_R) = 1$. In addition, the contact radius of the drop must remain constant throughout most of the penetration for both test and reference solvent (Figure 7).

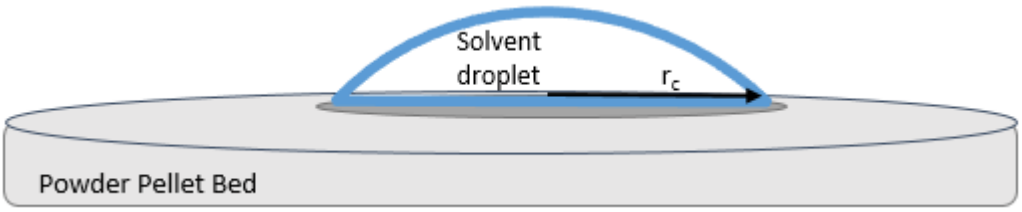

Figure 7 – Sessile droplet

View of a sessile drop as the liquid penetrates into the dry nanoparticle bed and begins wetting the surface using the drop penetration method.

Materials and Methods

Nanoparticle Powders

The metal oxide nanoparticles investigated in the present study were zinc oxide and titanium dioxide. Two types of commercially available zinc oxide nanoparticles have been tested: Nanogard™ (Lot: B13Y045, Alfa Aesar) and NanoTek™ (Lot: D22W010, Alfa Aesar). Nanogard™ nanoparticles are 40-100 nm in size and >99%

purity. The NanoTek^{TM} nanoparticles are similar at 40-100 nm in size and 99% purity, but they differ in being hydrophobic with an organosilane coating. Commercially available titanium dioxide nanoparticles of two sizes were examined as the second type of metal oxide nanoparticles. The first of the titanium dioxide nanopowders contained 21nm diameter particles comprised of a rutile and anatase mixture (Lot: MKCD9677, Aldrich). The second titanium dioxide nanopowder had larger particles (<100 nm), also containing a mixture of rutile and anatase (Lot: MKCG0376, Aldrich). The nanoparticles were used 'as received'.

Fabrication of specimens

A stainless-steel mold (25 mm I.D.) was used to fabricate flat disc shaped specimens composed of compacted nanoparticles' powders (either ZnO [with or without organosilane coating] or TiO_2). A pilot study was conducted to determine the necessary masses (1.4 g of ZnO and 1.0 g of TiO_2, respectively) of nanoparticles required to fabricate specimens with thicknesses that did not allow the complete penetration of solvent droplets through to the other side of the disc during CA measurements. Because the DPM is based on interaction of the solvent with particles, if the solvent penetrates completely through the disc to the other side, another interface is introduced to the testing environment. This is similar to wall effects in the Washburn method. To determine the necessary thickness, one considers the volume of the droplet, porosity, and horizontal spread of the solvent in the disc. Nanoparticles were placed into the cavity of the mold, were evenly distributed to produce wafers of similar porosity and roughness, and were subjected to 140 MPa (2 min, 25°C) of compressive

forces delivered by a manual press (Specac Atlas 15T hydraulic press). The rationale for the selection of compressive forces described was based on previously published reports[50,58,59] indicating that the utilization of compressive forces between 70 to 800 MPa resulted in specimens displaying acceptable compression and mechanical properties without adversely impacting the nanoparticles (e.g., textures, morphologies and structures). Fabricated specimens were then carefully removed from the mold and stored in Petri dishes (dry and dark conditions) until use (Figure 8).

Figure 8 – Nanogard disc after powder press

Solvents

Six solvents (distilled water [lab grade], diiodomethane [Lot: S7359453, MilliporeSigma], bromonaphthalene [Lot: S6971210, MilliporeSigma], formamide [Lot: 94011020, Roche], ethanol [Lot: SHBK0402, Sigma-Aldrich] and ethylene glycol [Lot: SHBK3427, Sigma-Aldrich]) were selected based on their ability to meet the requirements of a reference liquid (e.g., complete wetting) and were used to determine the CA of specimens' surfaces using the DPM method according to a method previously published[50]. Table 1 describes the viscosity, surface tension, and density properties of solvents investigated.

Table 1

Solvent	Viscosity x 10^3 (Pa.s)	Surface Tension x 10^3 (N/m)	Density x 10^3 (kg/m^3)
Diiodomethane	2.6	50.8	3.33
Formamide	3.34	58	1.13
Ethylene glycol	16.2	48	1.11
Bromonaphthalene	4.8[a]	44.4	1.48
Water	0.89	72.8	1
Ethanol	1.095	22.4	0.79

Liquid properties of solvents at 25°C; Note: All data cited from Van Oss et al. unless denoted otherwise[60]. a[61]

Contact angle measurements

A contact angle goniometer (OCA 15, Future Digital Scientific Corp.) coupled with a high-definition and high-speed digital camera (up to 50 frames/second), an environmental chamber and a computer-controlled solvent-dispensing system was used to individually dispense axisymmetric droplets of each solvent (volumes according to Table 2) onto the surfaces of separate specimens (n=2/group) at 3 random locations. Digital images (25 frames/s) were captured (1 min, 22 ± 1°C) to determine the evolution of the drop absorption by the compressed disc. The evolution of the droplet and its contact angle was determined using SCA 20 V.4.4.3 software program. The average of the contact angle measurements at $\tau_{\alpha=0.50}$ and $\tau_{\alpha=0.75}$ are used for contact angle data reporting. It is important to highlight that even though drop-volumes varied according to solvent considered, volumes used never exceeded the threshold of 10 µL to prevent gravitational forces from distorting the results[62]. The volumes of droplets were adjusted due to the considerable variability in physical properties of the solvents. This allowed the droplets to dispense consistently. Figure 9 (A-F) illustrates

representative images of the evolution of a droplet penetrating into a specimen fabricated using nanopowders. Each droplet dispensed was observed to exhibit a circular cross-section in shape during penetration.

Table 2 – Summary of dosing volume and rate for solvents in CA goniometer

Solvent	Dosing volume (µL)	Dosing rate (µL/sec)
Deionized water	3	2
Bromonaphthalene	3.5	2
Formamide	5	3
Diiodomethane	1.5	2
Ethanol	4	2
Ethylene glycol	3	2

The volume of droplets dispensed were calculated using Equation 3, below, for a spherical cap.

$$\textbf{Equation 3} \quad \textbf{Volume} = \frac{1}{3} * \pi * h\,(3 * a^2 - h^2)$$

where h represents the height of the spherical cap and a represents the radius.

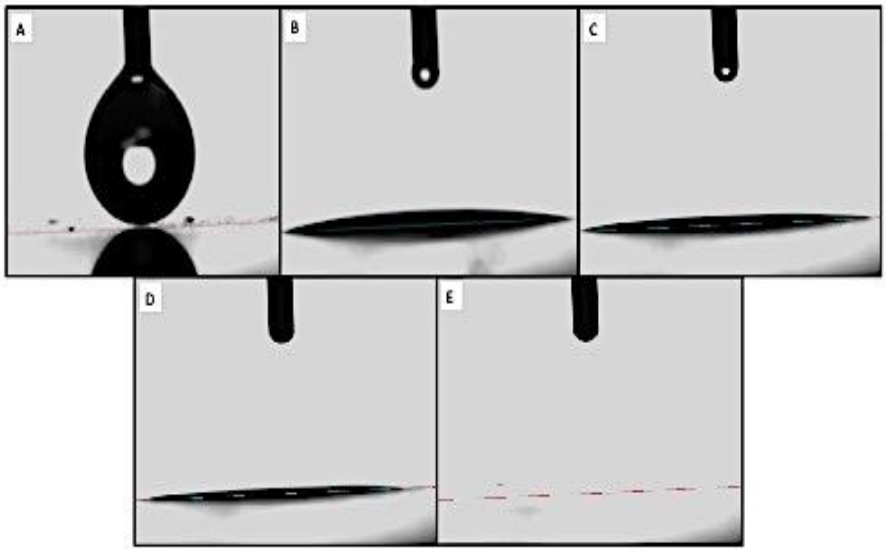

Figure 9 (A-E) – Formamide on Nanogard™

Representative images of formamide on Nanogard™; A) formamide droplet immediately before being dispensed onto the surface of the specimen, B) spreading of formamide droplet, C) aspect of droplet after 0.50 min, D) aspect of droplet after 0.75 min, E) aspect of the surface of the specimen at 1.00 min Note that the droplet dispensed is completely absorbed by the specimen over the time period of observation.

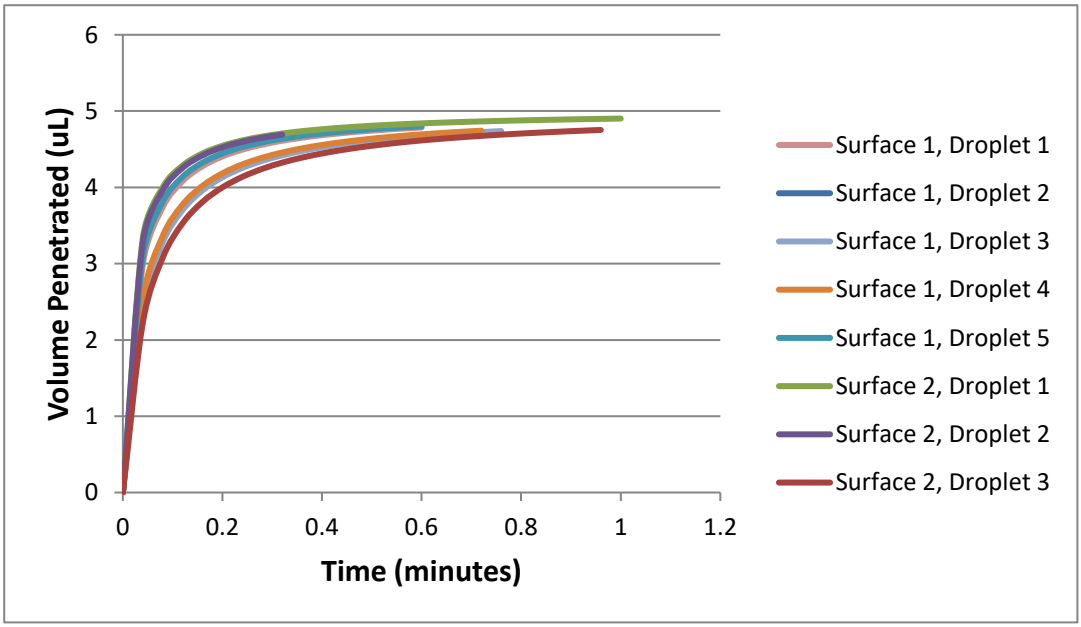

Figure 9F: Representative curves of time-dependent penetration of formamide (volume dispensed here) into specimens of packed Nanogard™ powders (either x or y). Surface numbers indicate separate specimens, while droplet numbers indicate separate droplets placed on the surface of same specimen.

Results and Discussion

The modified-DPM was employed in the present study to determine the wettability of deionized water, bromonaphthalene, formamide, diiodomethane, ethanol and ethylene glycol (in terms of contact angles) on the surfaces of specimens fabricated with packed nanopowders of Nanogard™ ZnO or TiO_2 to determine the utility of the modified-DPM investigated on nanostructured materials. In order for the modified protocol to render accurate contact angle measurements some fundamental criteria must be met, including (i) reference solvent's contact angles must tend to zero and exhibit complete wetting, (ii) contact radius should remain constant throughout penetration time, and iii) nondimensional time and volume (for different solvents on the same solid) should create an overlapping trend when graphed. The nondimensional time and volume takes the permeability, porosity and effective pore radius into account in order to determine the nondimensional values of the data shown in Equation 4.

$$\textbf{Equation 4} \quad t_c = \frac{\mu \varepsilon {r_c}^2}{k p_c}$$

Where t_c is the characteristic time, μ is viscosity, ε is the porosity, r_c is the contact radius, k is the permeability, and p_c is the capillary pressure inside of the powder bed. More details on the nondimensional analysis equations can be found in the article by Liu[56].

In the present study, the rationale for selection of nanoparticles was based on their utilization as antibacterial and bioactive agents for polymer-based dental

biomaterials, while solvents were selected based on their ability to determine the surface free energy components of the solids of interest,[49] and because this type of characterization, requires the utilization of a variety of solvents displaying a variety of affinity behaviors. Experimental results indicated that solvents investigated were partially capable to wet the surfaces of specimens fabricated using NanoTek^{TM} and, therefore, failed to meet the first criterion cited which resulted in the exclusion of NanoTek^{TM} from the present study. Table 3 lists the solvent used as the reference solvent for each contact angle analyzed. In addition, solvents investigated were observed to display droplets' radii that were nearly constant at $\tau_{\alpha=0.50}$ and $\tau_{\alpha=0.75}$, thereby fulfilling the second criterion cited. The volume and height of the droplet do change over time as each solvent penetrate into specimens investigated. Even though these characteristics are integral to determining the contact angles of the materials of interested, the nondimensional time and volume for different solvents on the same solid should create an overlapping trend when graphed. The results reported in present study were observed to completely fulfill this criterion (as seen in Figure 9F), thereby suggesting that despite intrinsic limitations associated to the utilization of solvent-specific drop volumes, high levels of accuracy and robustness were attained with the modified-DPM, which allowed us to perform intra-group comparisons.

The experimental data obtained revealed that the modified-DPM proved to be most effective when measuring contact angles between 20° and 80° (Figure 10A). When the contact angles exceeded 90 degrees (poor wettability) the solvent will experience weak capillary forces that are capable to promote solvent penetration. This

behavior not only impeded the recording of penetration time, but it has also indicated that the modified-DPM cannot be used to accurately assess contact angles for some specific solvent-material combinations. Experimental data from solvents displaying this type of behavior have been excluded from the present study because $\tau_{\alpha T}$ is very large, $\cos(\theta_T)$ is zero and all such samples yielded contact angles of 90°.

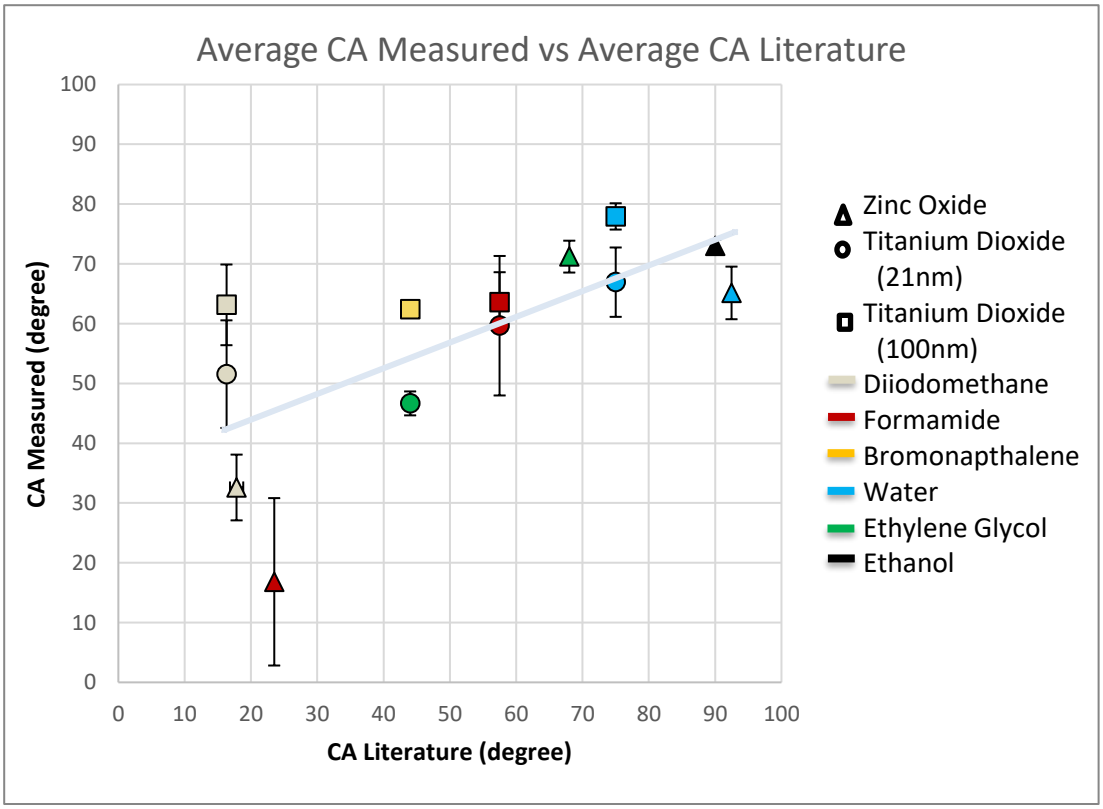

Figure 10A – Average contact angle measured vs average contact angle literature

Experimental contact angle versus literature contact angle based on substrate and solvent. A linear relationship can be seen in the data with the exception of points at low contact angles. The correlation value is 0.44 with a slope of 0.39 shown by the linear regression (light blue line). Symbol shape represents the nanoparticle tested and color indicates the solvent for the data point.

When examining which reference solvent would show promising results, it was found that the viscosity and surface tension of the test solvent and reference solvent were very important. If the value calculated using Equation 5 is ≤ 1, it is likely the reference and test solvent will be compatible and provide a reasonable contact angle data. All data with values ≤ 1 for this study returned reasonable contact angle results. If the value from Equation 5 was > 1 the reference solvent and test solvent combination usually proved unsatisfactory for the contact angle measurement.

$$\textbf{Equation 5} \quad \Pi = \frac{\mu_T}{\mu_R}\frac{\gamma_R}{\gamma_T}$$

The results obtained using the modified-DPM for solvents displaying contact angles smaller than 20° (e.g., diiodomethane) were not considered accurate because these types of solvents are volatile and displayed significant coefficients of variation and were not comparable to values previously reported in the literature (Table 3). These findings are in agreement with a previous report by Alghunaim et al. [50] that while investigating several techniques for determining contact angle and wettability of powders, have indicated that the SCA method also display limited performance for accurately determining contact angles that are below 20°. It is possible that modified-DPM was able to discern differences, though based on the results reported in the present study this seems unlikely. Figure 10B shows the results from the correlation analysis (R^2 = 0.82), between experimental (excluding results >90° and diiodomethane) and literature data. The results reported were obtained using the least squares regression method and indicate the presence of a strong, positive and linear

(slope=0.97) relationship between these two datasets, thereby further corroborating the present study's rationale for the selection of solvents and nanoparticles.

Table 3 – Summary of contact angles determined from the drop penetration method.

Powder	Measured Solvent	Reference	Experimental Contact angle	Literature Contact angle
ZnO Nanogard	Diiodomethane	Bromonaphthalene	35 ± 8	17, 28 [52]
		Ethylene Glycol	30 ± 3	
	Formamide	Bromonaphthalene	17 ± 14	25, 22 [52]
	Ethylene Glycol	Bromonaphthalene	73 ± 1	60.4, 75.6 [63]
		Diiodomethane	69 ± 4	
		Formamide	72 ± 3	
	Water	Bromonaphthalene	79 ± 2	88.6 [64], 81 [65]
		Diiodomethane	77 ± 1	
		Ethylene Glycol	47 ± 11	
		Formamide	78 ± 1	
		Ethanol	44 ± 7	
	Ethanol	Bromonaphthalene	75 ± 3	90 [66]
		Ethylene Glycol	71 ± 1	
		Formamide	73 ± 1	
TiO2 (21nm)	Diiodomethane	Bromonaphthalene	75 ± 3	16.3 [67]
		Ethylene Glycol	81 ± 2	
		Formamide	62 ± 1	
		Ethanol	34 ± 21	
	Formamide	Bromonaphthalene	56 ± 6	50-65 [51]
		Ethylene Glycol	71 ± 4	
	Bromonaphthalene	Ethylene Glycol	62 ± 1	38-50 [51]
	Water	Bromonaphthalene	84 ± 2	70-81 [51]
		Diiodomethane	67 ± 5	
		Ethylene Glycol	86 ± 1	
		Formamide	79 ± 2	
		Ethanol	73 ± 1	
	Ethanol	Bromonaphthalene	68 ± 10	
		Ethylene Glycol	77 ± 6	
		Formamide	48 ± 12	
TiO2 (100nm)	Diiodomethane	Bromonaphthalene	61 ± 5	16.3 [66]
		Ethylene Glycol	43 ± 13	
	Formamide	Bromonaphthalene	71 ± 8	50-65 [51]

	Diiodomethane	49 ± 13	
	Ethylene Glycol	60 ± 14	
Ethylene Glycol	Bromonaphthalene	47 ± 2	38-50 [51]
Water	Bromonaphthalene	82 ± 1	70-81 [51]
	Diiodomethane	73 ± 1	
	Ethylene Glycol	78 ± 2	
	Formamide	60 ± 10	
	Ethanol	41 ± 15	
Ethanol	Bromonaphthalene	78 ± 4	
	Diiodomethane	66 ± 5	
	Ethylene Glycol	72 ± 7	
	Formamide	49 ± 4	

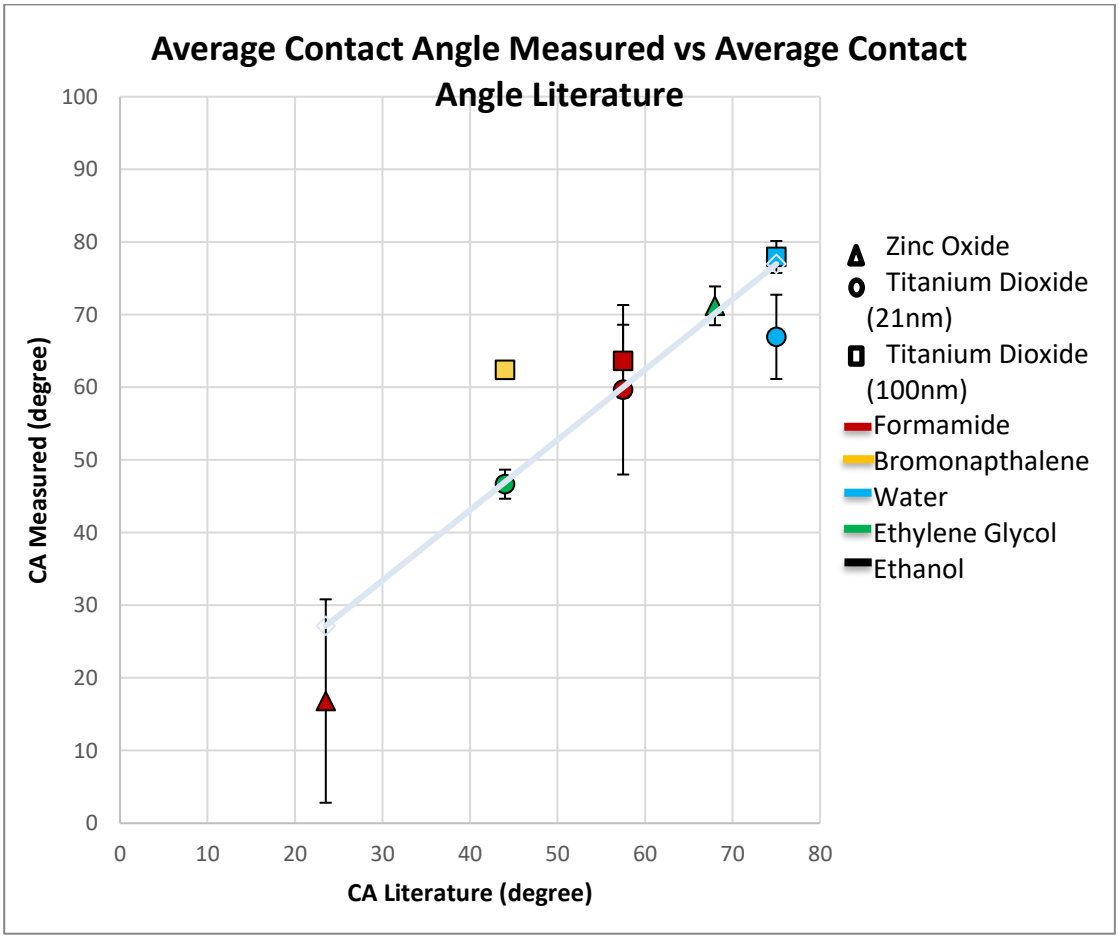

Figure 10B – Experimental contact angle versus literature contact angle with elimination of data >90 degrees and diiodomethane. A clear linear relationship can be seen giving a correlation value of 0.82 and a slope of 0.97. The literature values are an

average of the contact angle values using different measurement methods on a variety of surface types.

Previous studies[68–70] investigating the effects of particle size and shapes on the wetting properties of metal micropowders have indicated the presence of an inversely proportional relationship, wherein particles of smaller sizes were associated with higher contact angle values. The results of the present study contradict previous reports; however, there is was limited research conducted for this study. It was possible to observe a direct proportional trend between TiO_2 sizes and contact angle values observed where lower contact angle values were observed for particles of smaller dimensions (diameter≈ 21 nm). This finding could be partially explained by significant variations in capillary forces that result from materials fabricated using particles of different sizes and the effects of crystalline structure (e.g., rutile, anatase or brookite) as particle sizes decreases. One study reported that rutile has a somewhat higher surface energy than anatase which suggests it should have a low contact angle with water[71,72]. Conversely, Pantaroto et al. while investigating the antibacterial efficacy of different crystalline phases of TiO_2 photocatalysis against oral multispecies biofilms have indicated that the contact angle for rutile (θ=95^o) was higher when compared to that of anatase or that of a mixture of the two (θ=90^o), which indicates a lower surface energy[73]. Still according to the authors, the properties of titanium dioxide will change under depending on particle sizes and under certain conditions of temperature and pressure[41,74,75]. In this direction, even though anatase is more stable when particles sizes are small (typically below ~14.5 nm), increased pressures may cause anatase to become increasingly unstable[71].

The pressure used to compress the powders into discs has been demonstrated to affect the observed contact angles of compressed powders when assessed using different methods. Studies investigating the wettability of different types of materials using SCA or WPM have shown that contact angles tend to reduce as compression forces increase until a constant contact angle value is achieved[43,55]. Other studies[43,50] have shown that high compressive forces may plastically deform nanoparticles depending on their physical structure and their chemical compositions. The macroscopic manifestation of this behavior may adversely impact the penetration of solvents into materials by changing interparticle spacing, pore connectivity and changing capillary forces[43].

The greatest limitation to obtaining accurate measurements with the modified-DPM was directly related to the selection of solvents displaying contact angles less than 90^{o}. Despite this significant limitation when the criteria for use were met, the method reported provided values that comparable to those reported in the current literature. As discussed in the present study, there are different methods available to determine solvents' contact angles on the surfaces of specimens fabricated using compressed powders. Table 4 exemplifies many of the commonly used methods for contact angle measurement and the typical values of contact angles obtained from the utilization of each method described. Once the contact angle values have been obtained, the van-Oss-Good-Chaudhury technique can then be used to determine the surface free energy of the investigated surface; however, the vOCG technique has limitations when using the drop penetration method. The vOCG technique needs

solvents with a variety of characteristics. When using the drop penetration method, the characteristics of the solvent are limited because they must completely penetrate the surface but retain a nearly constant radius while penetrating. This means it should give a contact angle between 20º and 80º, therefore, limiting solvent choices and making the use of the vOCG technique somewhat unfavorable.

Table 4 – Summary of methods used for contact angle measurement in literature

Surface	Liquid	Method	Contact angle
Zinc Oxide	Diiodomethane	Thin-layer wicking method	17, 28
		Static contact angle	8.5
	Formamide	Thin-layer wicking method	25, 22
	Water	Static contact angle	88.6
		Static contact angle	81
Titanium Dioxide	Diiodomethane	Static contact angle	16.3
	Formamide	Washburn Method - Rutile	50-65
	Bromonaphthalene	Washburn Method - Rutile	38-50
	Water	Washburn Method - Rutile	70-81
		Static contact angle	74
	Ethylene Glycol	Static contact angle	44

The correlation between the experimental data reported in the present study and literature values has indicated that a clear correlation could not be found between the modified-DPM and the accuracy of the experimental results obtained (Figure 11). The thin layer wicking method is a variation of the WCR method. For the thin layer wicking method, a thin layer of powders is deposited onto a substrate to form a particle suspension. The surfaces in which the literature contact angle values were measured on varied across the studies reviewed where insufficient contact angles data on compact powders was observed; therefore, literature values typically reflect contact

angle measurements performed on solid specimens as well as on the surfaces of specimens fabricated using compacted powders.

Figure 11 – Contact angle measurement method vs. experimental contact angle

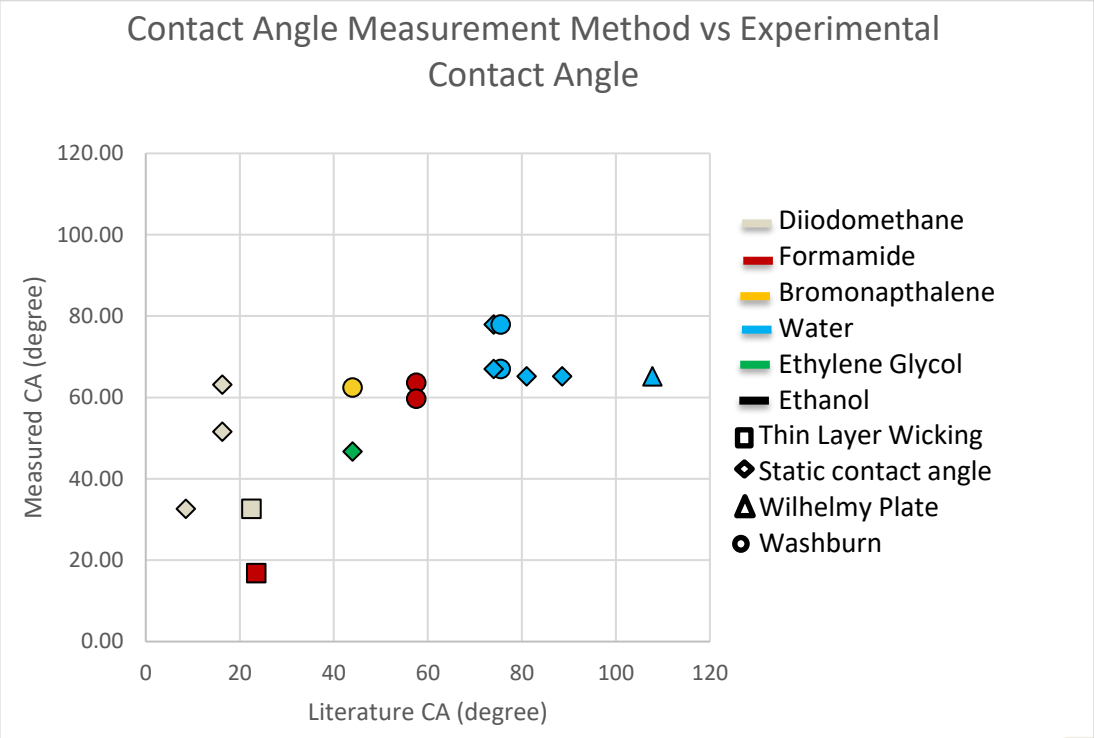

Comparison of modified DPM experimental values and literature contact angle values based on the type of technique used. The results have indicated that an obvious correlation between the experimental and literature contact angle values with any particular method could not be made. (The thin layer wicking method is a variation of the WCR method with powder deposited on a substrate.) Ideally, values would fall on a line with a slope equal to 1. This figure illustrates the challenge in obtaining reliable contact angles. Symbol shape represents measurement technique and color the solvent used for zinc oxide and titanium dioxide substrates.

Chapter 3 – Potential of Antibacterial Adhesives for Dental Applications

Introduction

Tooth decay resulting in caries is one of the most prevalent diseases in the world. If caries are left untreated, they can become a very painful problem that requires medical attention. Commonly the damage from dental caries results in the use of dental restorative techniques. The damage from caries is caused by bacterial adhesion to the tooth's surface.

A study conducted by Brighton University concluded that, "amine oxide showed high potential for controlling early biofilms caused by periodontal bacteria"[76]. A method of preventing bacterial adhesion to the tooth is to incorporate antibacterial materials such as zinc oxide nanoparticles and amine oxide surfactants into dental adhesive resins. This would inhibit the growth of bacteria and decrease the likelihood of secondary caries. It is desirable for the dental adhesive to possess antibacterial properties capable of deterring harmful bacterial growth, but not at the expense of the mechanical properties and bonding abilities of the dental adhesive. It important to determine the influence the nanoparticles and surfactant have on the mechanical properties of the adhesive resins. If the bonding is weak, the adhesive may fail at that site. One way this can be investigated is by measuring the contact angle of the adhesives with nanoparticle and surfactant incorporation. Knowing the hydrophobicity or hydrophilicity effects of the nanoparticles and surfactant when incorporated into the adhesive will give an idea of how the adhesive will react on the tooth's surface. It is favorable for the adhesive to show hydrophobic properties because water-based saliva

containing harmful bacteria will be deterred from entering possible gaps or cracks in the adhesive resin.

Another important factor to consider when incorporating metallic nanoparticles and amine oxide surfactants into dental adhesives is to the antibacterial effects. It is expected that when incorporating metal oxides into the dental adhesives, there will be less bacteria adhesion and growth on the adhesive due to the nanoparticle's antibacterial properties. The metallic nanoparticles will serve as a deterrent for bacteria. The main reason for nanoparticle incorporation into the dental adhesive resins is to prevent tooth decay from harmful bacteria found in the oral cavity; however, the surface wettability must also be examined in order to determine the surface properties of the modified adhesive. The wettability will help determine the overall mechanical strength of the adhesive.

Bacterial Influence

The oral cavity has a vast array of bacteria residing in it. There is thought to be over 700 bacterial species or phylotypes residing in the oral cavity[77]. The bacterium in the oral cavity can be beneficial to the host. The bacteria can also be harmful; however, in most cases, the bacteria provide a symbiotic relationship with the host. Some major benefits provided by the bacteria include: colonization resistance, down-regulation of potentially damaging host inflammatory responses, and active contributions to the normal development of the physiology of the mouth and the host defenses. The oral microbiome lives in harmony with the bacteria until there is a shift in the balance of the oral cavity that allows pathogenic bacteria to thrive and become harmful to the

host. The bacteria that are present in a healthy oral microbiome, commensal bacteria, are accustomed to the oral cavity's environment so when a harmful invader enters the cavity, the accustomed bacteria fight it off. However, it is proposed that when a major environmental shift occurs, the commensal bacteria are not equipped to survive and may lose the fight to pathogenic bacteria. These pathogenic bacteria will disrupt the normal bacteria in the oral microbiome and may eventually cause dental disease[7]. One of the most common bacterial infections in humans is dental caries[77].

Streptococcus mutans are primarily found in the mouth, pharynx, and intestine; thus, *Streptococcus mutans* (*S. mutans*) are one of the best-known bacteria for cause of dental caries. The formation of plaque can lead to an ideal breeding ground for *Streptococcus mutans*. There are multiple stages involved with dental plaque formation (Figure 12). First, salivary molecules are adsorbed to the enamel as soon as the tooth has been cleaned[78]. This forms the acquired pellicle layer on the tooth surface. This layer serves as a protection from acids after carbohydrate consumption and is normally present on the tooth. Next, bacterial interaction with the acquired pellicle happens through cell to surface interactions. These bacteria are known as primary or early colonizers. The primary colonizers grow and multiply throughout the mouth. Last, other bacterial species such as *Streptococcus mutans* adhere to the primary colonizers by cell-to-cell interactions. Bacterial growth on the tooth surface is what causes the formation of the biofilm on the teeth, also called dental plaque[78]. Once these bacteria are on the tooth surface, consuming carbohydrates can add to the

growth and proliferation of the bacteria in the biofilm. Carious lesions develop where oral biofilms are allowed to mature and remain on the teeth for long periods[79].

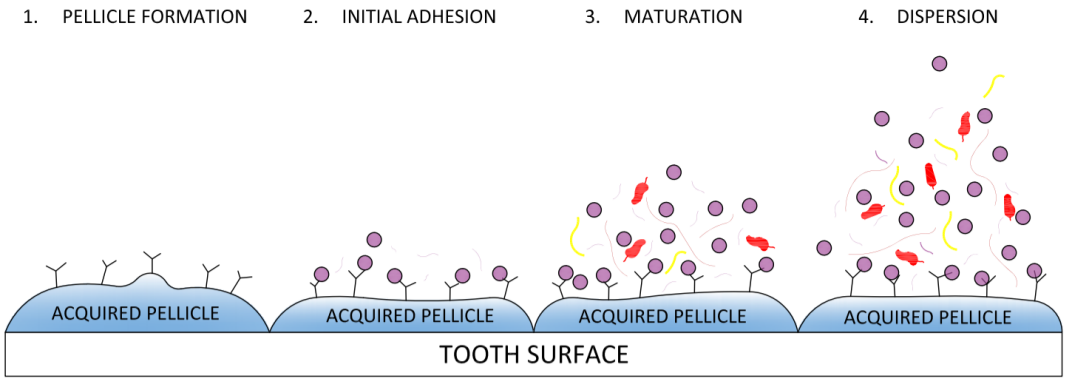

Figure 12 – Formation of biofilm on tooth surface

Carious lesions develop when the biofilm growth in uninterrupted and allowed to proliferate. 1) The tooth surface has a naturally acquired pellicle layer that protects the tooth from acids in foods. 2) The acquired pellicle layer experiences bacterial adhesion known as primary colonizers. 3) the bacterium matures and proliferates. 4) The tooth has likely experienced decay due to the bacteria and starts to disperse to other teeth.

Streptococcus mutans survive by metabolizing carbohydrates especially sugars[80]. Fermentation of carbohydrates by *Streptococcus mutans* is the principal source of energy production for the organism. *Streptococcus mutans* are able to metabolize a wider variety of carbohydrates than any other gram positive organism[80]. *Streptococcus mutans* can survive at low pH which is when the beneficial bacteria start to die. This means *Streptococcus mutans* survive, thrive, and eventually take over the places the commensal bacteria had once lived. In particular, *S. mutans* are known to live within the biofilm of the oral cavity. They are able to adhere and bind to receptors in the pellicle which allows them to be some of the primary colonizers; however, *S. mutans* are usually become part of the biofilm by adhering to the primary colonizers

such as *Streptococcus sanguis* and *Actinomyces* viscous by cell-to-cell interactions[78]. Even with the ability to adhere to the enamel and primary colonizers, *S. mutans* are not especially prominent in the oral cavity. However, when dietary sugars, particularly sucrose, become available, *S. mutans* are able to thrive and become dominant in the oral cavity allowing formation of cariogenic biofilms[81].

Secondary Caries

Secondary caries are mainly the result of micro cracks between the filling and the tooth tissue of a previous dental restoration. These micro cracks allow infiltration of bacteria and provide a nice environment for bacteria to grow. If secondary caries were preventable, a lot of time and money would be saved. To decrease the prevalence of secondary caries, the adhesive needs to be modified in a way that will allow it to inhibit the bacteria from entering the gaps between the tooth tissue and adhesive.

The incorporation of an amine oxide surfactant and metal oxide into dental adhesives are of interest particularly because of their potential antibacterial properties. The metal oxide nanoparticles observed in this study are zinc oxide nanoparticles. Nanoparticles are of interest because it has been found that decreasing the particle size of the material results in greater bactericidal efficacy[13,16]. The intention ultimately is to reduce the harmful effects of bacteria. Surfactants have shown also antimicrobial properties against a broad spectrum of microorganisms[11] which is one of the reasons they are key components in many disinfectant agents such as detergents and cleaning products. By working with *Streptococcus mutans*, a prevalent bacteria present when examining tooth decay[82], secondary caries can be reduced by using antibacterial

adhesive resins in the initial dental restoration. By combining the metallic nanoparticles and amine oxide surfactant there is a possibility of synergism. Because *Streptococcus mutans* are one of the main bacteria present in dental caries, it is believed that this bacterium may heavily contribute to the formation of dental caries. For this reason, the bacteria being used to test the effectiveness of zinc oxides nanoparticles and amine oxide surfactant will include *S. mutans*.

Materials

Antibacterial Blend (Composite)

Two types of commercially available zinc oxide nanoparticles were used: Nanogard™ (Lot # B13Y045, Alfa Aesar) and NanoTek™ (coated with organosilane, Lot # D22W010, Alfa Aesar). The Nanogard™ nanoparticles are 40-100nm in size and >99% purity. The NanoTek™ nanoparticles are 40-100nm in size and 99% purity. They are also hydrophobic and nonpolar. Surfactant solution was used to coat the nanoparticles: N,N-Dimethyldodecylamine N-oxide (DDAO (~30% in water, Lot# BCBQ8457V, Sigma Aldrich). The nanoparticles and surfactant are incorporated into dental adhesive resin as described in the methods (Optibond Solo Plus, Kerr Corporation, Orange, CA; Lot: 5112933).

Methods – Nanoparticle Fabrication

Six nanoparticle groups were created as follows:

Table 5

Sample	Composition
1	Uncoated NanoGard™ in water
2	Uncoated NanoTek™ in 70% Ethanol
3	DDAO Coated NanoGard™ in 70% Ethanol
4	DDAO Coated NanoTek™ in 70% Ethanol
5	DDAO Coated NanoGard™ in water
6	DDAO Coated NanoTek™ in water

For each group, 0.5 grams of nanoparticles were weighed and added to 10 mL of water or 70% ethanol. Surfactant solution was added at 68.7 µL for every 10mL of solution in Groups 3-6. The volumes and masses can be scaled proportionally for all groups. The solutions shook in a shaking bath for 48 ± 4 hours. The solution was mixed then sonicated on ice for 2 minutes at a 10% power output. The nanoparticles were filtered from the supernatant and dried at 72 ± 5 °C for 1 hour.

Methods – Contact Angle

Glass Cover Slips

The groups of adhesive mixtures were as follows:

Table 6

Sample	Composition
1	Control group (unaltered adhesive resin)
2	2.5 wt% Uncoated in water NanoGard™ in adhesive
3	4.0 wt% Uncoated in ethanol NanoTek™ in adhesive
4	2.5 wt% DDAO Coated in Ethanol NanoGard™ in adhesive
5	4.0 wt% DDAO Coated in Ethanol NanoTek™ in adhesive
6	0.033 wt% DDAO in adhesive

Dental adhesive resin was mixed with the fabricated nanoparticles. Each nanoparticle mixture was weighed on an analytical balance then put in a 3mL Eppendorf micro centrifuge tube with cap and 1mL of adhesive was added to each tube containing nanoparticles and/or surfactant. The tubes were wrapped in foil to prevent polymerization of the adhesive when exposed to light. The tube was sonicated using a microtip for 2 minutes total on amplitude 100 for three 40 second intervals with 15 second breaks in between intervals. The tube was submerged in an ice bath to prevent heating for the duration of sonication. Once sonication is complete, the adhesive is used to make the samples for measurement on the contact angle goniometer. The adhesive is wrapped in foil and stored in a dark, room temperature drawer and sonicated before each use. 10μL of adhesive mixture was pipetted in a small tray. A microtip brush is used to thinly coat the 12mm diameter circular glass

cover slips with adhesive then is light cured for 40 seconds in UV light. Three glass cover slips are used for each nanoparticle mixture.

Contact Angle Measurement

A contact angle goniometer (OCA 15, Future Digital Scientific Corp.) coupled with a high-definition and high-speed digital camera (up to 50 frames/second) were used to measure the contact angle of a droplet (Figure 13). Samples were stored in a temperature controlled experimental chamber. A computer-controlled solvent-dispensing system was used to dispense individual axisymmetric droplets of water onto the slips. The chamber can be moved up and down and side to side. The chamber can be connected to a water bath for a temperature-controlled chamber (Lauda Ecoline RE104 with a Lauda E100 circulator).

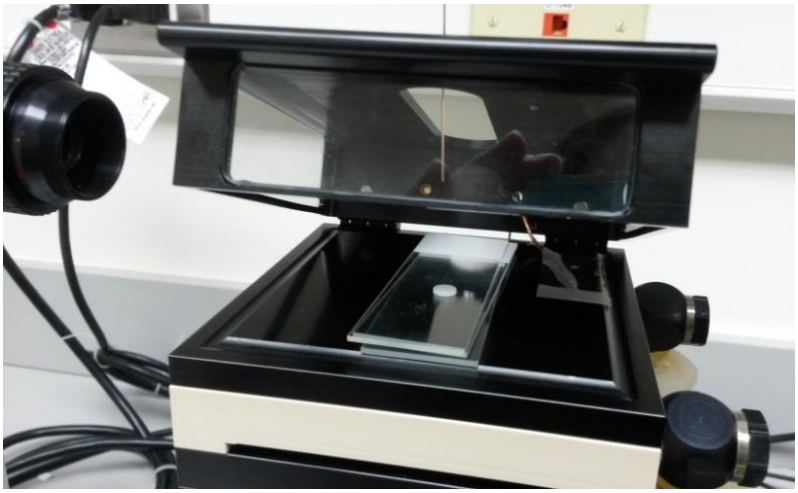

Figure 13 – Experimental chamber with syringe and camera on the contact angle goniometer

A 500μL syringe is suspended above the experimental chamber. It is cleaned and filled before every use. Once the equipment is set up, the sample is placed in the experimental chamber for at least 5 minutes if the water bath is being used. A drop of liquid is dispensed automatically, and the chamber is lifted manually until it is just below the droplet.

The water bath was set to 37±1°C and allowed to reach equilibrium before the specimens were tested. The water bath is set to 37°C because that is the temperature of the oral cavity and will help replicate the environment the adhesive will be used in. The syringe was filled with ultra-pure deionized water. The specimen stayed in the chamber for at least five minutes before being tested. A drop of 3μL was dispensed at 2μL/second from the syringe, the experimental chamber was raised, and the recording was started seconds before the drop came in contact with the specimen. There were three glass cover slips made for each of the groups. Each group had five droplets analyzed on it (n=15). The droplets did not overlap on the specimen even when fully spread out.

The contact angle goniometer uses the SCA 202 V.4.4.3 software program to capture and analyze the data. The recording software is started seconds before the drop makes contact with the surface. Data is collected at 25 frames per second for 60 ± 10 seconds for each data collection using the CAG. Once the data is collected and saved to the computer, the data can be analyzed. The software requires the user to manually set the base line of the sessile drop (Figure 14).

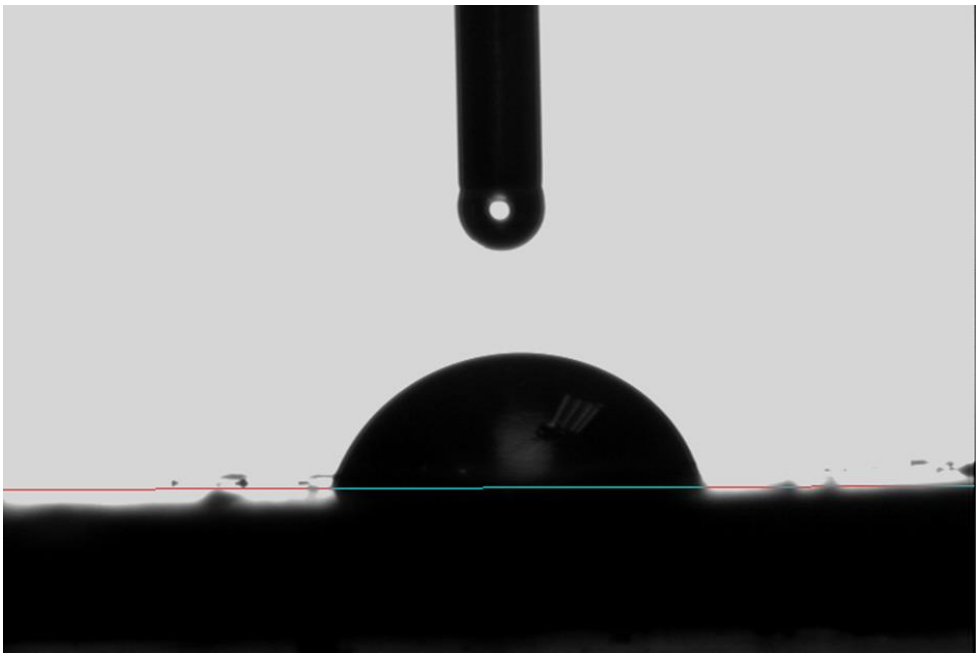

Figure 14 – Droplet with baseline

Image of a water droplet on a surface with the baseline manually set to the place where the droplet comes in contact with the surface.

The Young-Laplace fitting is used to analyze the data because a liquid is being dispersed onto a surface with air surrounding it. The Young-Laplace equation (Equation 6) determines the contact angle (θ) using the images from the sessile droplet recording. The process analyzes each frame and fits the curve to the drop. The drop is symmetrical so the Young-Laplace equation can be used and is commonly used to analyze drops on solid surfaces.[83] The Young-Laplace equation is as follows:

Equation 6 $$\gamma_{SG} = \gamma_{SL} + \gamma_{LG}\,(cos\,\theta)$$

Where γ_{SG}: Interfacial tension between the solid and gas

γ_{SL}: Interfacial tension between the solid and liquid

γ_{LG}: Interfacial tension between the liquid and gas

The use of the Young-Laplace equation assumes there is a relationship between the radii of curvature, the surface tension, and the Laplace pressure.[83] It is best used when the droplet is symmetrical on a level, smooth surface. Using SAS software, the contact angle measurements were analyzed to get θ_{intial} (θ at drop placement), θ_{slope} (rate of change of θ over time), and θ_{final} (θ at 60 seconds) for each specimen.

Methods – Bioluminescence Testing

Adhesive Pellets

The groups of adhesive mixtures were as follows:

Table 7

Sample	Composition
1	Control group (unaltered adhesive resin)
2	20% Uncoated NanoGard™ in water
3	20% Uncoated NanoTek™ in ethanol
4	20% DDAO Coated NanoGard™ in ethanol
5	20% DDAO Coated NanoTek™ in ethanol
6	20% DDAO Coated NanoGard™ in water
7	20% DDAO Coated NanoTek™ in water
8	20% DDAO solution

Fabricated nanoparticles were added to the dental adhesive resin at 20% (wt/wt). Each nanoparticle mixture was weighed on an analytical balance at 1.39 ± 0.05 grams then added to 5.56 grams of adhesive. For group 8, 1.25 mL of DDAO was

added to 5 mL of adhesive. The tubes were wrapped in foil to prevent polymerization of the adhesive when exposed to light. The tube was sonicated using a microtip for 2 minutes total on amplitude 100 for three 40 second intervals with 15 second breaks in between intervals. The tube was submerged in an ice bath to prevent heating for the duration of sonication. Once sonication is complete, the adhesive is used to make the samples for measurement on the contact angle goniometer. The adhesive is wrapped in foil and stored in a dark, room temperature drawer and sonicated before each use.

After the nanoparticles were added to the adhesive, small disc-like pellets were made by using approximately 200µL of adhesive mixture per pellet. A metal mold with eight small circles (diameter of 6mm x height 1.1mm) was used to create the pellets (Figure 15). Each circular cut out was identical.

Figure 15 – Silver mold for adhesive pellets

A glass cover slip, 12mm diameter, was placed over each of the circular cut out on the bottom of the mold. One piece of double-sided tape was placed over all the holes with cover slips on them. A gloved hand was used to create the seal between the tape, mold, and glass cover slip. The mold was turned over and stuck to a glass block and was sealed again using a gloved hand. A flat tipped tool was used to press the

inside of the glass cover slip to the double-sided tape. The mold was filled with Optibond adhesive and another glass cover slip was dropped over the mold to create a smooth pellet surface. UV light was used to cure the adhesive for four cycles of 20 seconds on the top of each pellet. The mold was turned over and cured with UV light for two cycles of 20 seconds. Then the tape was pulled off along with the glass slips on the back side and the pellets were removed from the mold. If there was access adhesive on the pellet, the pellet was pushed back through the mold to ensure a circular pellet (Figure 16). Six replicates were made for each of the groups every time the specimens were tested (n=6 for every test). Bioluminescence testing was conducted once a week for three weeks (n total=18 per sample group).

Figure 16 – Optibond Pellets with uncoated Nanogard

Bacterial strain and in vitro growth of biofilms

Bioluminescent *S. mutans* strain JM10, a derivative of wild type UA159 was used. Details about the strain construction were reported by Merritt et al[84]. Working stocks of *S. mutans* were grown on TH agar plates (Todd-Hewitt, BD Difco, USA) supplemented with 0.3% yeast extract (EMD Millipore, USA), and 800 μg/mL of Spectinomycin (MP Biomedicals, USA). Colonies were cultivated under anaerobic conditions at 37°C for 48 hours.

Planktonic cultures of JM10 were grown in TH culture medium supplemented with 0.3% yeast extract (THY) and Spectinomycin. A single colony was inoculated in 4mL THY broth with 32μL of Spectinomycin (100mg/mL). The cultures were incubated at 37°C for 16 hours (static cultures, anaerobic conditions). Overnight planktonic cultures having an optical density of ≥0.900 were used in biofilm growth. A 1:50 dilution of the selected overnight culture was added to 0.65x THY media supplemented with 0.1% (w/v) sucrose. Aliquots (1mL) of the culture medium were added to the wells of a sterile-24 well microtiter plate containing the previously manufactured and sterilized specimens (procedure in Adhesive Pellets section). Previously, specimens were UV-sterilized (254 nm, 800,000 uJ/cm^2, model CL-1000 UVP Crosslinker, UVP, LLC, USA) and stored in sterile ultra-pure water at 37°C for 24 hours to extract unreacted monomers. The specimens were incubated at 37°C for 24 hours (static cultures, anaerobic conditions). Method development described in detail by Florez et al[12].

Bioluminescence Assay

After incubation, the biofilms were removed and washed twice with PBS (pH 7.4, 15 sec/wash), before being transferred to a sterile 24-well plate. Fresh 1x THY supplemented with 1%(wt/vol) glucose culture medium (recharge medium) was added in the same volume as the original inoculum volume. The biofilms were incubated at 37°C for one hour before measuring the bioluminescence activity.

After the recharge period, D-Luciferin aqueous solution (100mM) suspended in 0.1 M citrate buffer (pH 6) was added in a 1:2 (v/v) ratio to the wells containing the biofilms and recharge medium. Luciferase activity was measured using a Synergy HT Multi-mode microplate reader equipped with Gen5 software (Biotek, USA) in 2-min increments (six minutes in total) after the addition of D-luciferin substrate[12]. Bioluminescence was evaluated at 590nm.

Methods – Verification of Antibacterial Properties

MBC (minimum bactericidal count) testing was conducted on nanoparticle mixtures corresponding to Table 8. Nanoparticles are dispersed in sodium hydroxide, sodium chloride, or hydrochloric acid. For uncoated NanoTek^{TM}, sample 2, 15 M sodium hydroxide is used. For samples 4 and 6, 1 M hydrochloric acid is used. For samples 1, 3 and 5, 1 M sodium chloride is used. The final concentration of the nanoparticles in solution should be 40 mg/mL.

Table 8

Sample	Composition
1	Uncoated NanoGard™ in water
2	Uncoated NanoTek™ in 70% Ethanol
3	DDAO Coated NanoGard™ in 70% Ethanol
4	DDAO Coated NanoTek™ in 70% Ethanol
5	DDAO Coated NanoGard™ in water
6	DDAO Coated NanoTek™ in water
7	DDAO solution

Once the nanoparticles were added to the respective solutions, they were sonicated in a water bath for approximately 1.5 hours with intermittent vortexing for 2 minutes every 30 minutes. Sonicating of the solution continued for additional 30 minute increments until nanoparticle agglomerates were broken apart and dispersed into the solution. Centrifuged solutions at 8000 rpm for 25 minutes then removed the supernatant (NaOH or HCl).

The nanoparticles were washed by adding 20 mL ethyl alcohol and mixing the solution. Nanoparticles were resuspended in the ethyl alcohol by sonicating in a water bath at room temperature for 30 minutes with intermittent mixing. Solutions were centrifuged at 8000 rpm for 25 minutes and supernatant removed. Steps were repeated until 3-5 wash steps were completed. Once at least three washes have been completed, before centrifuging a fourth time, split the nanoparticles based on mass between 2

tubes. One of the tubes was saved for testing of the nanoparticles suspended in ethyl alcohol. The other tube was centrifuged, and the ethanol replaced with 20 mL ultra-pure water.

The nanoparticle solution in water was added to 1x THY media to create an 80% concentration of the nanoparticle solution. A 1:2 dilution was conducted and repeated 12-fold. Once the serial dilutions were complete, a 1:50 dilution of an S. mutans overnight culture was added to each of the tubes. The tubes were inverted several times to ensure good mixing, then the bacteria culture was streaked on a 1x THY Spec-plate to check for the presence or absence of bacterial growth[85].

Results and Discussion – Contact Angle

It is important to evaluate the hydrophilic properties of the adhesive with nanoparticles and surfactant incorporated into it. The antibacterial properties of the nanoparticles on their own are important, but in addition to this, an adhesive with hydrophobic properties is more desirable. If the surface exhibits more hydrophobic properties, the likelihood of bacteria infiltrating through saliva decreases significantly; however, if the material is too hydrophobic, this will cause issues for the adhesion of the adhesive to the tooth surface. When the adhesive is too hydrophobic, it will not adhere to the tooth surface which could cause gaps and crevices between the tooth surface and adhesive resin. Pathogenic bacteria could infiltrate the gaps where the antibacterial adhesive is not bonded to the tooth and cause additional harm to the tooth surface leading to secondary caries. For this reason, the contact angle of the different

adhesive compositions is measured and evaluated to find the most well-rounded nano composition for antibacterial purposes.

The Nanogard^{TM} powder is known to have hydrophilic properties so it was expected that the water droplet would spread out more over the specimen containing Nanogard^{TM}. This would result in a smaller contact angle reading for the adhesive with Nanogard^{TM} materials incorporated in it. The opposite is expected for the NanoTek^{TM} samples which are expected to be hydrophobic due to the organosilane coating. NanoTek^{TM} was examined due to its organosilane coating. Silanation can help to create a strong bond between the nanoparticles and the adhesive. Because the DDAO surfactant has a long carbon chain, it is possible for it to form micelles that could affect the contact angle. It is possible that the surfactant could also coat the nanoparticles which would improve dispersion and bonding. The analysis of the wettability testing can be seen in Figure 17Figure 17 – Contact angle from computer software.

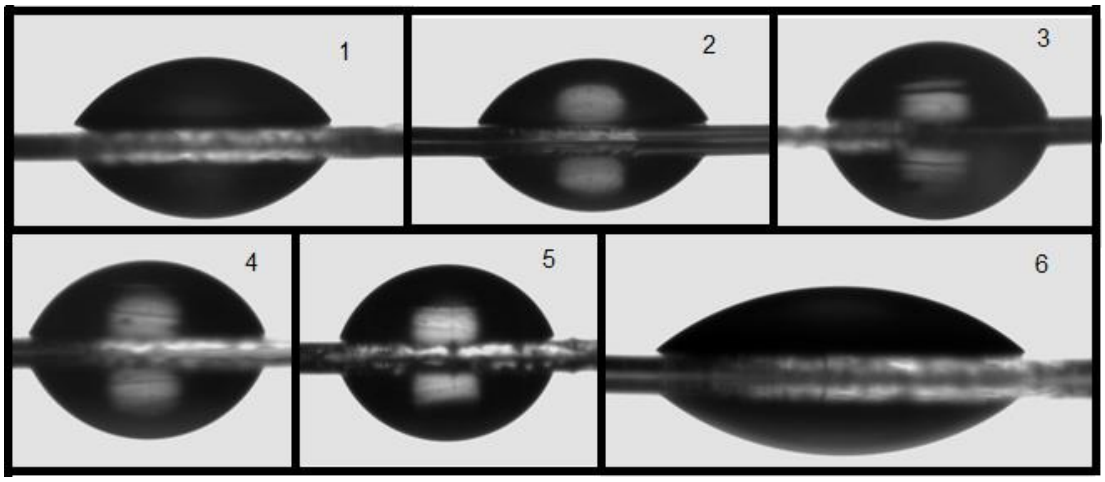

Figure 17 – Contact angle from computer software

Images of the water droplet after analysis. Numbers in upper right corner correspond to the sample numbers shown in Table 6 and Table 9.

The specimen containing Nanogard™ nanoparticles, samples 2 and 4, experienced a slightly less hydrophilic response when compared to the control (sample 1). As expected, the samples with specimen containing NanoTek™ nanoparticles, samples 3 and 5, have a the most hydrophobic response of all the specimen. Sample 6 shows a hydrophilic response as it spreads out more than the control did (Figure 18). A more quantitative analysis can be seen in Table 9. Using Equation 7 the following functional form is used to describe relation between water contact angle (y) and time (t).

$$\textbf{Equation 7} \quad y = \alpha + (\theta - \alpha)\exp(-t/\beta)$$

Where θ is the contact angle at frame number 0, α is the contact angle at time infinity, β is the exponential decay rate, t is the time (seconds), and y is the contact angle.

Table 9

Sample	Group	θ	α	β
1	Control	74.7 ± 0.22	53.1 ± 0.07	227.3 ± 4.2
2	Uncoated Nanogard™	73.6 ± 0.17	54.8 ± 0.15	471.3 ± 12.4
3	Uncoated NanoTek™	103.0 ± 0.18	63.9 ± 0.12	400.0 ± 4.6
4	Coated Nanogard™	74.2 ± 0.15	59.2 ± 0.30	719.2 ± 33.4
5	Coated NanoTek™	99.3 ± 0.16	66.9 ± 0.17	525.5 ± 8.3
6	Surfactant (DDAO)	167.7 ± 1.2	45.3 ± 0.04	8.3 ± 0.11

Estimated values for 3 shape parameters used in the exponential function using Equation 7.

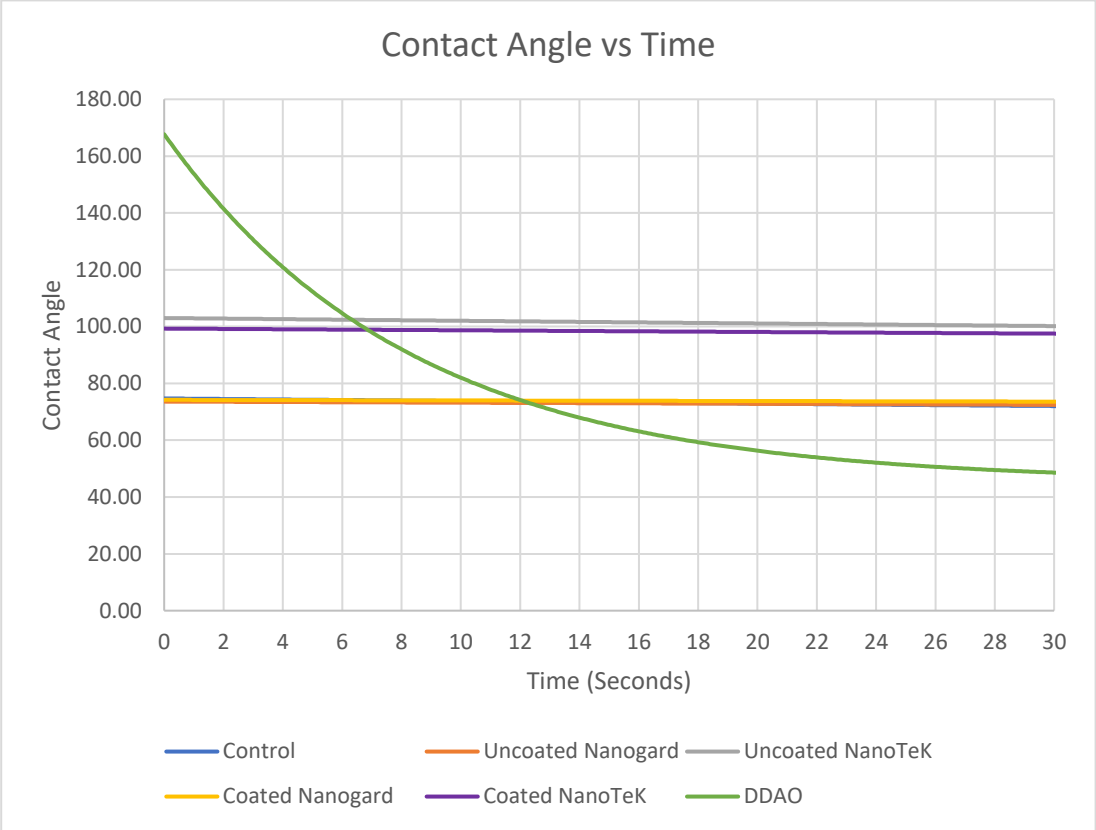

Figure 18 – Contact angle vs time

Figure 18 demonstrates how the contact angle of the water progresses over time.

The control, sample 1, has an initial water contact angle of about 75° then spreads out fairly quickly over the 1 minutes testing period. The two Nanogard™ specimen, samples 2 and 4, have an initial water contact angle of about 75° and stays fairly constant through the 1 minute testing period ending around 70°. The two specimen with NanoTek™, samples 3 and 5, have an initial water contact angle of about 100° and spreads out through the 1 minute testing period to around 75°. Sample 1-5 have a consistently have about a 70° water contact angle at the end of the 1 minute period. The speciman with only surfactant, sample 6, starts at over 100° but spreads out to 45° water contact angle making it the most hydrophilic specimen tested. The

contact angles are analyzed by the SCA software using the Laplace-Young fitting analysis (Equation 6).

An examination of the data in Table 9 suggest that the water contact angle is dominated by the properties of the adhesive. From the control values, it appears that water causes conformational changes with reorientation of functional groups to make the adhesive more hydrophilic. Hydrophilic Nanogard^{TM} does little to change this result (Sample 2) while the presence of surfactant strongly adsorbed on the nanoparticles as hemimicelles can explain a somewhat less equilibrium hydrophilicity (Sample 5). The hydrophobic NanoTek^{TM} particles (Samples 3 and 5) resulted in higher initial and static contact angles after equilibrium. The very high initial contact angle of Sample 6 indicates surface roughness was a factor while reordering of labile surfactant located the hydrophilic head group at the interface to lower the contact angle below that of the control.

Results and Discussion – Bioluminescence Assay

In order to quantify the antibacterial viability of the nanoparticles and surfactant incorporated into the adhesive, a bioluminescence assay is conducted based on the North American firefly luciferase[86]. *Streptococcus mutans* are the bacteria used to measure the antibacterial properties of the adhesives due to it being a prevalent bacterium found in the oral cavity where caries are present. The *S. mutans* are modified in a laboratory for use in this assay. The luciferase gene is placed under control of the *S. mutans* lactate dehydrogenase (ldh) promoter[84]. The ldh-luc reporter system can monitor the metabolic status and viability of *S. mutans* in biofilms. This allows any

drug that affects the ldh promoter activity to be quantitatively measured in a noninvasive, high throughput manner due to nearly all the ATP pool being converted into light[12].

The eight groups tested included 18 data points for each group. There was considerable variation in bacteria counts from week to week, but the average results across all specimen for each individual week was comparable (Figure 19).

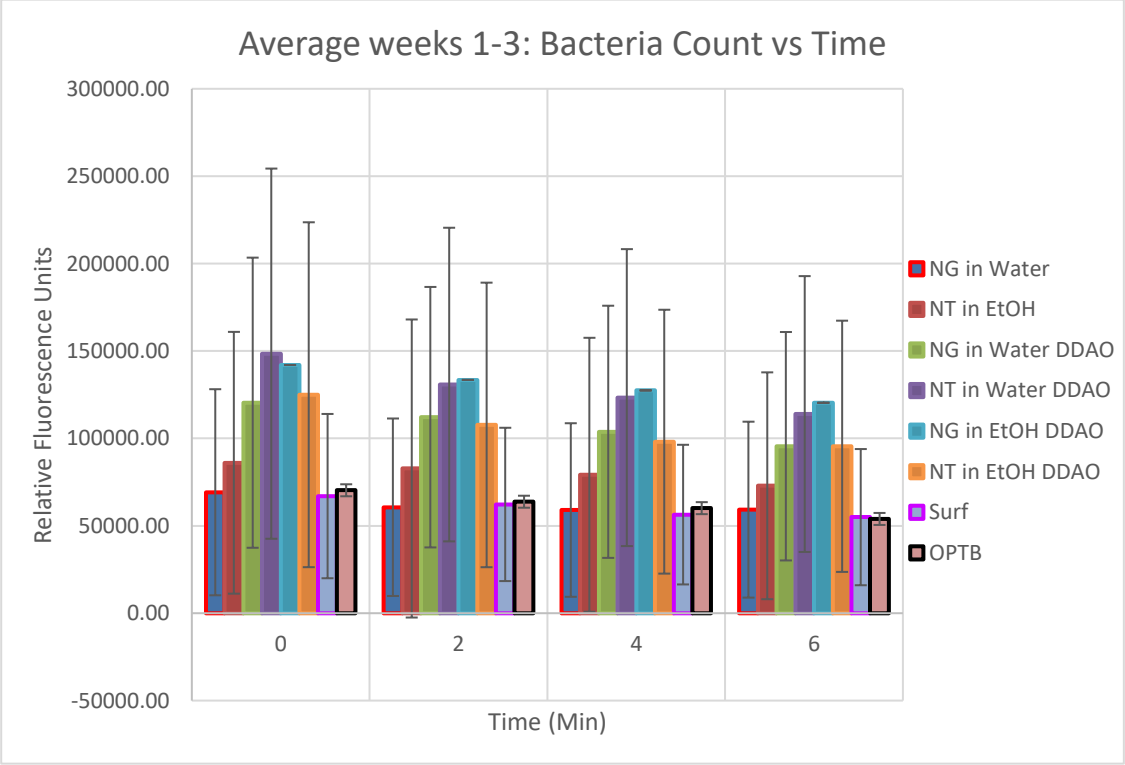

Figure 19 – Bacteria count vs. time

Average results on biofilms' bacteria count for 3 weeks across eight groups each having a sample size of n=18 versus time over six minutes of testing.

The Optibond adhesive alone showed one of the least variances and lowest error from week to week. It appears that the addition of nanoparticles to the adhesive may have caused inconsistencies in the surface composition. When nanoparticles were

incorporated to the adhesive, this may have caused an aeration in the adhesive resulting in nanosized areas for the bacteria to settle and grow in. It would need to be confirmed that the surface is completely smooth and void of air pockets that could encourage bacteria growth. The nanoparticles with surfactant coating showed the highest bacteria count.

The antibacterial effects of the nanoparticles incorporated into the dental adhesive was not apparent. There are several factors that could have contributed to the lack of antibacterial properties from the zinc oxide nanoparticles. It is likely that the polymer interfered with the antibacterial mechanism by causing the agglomeration of the nanoparticles in the adhesive. This did not allow for a consistent distribution of nanoparticles exposed to the surface for the *S. mutans* to encounter. For some of the articles citing zinc oxide as antibacterial in nature, it was found that low concentrations of the nanoparticles did not seem to have a significant effect on reducing the bacteria[13,16,87]. This could be a potential health hazard due to high concentration of metal oxides necessary in dental adhesives to exhibit antibacterial effects. This would not be a viable option when considering fabrication of an oral adhesive which would allow continued and extended exposure to the nanoparticles. Due to the adhesive polymerization, it is possible that the nanoparticles might be contained within the adhesive eliminating much of the risk associated with nanoparticles being continually present in the oral cavity. More research would need to be conducted on the toxicity of nanoparticles polymerized in dental adhesives. Changing the concentration of the nanoparticles would also change the ratio of adhesive to nanoparticles. This might

cause the adhesive to gain antibacterial properties at the expense of compromising the adhesive's mechanical properties. More research would need to be conducted on dispersion of the nanoparticles throughout the adhesive. Some studies found that decreasing particle size of nanoparticles resulted in greater bactericidal efficacy[13,16]. The nanoparticles used in this study may have needed to be smaller in particle size in order to exhibit quantifiable antibacterial properties. Some studies have shown the increase in antibacterial properties in metal ion doped nanoparticles[14,15,17]. The metal ion doped nanoparticles differ from these nanoparticles in the way they were synthesized. Metal ion doped nanoparticles are synthesized by utilizing metal ion exchange methods to enhance the interfacial charge transfer at the interface[88]. This method allows a trace of impurity element to be introduced to the chemical material to alter its properties.

It is possible the bacteria used in other studies (i.e. *S. sobrinus* and *E. coli*) were more susceptible to the nanoparticles' antibacterial properties while *S. mutans* may have been more resistant unless further action was taken, such as: metal ion doped nanoparticles or smaller nanoparticle sizes.

Results and Discussion – Verification of Antibacterial Properties

A minimum bactericidal count (MBC) was conducted to evaluate the antibacterial properties of the zinc oxide nanoparticles by groups corresponding to Table 10.

Table 10

Sample	Composition
1	Uncoated NanoGard™ in water
2	Uncoated NanoTek™ in 70% Ethanol
3	DDAO Coated NanoGard™ in 70% Ethanol
4	DDAO Coated NanoTek™ in 70% Ethanol
5	DDAO Coated NanoGard™ in water
6	DDAO Coated NanoTek™ in water
7	DDAO only

Each of the groups had 12 serial dilutions per plate pictured in Figure 20. Originally, the samples were only diluted in 15 M NaOH or 1 M HCl, but samples 1 and 5 completely dissolved in the solutions and it was determined these solutions were too harsh on the NanoGard™ and a new diluent would be needed. Sodium chloride was used for NanoGard™, and the nanoparticles did not completely dissolve, but were effectively deagglomerated for the MBC. The samples needed to disperse into the diluent to make white milky solutions.

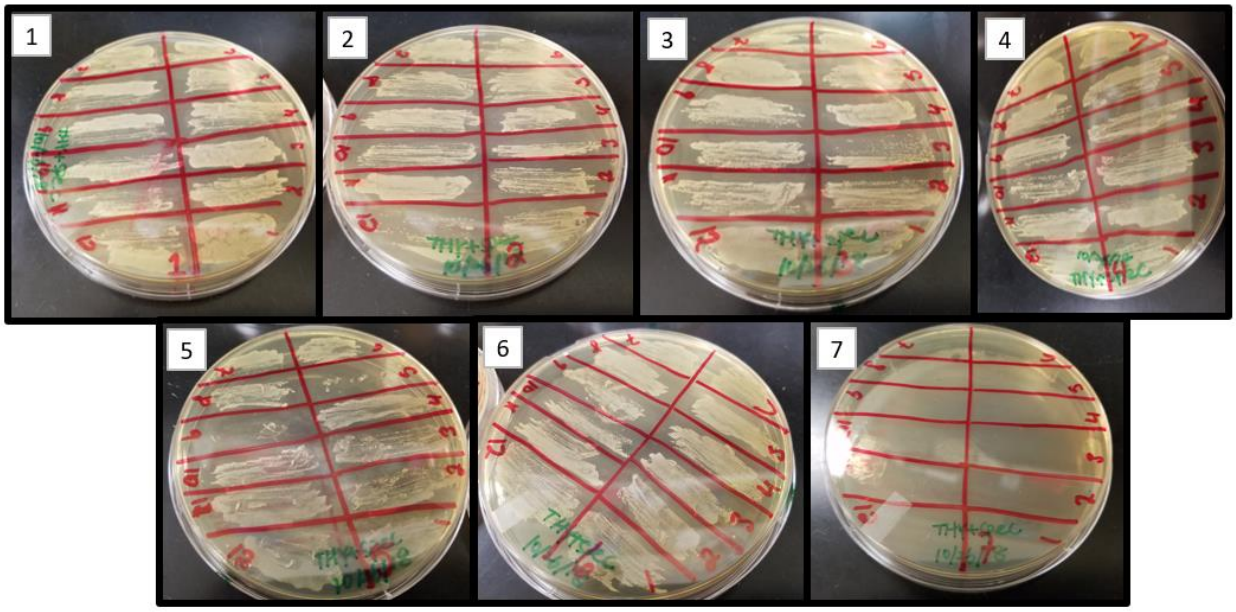

Figure 20 – MBC plates

Images of the MBC for all groups. Numbers in upper left corner correspond to the sample numbers shown in Table 10.

None of the plates with nanoparticles showed antibacterial properties for any of the solutions against the *S. mutans*, plates 1-6. The surfactant on its own, however, did show inhibition of bacterial growth at all dilutions on plate 7. Unfortunately, this shows that these zinc oxide nanoparticles do not possess a bacterial resistance to *S. mutans*. It is possible that with some modifications to the synthesis of the nanoparticles that they could show antibacterial properties.

Chapter 4 – Conclusion

In summary, the modified-DPM is a good technique for determining contact angles on lyophilic surfaces of nanoparticles when solvents are expected to display contact angle values varying between 20^{o} and 80^{o}. This method can be easily learned and uses inexpensive equipment that are typically found in surface chemistry laboratories; however, if accurate measurements using a variety of solvents are made necessary, a different technique may be necessary. This method is valuable due to the ability to measure the contact angle of nanoparticles with various solvents. This method can then be applied and used in the vOGC method to determine surface free energy of the nanoparticle granted the solvents meet criteria. The greatest impediment to use of the modified-DPM is identification of solvents that fit the criteria required for the adequate use of the modified-DPM. It is difficult to predict which solvents will fit the criteria before testing the solvent on the test surface. The most promising way to determine reference and test solvent compatibility is by using the parameter defined by Equation 5. If the value from Equation 5 is ≤ 1, it is very likely that the reference and test solvents are compatible and will give a quantitative contact angle measurement when using the DPM.

NanoTek™ and NanoGard™ do not appear to possess antibacterial properties against S. mutans. In contrast, some studies have found that zinc oxide does possess antimicrobial properties against *S. mutans* and other bacteria[1,13,18]. These properties may not have been expressed due to the addition of the nanoparticles to the adhesive. The adhesive with NanoGard™ did show the slight hydrophilic properties that were

expected while the adhesive with NanoTek™ showed less hydrophilic character. The addition of the DDAO to the NanoGard™ suggests that the hydrophilicity of the two compounds might be influenced by their interactions. Reduced hydrophilicity of adhesive samples with DDAO and NanoGard™ may have been the result of hemimicelle formation on the nanoparticles.

Chapter 5 – Future Work Suggestions

In the future, the wettability of the nanoparticles could be tested on a wider range of solvents. Finding more solvents that meet the criteria described in Chapter 2 is critical to gathering useful data using the DPM. Once more and reliable data is obtained, the surface free energy values of the zinc oxide should be evaluated again. This might show the ability to use this method to find surface free energies of nanoparticles in a cost and time effective manner. However, the limited range of the DPM between 20 and 80 degrees severely limits the solvents available for testing which may not provide reliable results for surface energy analysis.

It is possible antimicrobial properties would have been more readily observed on metal doped nanoparticles. I would recommend trying the antibacterial testing again on newly synthesized nanoparticles that have been metal doped. I would suggest confirming that nanoparticles are dispersed evenly when adding them to the dental resin. It is important to minimize agglomerates and prevent the gathering of nanoparticles on the inside of the adhesive resin.

References

1. Aydin Sevinç B, Hanley L. Antibacterial activity of dental composites containing zinc oxide nanoparticles. *J Biomed Mater Res Part B Appl Biomater*. 2010;94B(1):22-31. doi:10.1002/jbm.b.31620

2. Khushbu Y, Satyam P. Dental Caries: A Microbiological Approach. *J Clin Infect Dis Pract*. 2017;2:1-15.

3. Dye BA, Hsu KLC, Afful J. Prevalence and Measurement of Dental Caries in Young Children. *Pediatr Dent*. 2015;37(3):200-216.

4. Berdan AS, Luke H. Antibacterial activity of dental composites containing zinc oxide nanoparticles. *J Biomed Mater Res Part B Appl Biomater*. 2010;94B(1):22-31. doi:doi:10.1002/jbm.b.31620

5. Shen M, Liang G, Gu A, Yuan L. Development of high performance dental resin composites with outstanding antibacterial activity, high mechanical properties and low polymerization shrinkage based on a SiO2 hybridized tetrapod-like zinc oxide whisker with C-C bonds. *RSC Adv*. 2016;6(61):56353-56364. doi:10.1039/C6RA13498J

6. Featherstone JDB. The Continuum of Dental Caries—Evidence for a Dynamic Disease Process. *J Dent Res*. 2004;83(1_suppl):39-42. doi:10.1177/154405910408301s08

7. Marsh PD. Dental plaque as a biofilm and a microbial community - implications for health and disease. *BMC Oral Health*. 2006;6 Suppl 1(Suppl 1):S14-S14. doi:10.1186/1472-6831-6-S1-S14

8. Sheiham A, James WPT. Diet and Dental Caries: The Pivotal Role of Free Sugars Reemphasized. *J Dent Res*. 2015;94(10):1341-1347. doi:10.1177/0022034515590377

9. Steindorff MM, Lehl H, Winkel A, Stiesch M. Innovative approaches to regenerate teeth by tissue engineering. *Arch Oral Biol*. 2014;59(2):158-166. doi:10.1016/j.archoralbio.2013.11.005

10. van Manen EH, Zhang W, Walboomers XF, et al. The influence of electrospun fibre scaffold orientation and nano-hydroxyapatite content on the development of tooth bud stem cells in vitro. *Odontology*. 2014;102(1):14-21. doi:10.1007/s10266-012-0087-9

11. Devínsky F, Kopecka-Leitmanová A, Šeršeň F, Balgavý P. Cut-off Effect in Antimicrobial Activity and in Membrane Perturbation Efficiency of the Homologous Series of N,N-Dimethylalkylamine Oxides†. *J Pharm Pharmacol*. 1990;42(11):790-794. doi:10.1111/j.2042-7158.1990.tb07022.x

12. Esteban Florez FL, Hiers RD, Smart K, et al. Real-time assessment of Streptococcus mutans biofilm metabolism on resin composite. *Dent Mater*. 2016;32(10):1263-1269. doi:10.1016/j.dental.2016.07.010

13. Hernández-Sierra JF, Ruiz F, Cruz Pena DC, et al. The antimicrobial sensitivity of Streptococcus mutans to nanoparticles of silver, zinc oxide, and gold. *Nanomedicine Nanotechnology, Biol Med*. 2008;4(3):237-240. doi:https://doi.org/10.1016/j.nano.2008.04.005

14. Gupta K, Singh RP, Pandey A, Pandey A. Photocatalytic antibacterial performance of TiO2 and Ag-doped TiO2 against S. aureus. P. aeruginosa and E. coli. *Beilstein J Nanotechnol*. 2013;4:345-351.

15. Esteban Florez FL, Hiers RD, Larson P, et al. Antibacterial dental adhesive resins containing nitrogen-doped titanium dioxide nanoparticles. *Mater Sci Eng C*. 2018;93:931-943. doi:https://doi.org/10.1016/j.msec.2018.08.060

16. Azam A, Ahmed AS, Oves M, Khan MS, Habib SS, Memic A. Antimicrobial activity of metal oxide nanoparticles against Gram-positive and Gram-negative bacteria: a comparative study. *Int J Nanomedicine*. 2012;7:6003-6009. doi:10.2147/IJN.S35347

17. Sun T, Hao H, Hao W, Yi S, Li X, Li J. Preparation and antibacterial properties of titanium-doped ZnO from different zinc salts. *Nanoscale Res Lett*. 2014;9(1):98. doi:10.1186/1556-276X-9-98

18. Kasraei S, Sami L, Hendi SS, Alikhani M, Rezaei-Soufi L, Khamverdi Z. Antibacterial properties of composite resins incorporating silver and zinc oxide nanoparticles on Streptococcus mutans and Lactobacillus. *Restor Dent Endod*. 2014;39:109-114. doi:10.5395/rde.2014.39.2.109

19. Lemire JA, Harrison JJ, Turner RJ. Antimicrobial activity of metals: mechanisms, molecular targets and applications. *Nat Rev Microbiol*. 2013;11(6):371-384. doi:10.1038/nrmicro3028

20. Imlay JA. Pathways of Oxidative Damage. *Annu Rev Microbiol*. 2003;57(1):395-418. doi:10.1146/annurev.micro.57.030502.090938

21. Applerot G, Perkas N, Amirian G, Girshevitz O, Gedanken A. Coating of glass with ZnO via ultrasonic irradiation and a study of its antibacterial properties. *Appl Surf Sci*. 2009;256(3, Supplement):S3-S8. doi:https://doi.org/10.1016/j.apsusc.2009.04.198

22. Jiao L, Lin F, Cao S, et al. Preparation, characterization, antimicrobial and cytotoxicity studies of copper/zinc- loaded montmorillonite. *J Anim Sci Biotechnol*. 2017;8(1):27. doi:10.1186/s40104-017-0156-6

23. Sharma V, Singh P, Pandey AK, Dhawan A. Induction of oxidative stress, DNA damage and apoptosis in mouse liver after sub-acute oral exposure to zinc oxide nanoparticles. *Mutat Res Toxicol Environ Mutagen*. 2012;745(1):84-91. doi:https://doi.org/10.1016/j.mrgentox.2011.12.009

24. Li C-H, Shen C-C, Cheng Y-W, et al. Organ biodistribution, clearance, and genotoxicity of orally administered zinc oxide nanoparticles in mice. *Nanotoxicology*. 2012;6(7):746-756. doi:10.3109/17435390.2011.620717

25. Bundy KJ, Butler MF, Hochman RF. An investigation of the bacteriostatic properties of pure metals. *J Biomed Mater Res*. 1980;14(5):653-663. doi:10.1002/jbm.820140511

26. He X, Hartlieb E, Rothmund L, et al. Intracellular uptake and toxicity of three different Titanium particles. *Dent Mater*. 2015;31(6):734-744. doi:https://doi.org/10.1016/j.dental.2015.03.017

27. Mohammadi S, Mohammadi P, Hosseinkhani S, Shipour R. Antifungal Activity of TiO2 nanoparticles and EDTA on Candida albicans Biofilms. *Infect Epidemiol Med*. 2013;1:33-38.

28. Dizaj SM, Lotfipour F, Barzegar-Jalali M, Zarrintan MH, Adibkia K. Antimicrobial activity of the metals and metal oxide nanoparticles. *Mater Sci Eng C*. 2014;44:278-284. doi:https://doi.org/10.1016/j.msec.2014.08.031

29. Yu JC, Ho W, Lin J, Yip H, Wong PK. Photocatalytic Activity, Antibacterial Effect, and Photoinduced Hydrophilicity of TiO2 Films Coated on a Stainless Steel Substrate. *Environ Sci Technol*. 2003;37(10):2296-2301. doi:10.1021/es0259483

30. Rincón A-G, Pulgarin C. Effect of pH, inorganic ions, organic matter and H2O2 on E. coli K12 photocatalytic inactivation by TiO2: Implications in solar water disinfection. *Appl Catal B Environ*. 2004;51(4):283-302. doi:https://doi.org/10.1016/j.apcatb.2004.03.007

31. Besinis A, De Peralta T, Handy RD. The antibacterial effects of silver, titanium dioxide and silica dioxide nanoparticles compared to the dental disinfectant chlorhexidine on Streptococcus mutans using a suite of bioassays. *Nanotoxicology*. 2014;8(1):1-16. doi:10.3109/17435390.2012.742935

32. Allahverdiyev AM, Abamor ES, Bagirova M, Rafailovich M. Antimicrobial effects of TiO2 and Ag2O nanoparticles against drug-resistant bacteria and leishmania parasites. *Future Microbiol*. 2011;6(8):933-940. doi:10.2217/fmb.11.78

33. Zaleska A. Doped-TiO2: A Review. *Recent Patents Eng*. 2008;2(3):157-164. doi:http://dx.doi.org/10.2174/187221208786306289

34. Ishikawa S, Matsumura Y, Katoh-Kubo K, Tsuchido T. Antibacterial activity of surfactants against Escherichia coli cells is influenced by carbon source and anaerobiosis. *J Appl Microbiol*. 2002;93(2):302-309. doi:10.1046/j.1365-2672.2002.01690.x

35. Rosen MJ. Characteristic Features of Surfactants. *Surfactants Interfacial Phenom*. July 2004:1-33. doi:doi:10.1002/0471670561.ch1

36. Subík J, Takácsová G, Pšenák M, Devínsky F. Antimicrobial Activity of Amine Oxides: Mode of Action and Structure-Activity Correlation. *Antimicrob Agents Chemother*. 1977;12:139-146. doi:10.1128/AAC.12.2.139

37. Jaine JE, Mucalo MR. Measurements of the wettability of catalyst support materials using the Washburn capillary rise technique. *Powder Technol*. 2015;276:123-128. doi:https://doi.org/10.1016/j.powtec.2015.02.026

38. Lefebvre G, Galet L, Chamayou A. Dry coating of talc particles with fumed silica: Influence of the silica concentration on the wettability and dispersibility of the composite particles. *Powder Technol*. 2011;208(2):372-377. doi:https://doi.org/10.1016/j.powtec.2010.08.031

39. Ji L, Shi B. A novel method for determining surface free energy of powders using Washburn's equation without calculating capillary factor and contact angle. *Powder Technol*. 2015;271:88-92. doi:https://doi.org/10.1016/j.powtec.2014.11.002

40. N. S. Da-Silva, F. Marciano, A. O Lobo, V. Trava-Airoldi, C. Pacheco-Soares, C. C Wachesk. Thermodynamic aspects of fibroblastic spreading on diamond-like carbon films containing titanium dioxide nanoparticles. *Theor Chem Acc*. 2011;130(4-6):1085-1093. doi:https://doi.org/10.1007/s00214-011-1018-5

41. Barnard AS, Zapol P, Curtiss LA. Modeling the morphology and phase stability of TiO2 nanocrystals in water. *J Chem Theory Comput*. 2005;1(1):107-116. doi:10.1021/ct0499635

42. Dzwigaj S, Arrouvel C, Breysse M, et al. DFT makes the morphologies of anatase-TiO2 nanoparticles visible to IR spectroscopy. *J Catal*. 2005;236(2):245-250. doi:https://doi.org/10.1016/j.jcat.2005.09.034

43. Buckton G, Newton JM. Assessment of the wettability of powders by use of compressed powder discs. *Powder Technol*. 1986;46(2):201-208. doi:https://doi.org/10.1016/0032-5910(86)80027-4

44. Honda RJ, Keene V, Daniels L, Walker SL. Removal of TiO2 nanoparticles during primary water treatment: role of coagulant type, dose, and nanoparticle concentration. *Environ Eng Sci*. 2014;31(3):127-134.

doi:10.1089/ees.2013.0269

45. Pérez-Díaz MA, Boegli L, James G, et al. Silver nanoparticles with antimicrobial activities against Streptococcus mutans and their cytotoxic effect. *Mater Sci Eng C*. 2015;55:360-366. doi:https://doi.org/10.1016/j.msec.2015.05.036

46. Tavassoli Hojati S, Alaghemand H, Hamze F, et al. Antibacterial, physical and mechanical properties of flowable resin composites containing zinc oxide nanoparticles. *Dent Mater*. 2013;29(5):495-505. doi:https://doi.org/10.1016/j.dental.2013.03.011

47. Good RJ, van Oss CJ. *Modern Approaches to Wettability: Theory and Applications*.; 1992.

48. Redzuan M, Tripathy M, Majeed A. Solubility enhancement of simvastatin and atorvastatin by arginine: Contact angle determination, wettability and surface energy characteristics. *J Mol Liq*. 2017;240. doi:10.1016/j.molliq.2017.05.068

49. van Oss CJ, Chaudhury MK, Good RJ. Monopolar surfaces. *Adv Colloid Interface Sci*. 1987;28:35-64. doi:https://doi.org/10.1016/0001-8686(87)80008-8

50. Alghunaim A, Kirdponpattara S, Newby BZ. Techniques for determining contact angle and wettability of powders. *Powder Technol*. 2016;287:201-215. doi:https://doi.org/10.1016/j.powtec.2015.10.002

51. Hwang JS, Lee J, Chang YH. Surface properties of silane-treated titania nanoparticles and their rheological behavior in silicone oil. *Macromol Res*. 2005;13:409-417. doi:10.1007/BF03218474

52. Durán JDG, Delgado A V, González-Caballero F, Chibowski E. Surface free energy components of monodisperse zinc sulfide. *Mater Chem Phys*. 1994;38(1):42-49. doi:https://doi.org/10.1016/0254-0584(94)90143-0

53. Van Oss CJ, Giese RF, Li Z, et al. Determination of contact angles and pore sizes of porous media by column and thin layer wicking. *J Adhes Sci Technol*. 1992;6(4):413-428. doi:10.1163/156856192X00755

54. C. Ramírez-Flores J, Bachmann J. Analyzing capillary-rise method settings for contact-angle determination of granular media. *J Plant Nutr Soil Sci*. 2013;176(1):16-19. doi:10.1002/jpln.201100431

55. Chawla A, Buckton G, Taylor KMG, Newton JM, Johnson MCR. Wilhelmy plate contact angle data on powder compacts: considerations of plate perimeter. *Eur J Pharm Sci*. 1994;2(3):253-258.

doi:https://doi.org/10.1016/0928-0987(94)90030-2

56. Liu Z, Wang Y, Muzzio FJ, Callegari G, Drazer G. Capillary drop penetration method to characterize the liquid wetting of powders. *Langmuir*. 2017;33(1):56-65. doi:10.1021/acs.langmuir.6b03589

57. Bautista EV, Barillas JLM, Dutra TV, da Mata W. Capillary, viscous and gravity forces in gas-assisted gravity drainage. *J Pet Sci Eng*. 2014;122:754-760. doi:https://doi.org/10.1016/j.petrol.2014.09.018

58. Mišljenović N, Mosbye J, Schüller RB, Lekang O-I, Salas-Bringas C. Physical quality and surface hydration properties of wood based pellets blended with waste vegetable oil. *Fuel Process Technol*. 2015;134:214-222. doi:https://doi.org/10.1016/j.fuproc.2015.01.037

59. Wang Y, Liu Z, Muzzio F, Drazer G, Callegari G. A drop penetration method to measure powder blend wettability. *Int J Pharm*. 2018;538(1):112-118. doi:https://doi.org/10.1016/j.ijpharm.2017.12.034

60. (ed.) CJ van O. *Interfacial Forces in Aqueous Media*. Vol 64. 2nd ed.; 2006. doi:doi:10.1002/jctb.280640321

61. Wildemuth CR, Williams MC. A new interpretation of viscosity and yield stress in dense slurries: Coal and other irregular particles. *Rheol Acta*. 1985;24(1):75-91. doi:10.1007/BF01329266

62. de Villiers MM, Lötter AP, van der Watt JG. Influence of surfactants and interactive mixing on the cohesiveproperties of a poorly wettable solid. *Powder Technol*. 1993;75(2):159-165. doi:https://doi.org/10.1016/0032-5910(93)80077-N

63. Patel KH, Rawal SK. Contact angle hysteresis, wettability and optical studies of sputtered zinc oxide nanostructured thin films. *Indian J Eng Mater Sci*. 2017;24(6):469-476.

64. Muster TH, Cole IS. The protective nature of passivation films on zinc: surface charge. *Corros Sci*. 2004;46(9):2319-2335. doi:https://doi.org/10.1016/j.corsci.2004.01.002

65. Trino LD, Dias LFG, Albano LGS, et al. Zinc oxide surface functionalization and related effects on corrosion resistance of titanium implants. *Ceram Int*. 2018;44(4):4000-4008. doi:10.1016/j.ceramint.2017.11.195

66. J. Lee YHCH. Surface modification and characterization of zinc oxide for use in organic photovaltaic devices. August 2011. doi:10.13140/RG.2.1.1355.4324

67. Stepien M, Saarinen JJ, Teisala H, et al. Surface chemical characterization of

nanoparticle coated paperboard. *Appl Surf Sci*. 2012;258(7):3119-3125. doi:10.1016/j.apsusc.2011.11.048

68. Kirchberg S, Abdin Y, Ziegmann G. Influence of particle shape and size on the wetting behavior of soft magnetic micropowders. *Powder Technol*. 2011;207(1):311-317. doi:https://doi.org/10.1016/j.powtec.2010.11.012

69. Garbacz H, Wieciński P, Kuczyńska D, Kubacka D, Kurzydłowski KJ. The effect of grain size on the surface properties of titanium grade 2 after different treatments. *Surf Coatings Technol*. 2018;335:13-24. doi:https://doi.org/10.1016/j.surfcoat.2017.12.005

70. Kirdponpattara S, Phisalaphong M, Zhang Newby B. Applicability of washburn capillary rise for determining contact angles of powders and porous materials. *J Colloid Interface Sci*. 2013;397. doi:10.1016/j.jcis.2013.01.033

71. Zhang H, Banfield JF. Nanoparticles in the environment. *Rev Mineral geochemistry*. 2001;44(1):1-58. doi:10.2138/rmg.2001.44.01

72. Bourikas K, Kordulis C, Lycourghiotis A. Titanium dioxide (anatase and rutile): surface chemistry, liquid–solid interface chemistry, and scientific synthesis of supported catalysts. *Chem Rev*. 2014;114(19):9754-9823. doi:10.1021/cr300230q

73. Pantaroto H, Filho AP, Bertolini M, et al. Antibacterial photocatalytic activity of different crystalline TiO2 phases in oral multispecies biofilm. *Dent Mater*. 2018;34(7):3182-3195. doi:10.1016/j.dental.2018.03.011

74. Ranade MR, Navrotsky A, Zhang HZ, et al. Energetics of nanocrystalline TiO2. *Proc Natl Acad Sci*. 2002;99(suppl 2):6476 LP - 6481. doi:10.1073/pnas.251534898

75. Grzmil B, Gleń M, Kic B, Lubkowski K. Study of the anatase to rutile transformation kinetics of the modified TiO2. *Polish J Chem Technol*. 2013;15(2):73-80. doi:https://doi.org/10.2478/pjct-2013-0026

76. Fraud S, Maillard J-Y, Kaminski MA, Hanlon GW. Activity of amine oxide against biofilms of Streptococcus mutans: a potential biocide for oral care formulations. *J Antimicrob Chemother*. 2005;56(4):672-677. doi:10.1093/jac/dki325

77. Aas JA, Paster BJ, Stokes LN, Olsen I, Dewhirst FE. Defining the normal bacterial flora of the oral cavity. *J Clin Microbiol*. 2005;43(11):5721-5732. doi:10.1128/JCM.43.11.5721-5732.2005

78. Forssten SD, Björklund M, Ouwehand AC. Streptococcus mutans, caries and simulation models. *Nutrients*. 2010;2(3):290-298. doi:10.3390/nu2030290

79. Silverstone LM, Johnson NW, Hardie JM, Williams RAD. The Microbiology of Dental Caries BT - Dental Caries: Aetiology, Pathology and Prevention. In: Silverstone LM, Johnson NW, Hardie JM, Williams RAD, eds. London: Macmillan Education UK; 1981:48-69. doi:10.1007/978-1-349-16547-6_3

80. Ajdic D, Mcshan M, Mclaughlin R, et al. Genome sequence of Streptococcus mutans UA159, a cariogenic dental pathogen. *Proc Natl Acad Sci U S A*. 2002;99:14434-14439. doi:10.1073/pnas.172501299

81. Lemos JA, Quivey RG, Koo H, Abranches J. Streptococcus mutans: a new Gram-positive paradigm? *Microbiology*. 2013;159(Pt 3):436-445. doi:10.1099/mic.0.066134-0

82. Loesche WJ. Role of Streptococcus mutans in human dental decay. *Microbiol Rev*. 1986;50(4):353-380.

83. Ip SW, Toguri JM. The equivalency of surface tension, surface energy and surface free energy. *J Mater Sci*. 1994;29(3):688-692. doi:10.1007/bf00445980

84. Merritt J, Kreth J, Qi F, Sullivan R, Shi W. Non-disruptive, real-time analyses of the metabolic status and viability of Streptococcus mutans cells in response to antimicrobial treatments. *J Microbiol Methods*. 2005;61(2):161-170. doi:https://doi.org/10.1016/j.mimet.2004.11.012

85. Merritt JH, Kadouri DE, O'Toole GA. Growing and analyzing static biofilms. *Curr Protoc Microbiol*. 2005;Chapter 1:Unit-1B.1. doi:10.1002/9780471729259.mc01b01s00

86. Fan F, Wood K V. Bioluminescent Assays for High-Throughput Screening. *Assay Drug Dev Technol*. 2007;5(1):127-136. doi:10.1089/adt.2006.053

87. Buzea C, Pacheco II, Robbie K. Nanomaterials and nanoparticles: Sources and toxicity. *Biointerphases*. 2007;2(4):MR17-MR71. doi:10.1116/1.2815690

88. Belver C, Bedia J, Gómez-Avilés A, Peñas-Garzón M, Rodriguez J. Semiconductor Photocatalysis For Water Purification. In: ; 2018:581. doi:10.1016/B978-0-12-813926-4.00001-X

Appendix

Appendix 1 – Contact angle experiments on nanoparticle pellets

Volume Penetrated (uL) vs Time (sec)

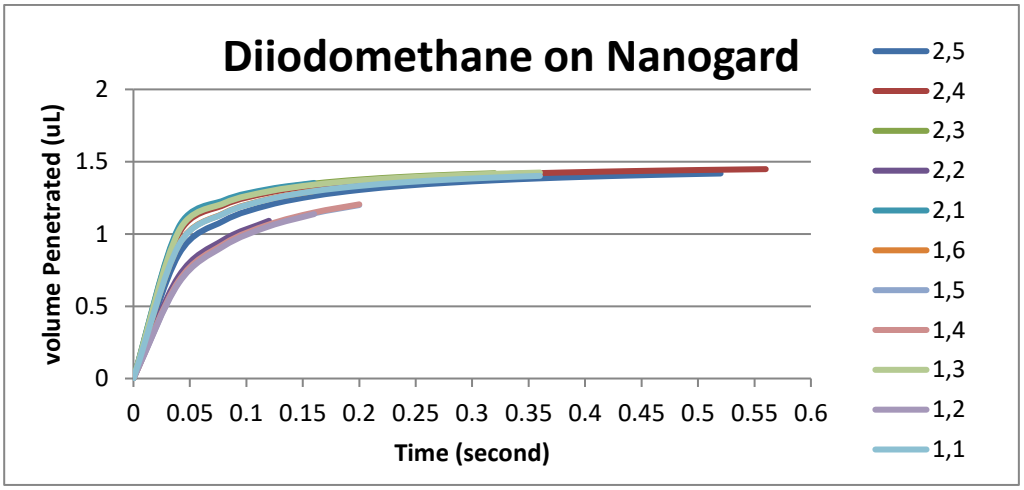

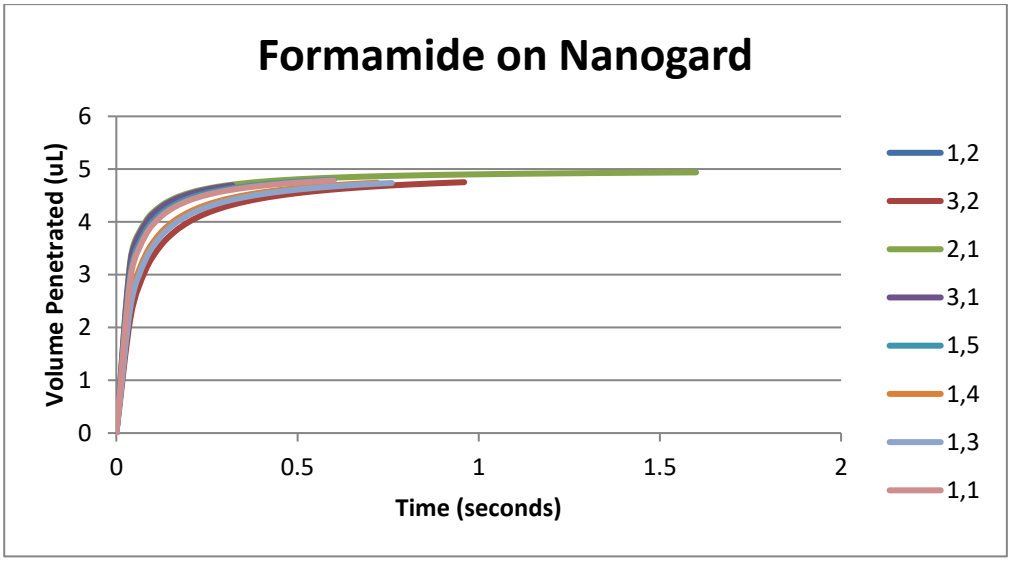

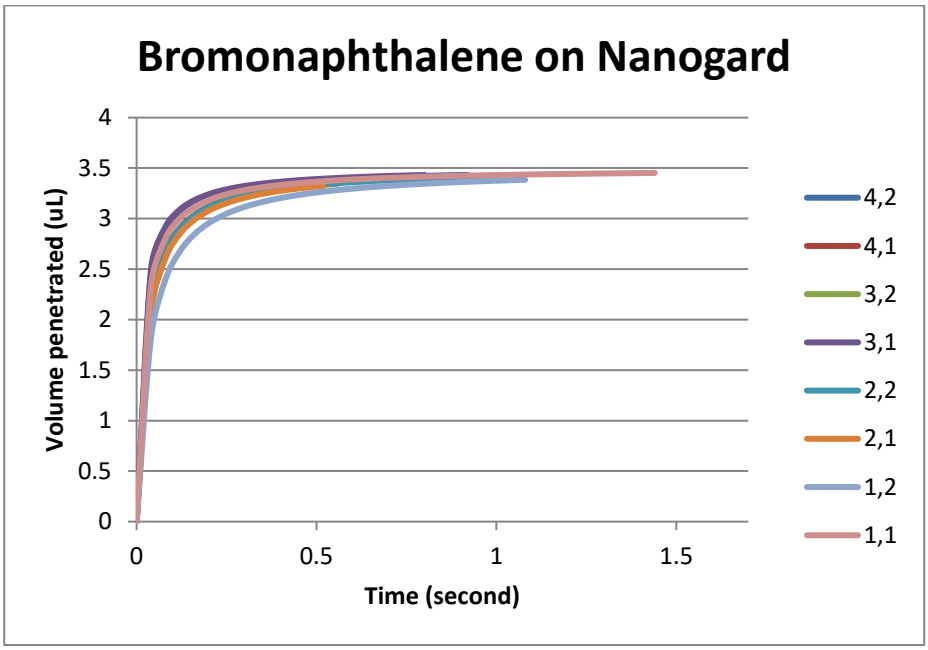
Bromonaphthalene on Nanogard
Volume penetrated (uL)
4
3.5
3
2.5
2
1.5
1
0.5
0
0
0.5
1
1.5
Time (second)
4,2
4,1
3,2
3,1
2,2
2,1
1,2
1,1

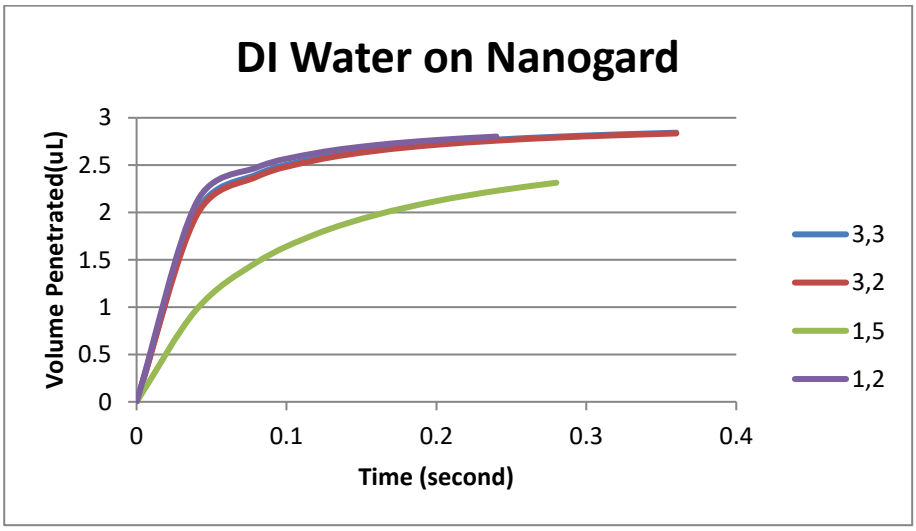
DI Water on Nanogard
Volume Penetrated(uL)
3
2.5
2
1.5
1
0.5
0
0
0.1
0.2
0.3
0.4
Time (second)
3,3
3,2
1,5
1,2

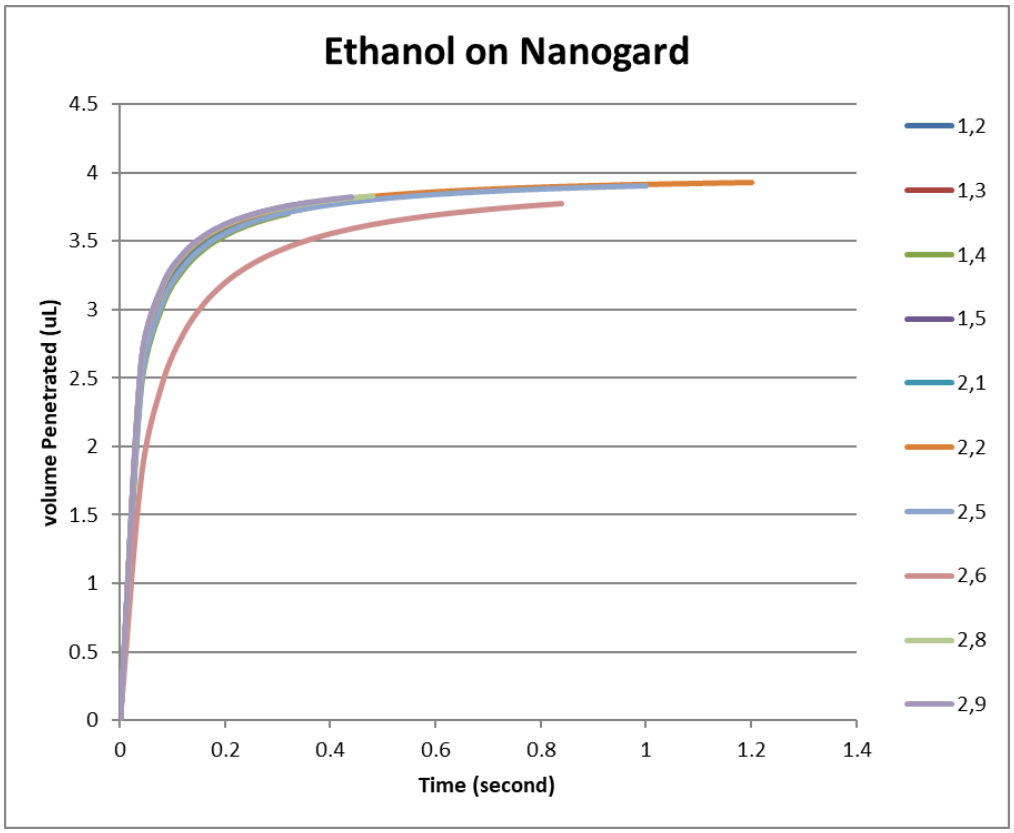
Ethanol on Nanogard
volume Penetrated (uL)
Time (second)
4.5
4
3.5
3
2.5
2
1.5
1
0.5
0
0
0.2
0.4
0.6
0.8
1
1.2
1.4
1,2
1,3
1,4
1,5
2,1
2,2
2,5
2,6
2,8
2,9

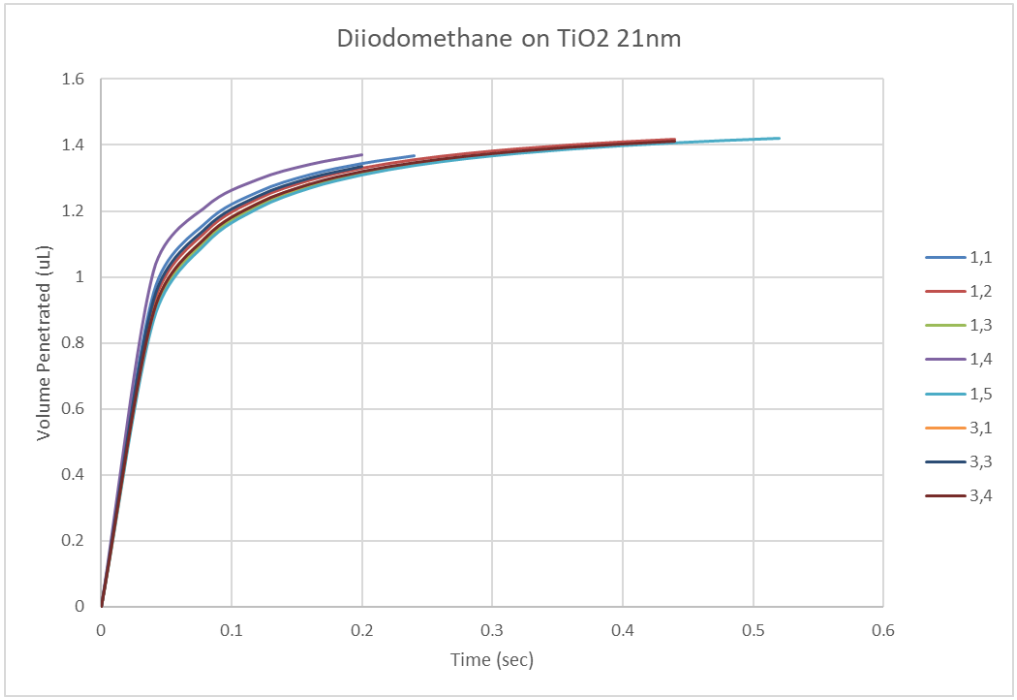
Diiodomethane on TiO2 21nm
Volume Penetrated (uL)
Time (sec)
1.6
1.4
1.2
1
0.8
0.6
0.4
0.2
0
0
0.1
0.2
0.3
0.4
0.5
0.6
1,1
1,2
1,3
1,4
1,5
3,1
3,3
3,4

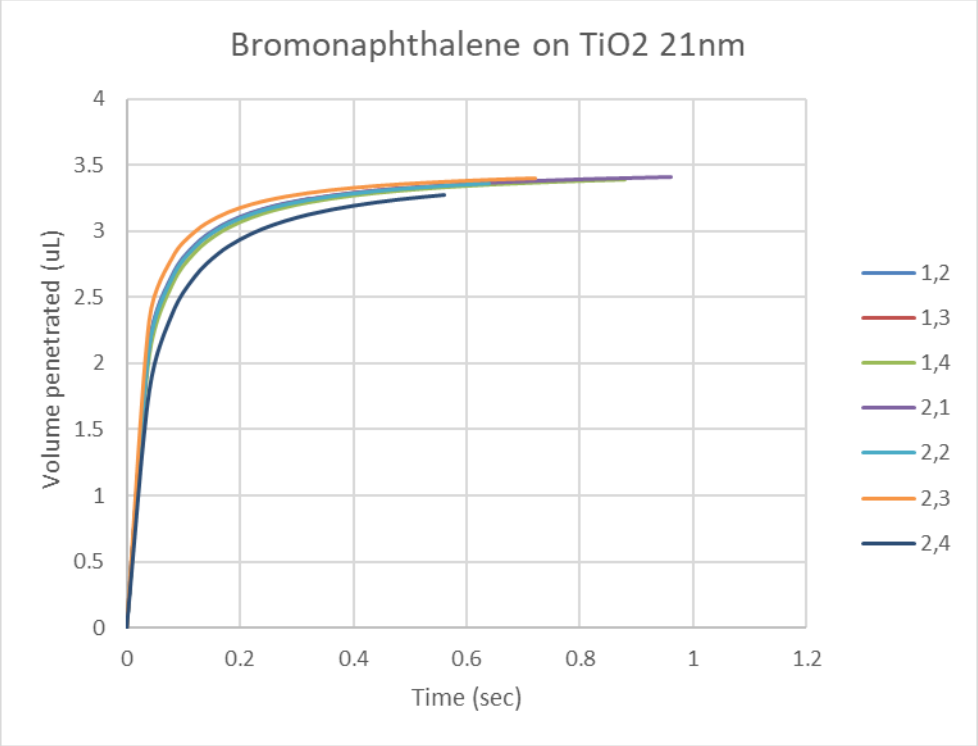
Bromonaphthalene on TiO2 21nm
Volume penetrated (uL)
Time (sec)
0
0.5
1
1.5
2
2.5
3
3.5
4
0
0.2
0.4
0.6
0.8
1
1.2
1,2
1,3
1,4
2,1
2,2
2,3
2,4

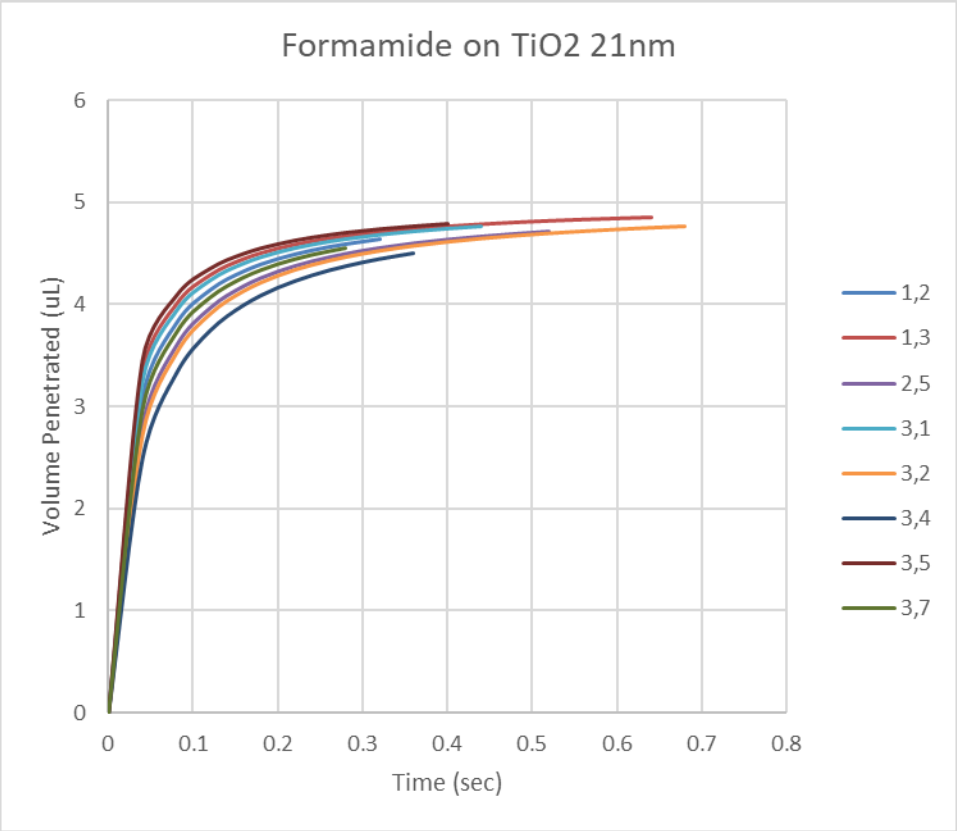
Formamide on TiO2 21nm
Volume Penetrated (uL)
Time (sec)
0
1
2
3
4
5
6
0
0.1
0.2
0.3
0.4
0.5
0.6
0.7
0.8
1,2
1,3
2,5
3,1
3,2
3,4
3,5
3,7

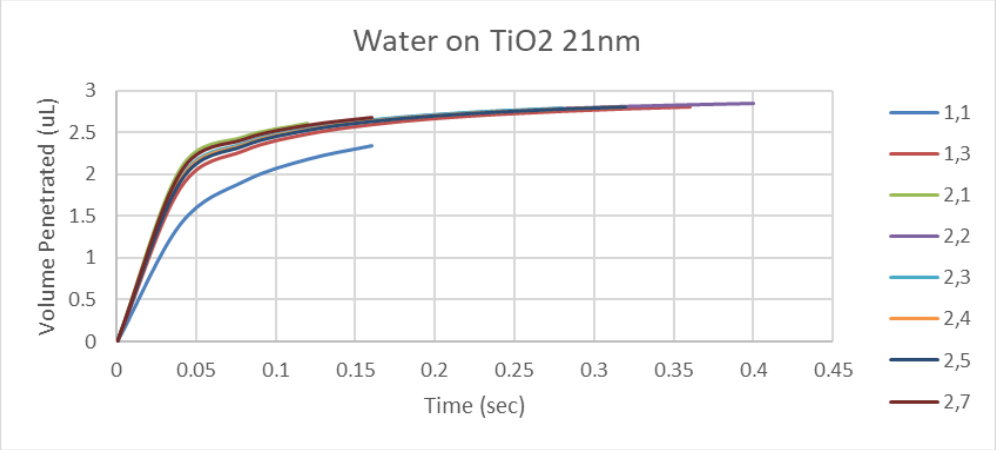
Water on TiO2 21nm
Volume Penetrated (uL)
Time (sec)
0
0.5
1
1.5
2
2.5
3
0.05
0.1
0.15
0.2
0.25
0.3
0.35
0.4
0.45
1,1
1,3
2,1
2,2
2,3
2,4
2,5
2,7

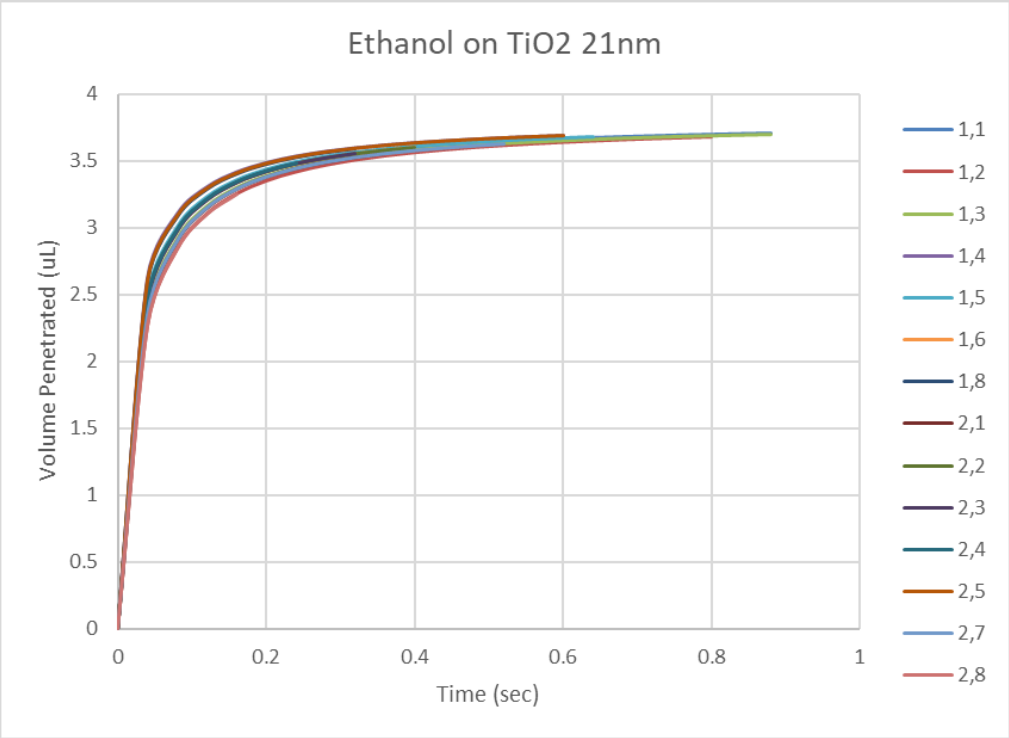
Ethanol on TiO2 21nm
Volume Penetrated (uL)
Time (sec)
0
0.5
1
1.5
2
2.5
3
3.5
4
0.2
0.4
0.6
0.8
1
1,1
1,2
1,3
1,4
1,5
1,6
1,8
2,1
2,2
2,3
2,4
2,5
2,7
2,8

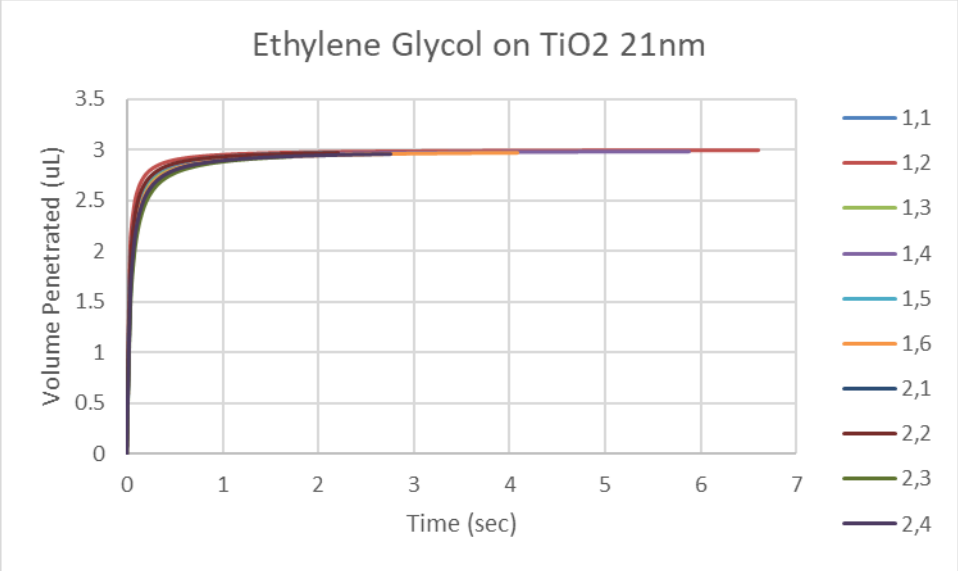
Ethylene Glycol on TiO2 21nm
Volume Penetrated (uL)
Time (sec)
1,1
1,2
1,3
1,4
1,5
1,6
2,1
2,2
2,3
2,4

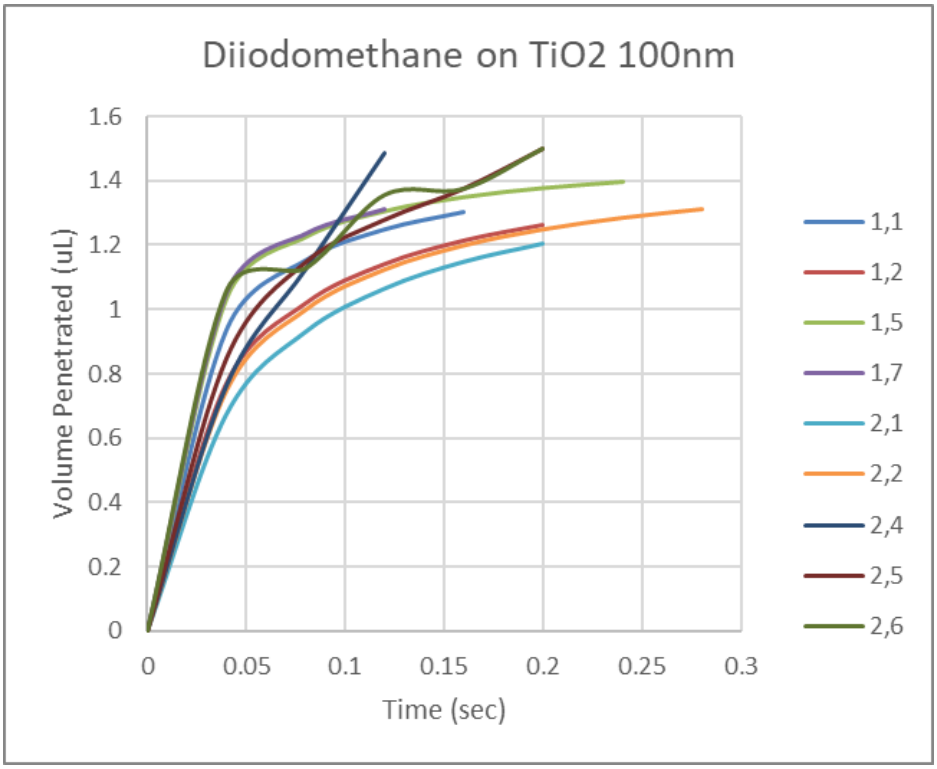
Diiodomethane on TiO2 100nm
Volume Penetrated (uL)
Time (sec)
1,1
1,2
1,5
1,7
2,1
2,2
2,4
2,5
2,6

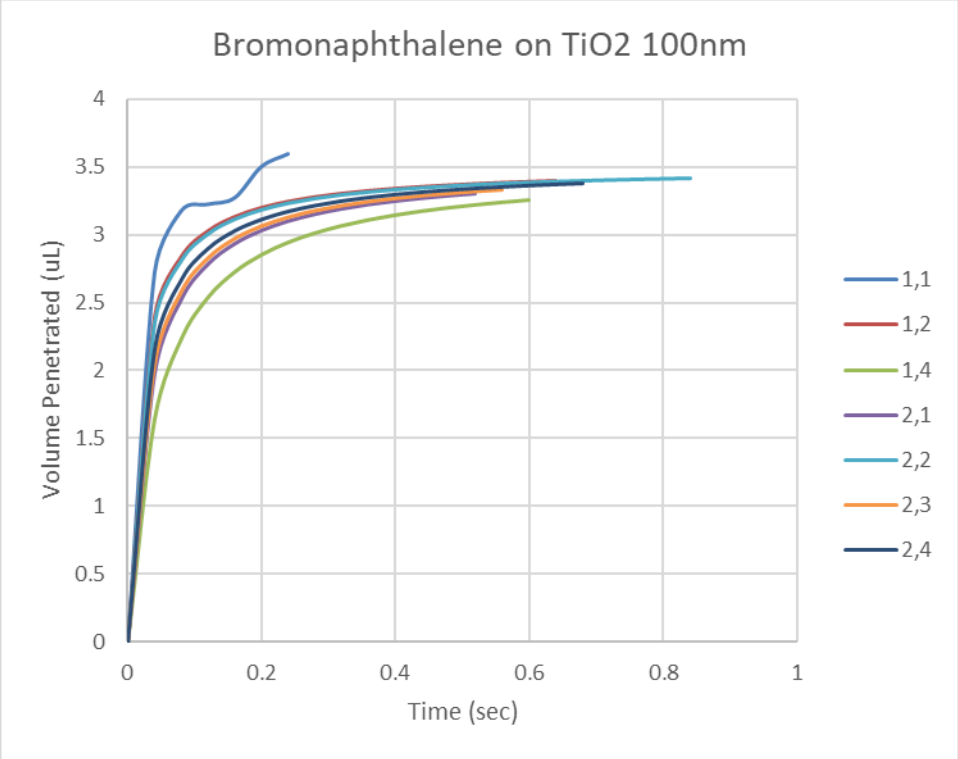
Bromonaphthalene on TiO2 100nm
Volume Penetrated (uL)
Time (sec)
0
0.5
1
1.5
2
2.5
3
3.5
4
0
0.2
0.4
0.6
0.8
1
1,1
1,2
1,4
2,1
2,2
2,3
2,4

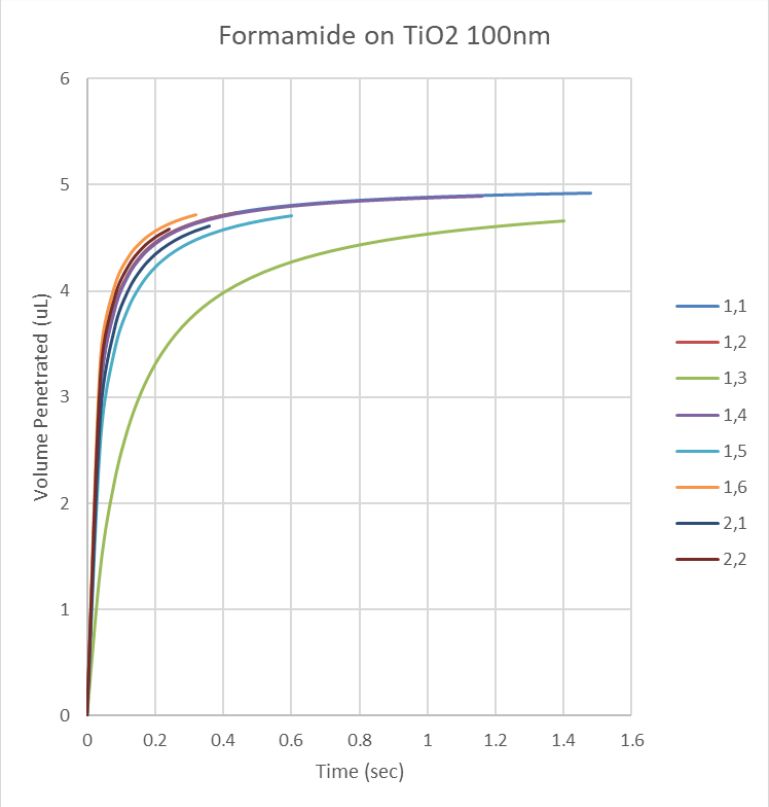
Formamide on TiO2 100nm
Volume Penetrated (uL)
Time (sec)
0
1
2
3
4
5
6
0
0.2
0.4
0.6
0.8
1
1.2
1.4
1.6
1,1
1,2
1,3
1,4
1,5
1,6
2,1
2,2

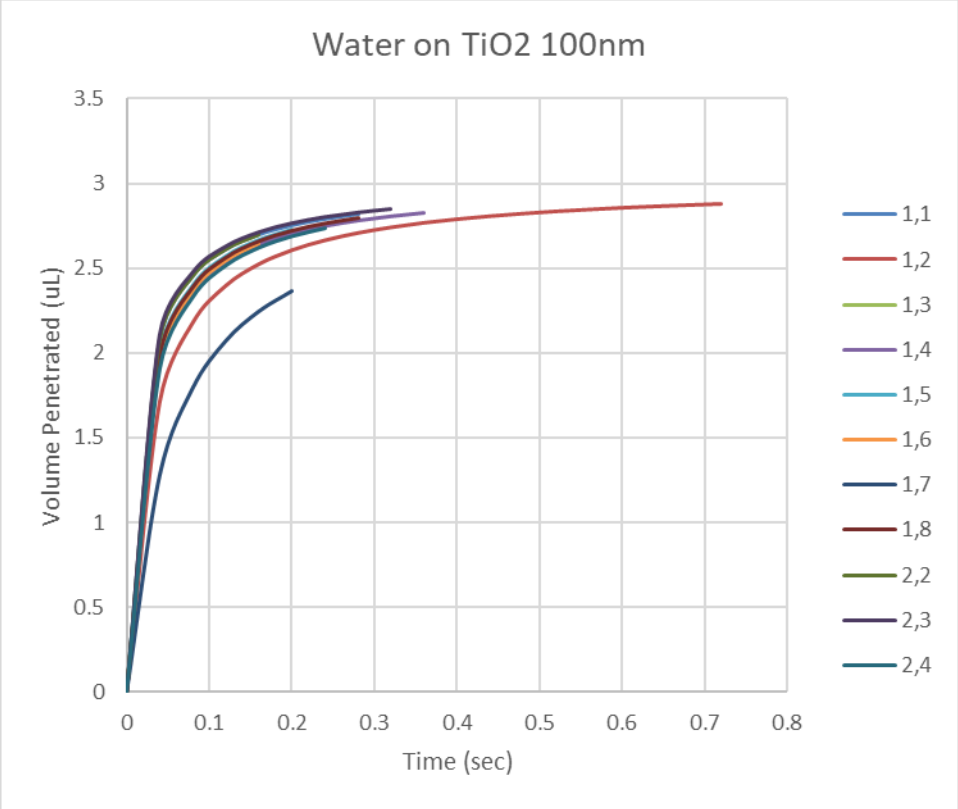
Water on TiO2 100nm
Volume Penetrated (uL)
Time (sec)
0
0.5
1
1.5
2
2.5
3
3.5
0
0.1
0.2
0.3
0.4
0.5
0.6
0.7
0.8
1,1
1,2
1,3
1,4
1,5
1,6
1,7
1,8
2,2
2,3
2,4

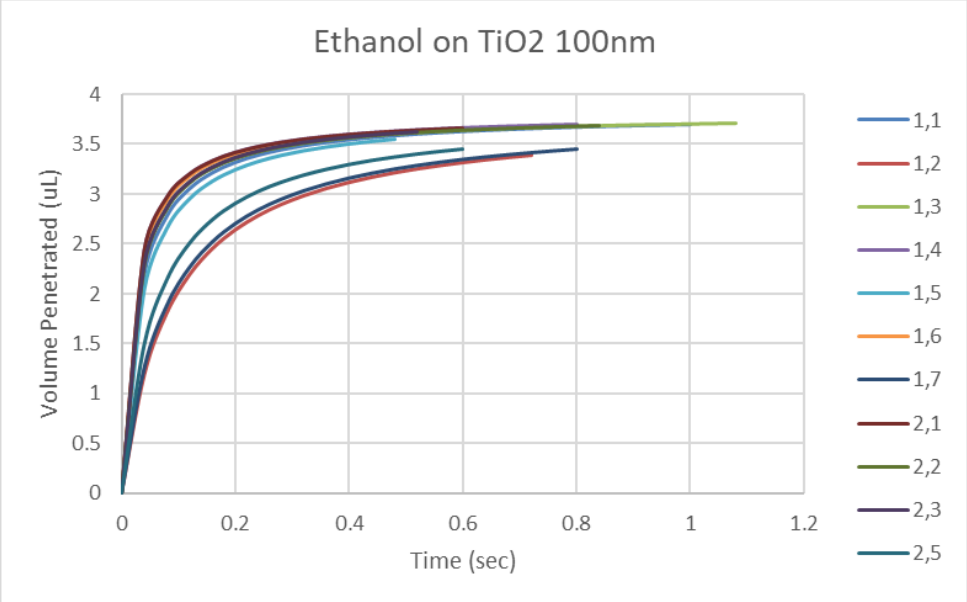
Ethanol on TiO2 100nm
Volume Penetrated (uL)
Time (sec)
0
0.5
1
1.5
2
2.5
3
3.5
4
0
0.2
0.4
0.6
0.8
1
1.2
1,1
1,2
1,3
1,4
1,5
1,6
1,7
2,1
2,2
2,3
2,5

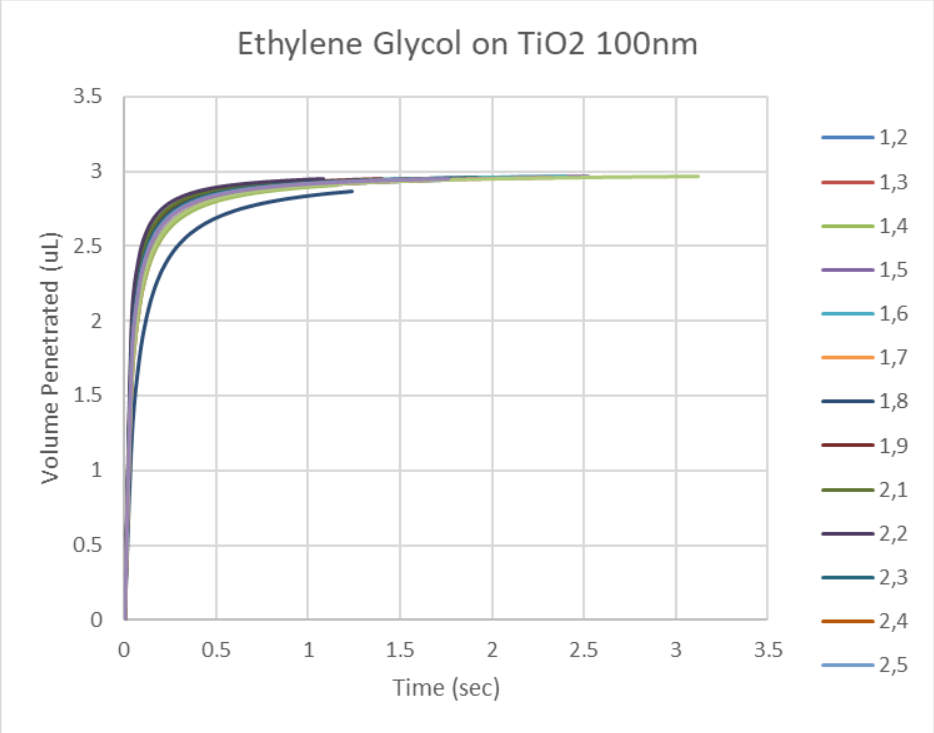

Appendix 2 – Contact angle experiments on adhesives

Original processed data through the SAS System

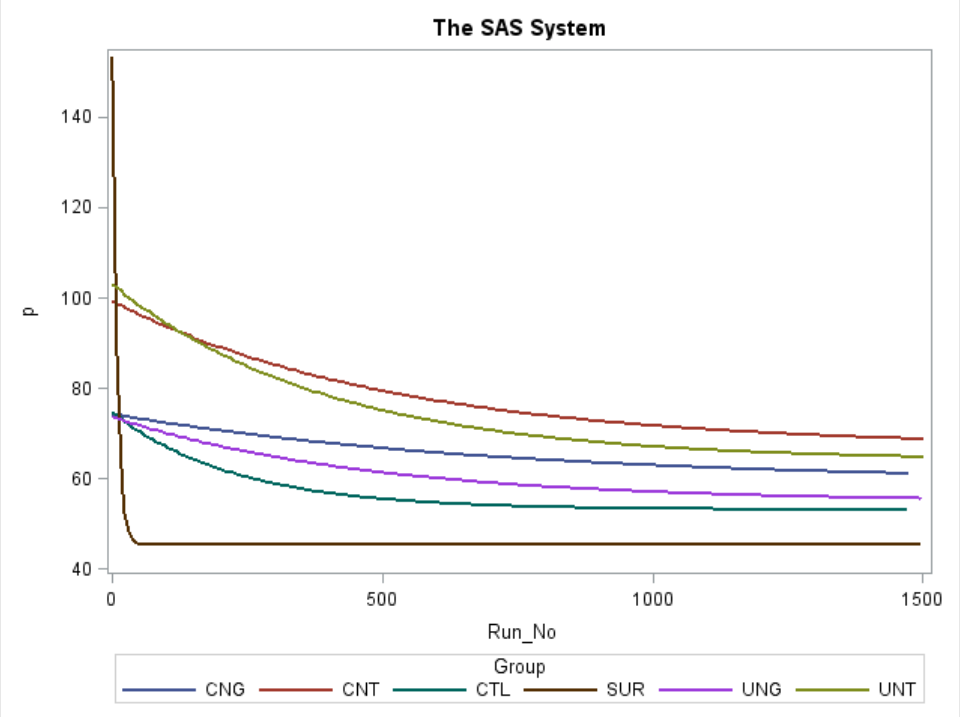

Appendix 3 – Bioluminescence Assay Experiments

Week 1:

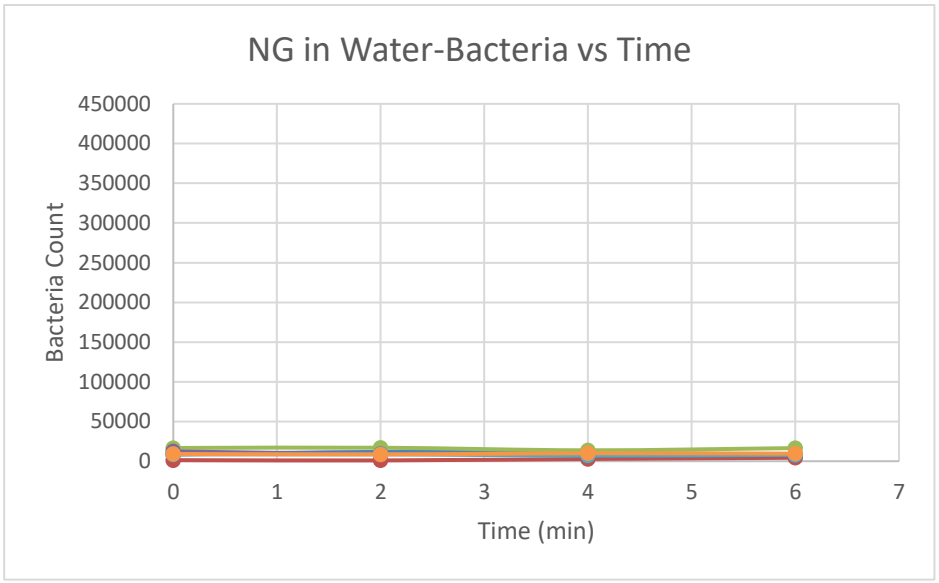

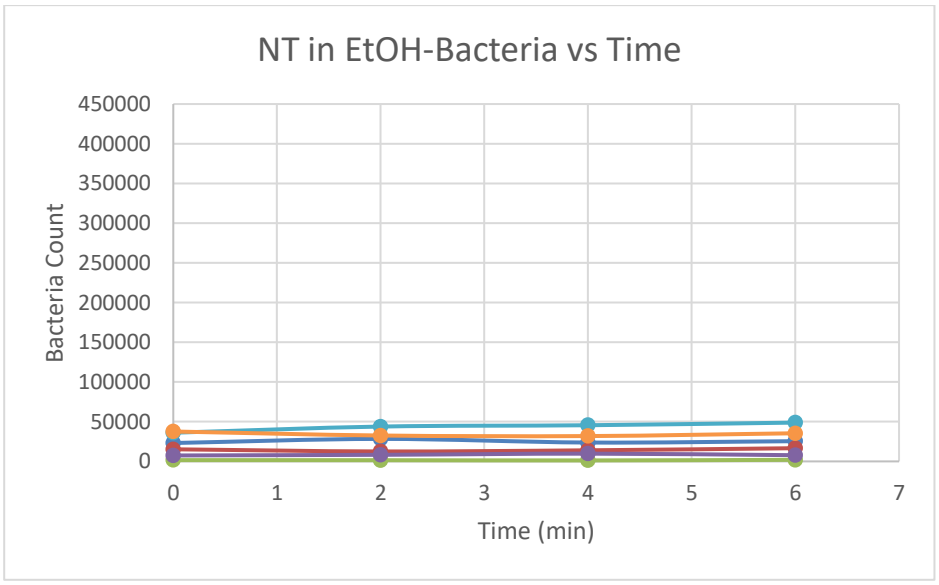

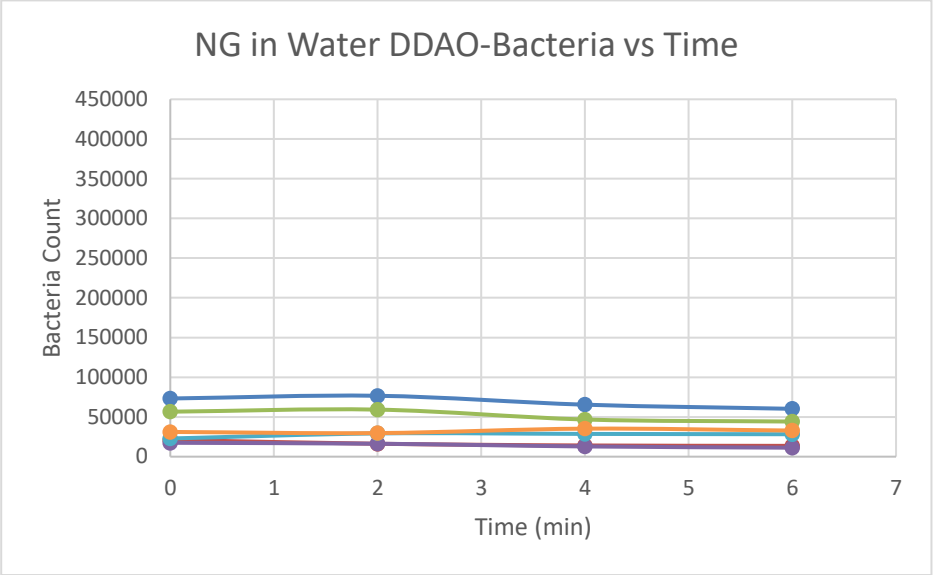
NG in Water DDAO-Bacteria vs Time
Bacteria Count
450000
400000
350000
300000
250000
200000
150000
100000
50000
0
0
1
2
3
4
5
6
7
Time (min)

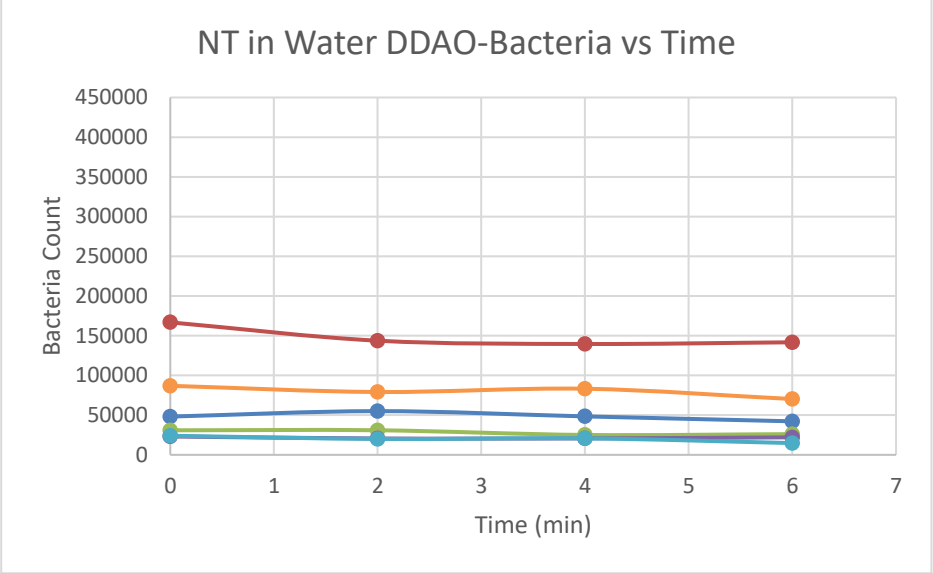
NT in Water DDAO-Bacteria vs Time
Bacteria Count
450000
400000
350000
300000
250000
200000
150000
100000
50000
0
0
1
2
3
4
5
6
7
Time (min)

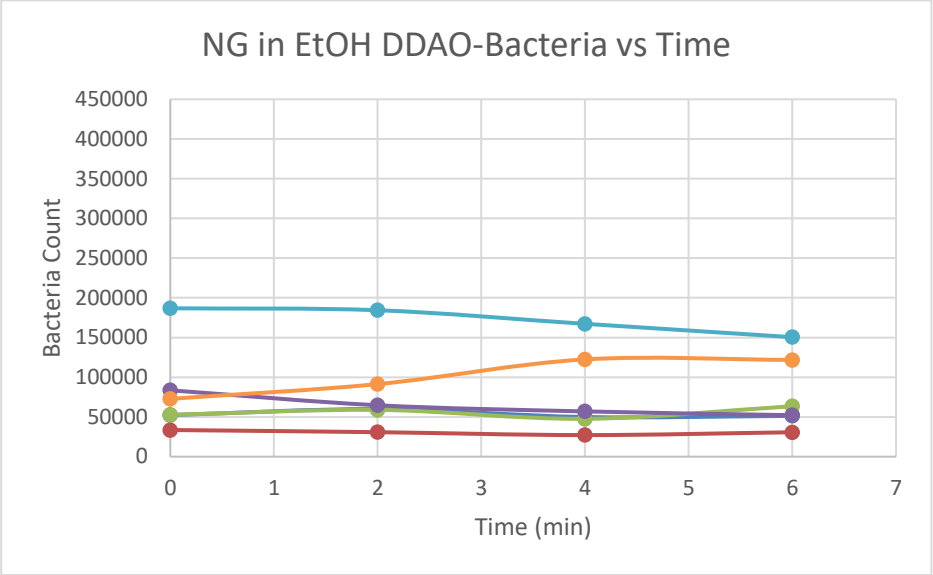
NG in EtOH DDAO-Bacteria vs Time
Bacteria Count
450000
400000
350000
300000
250000
200000
150000
100000
50000
0
0
1
2
3
4
5
6
7
Time (min)

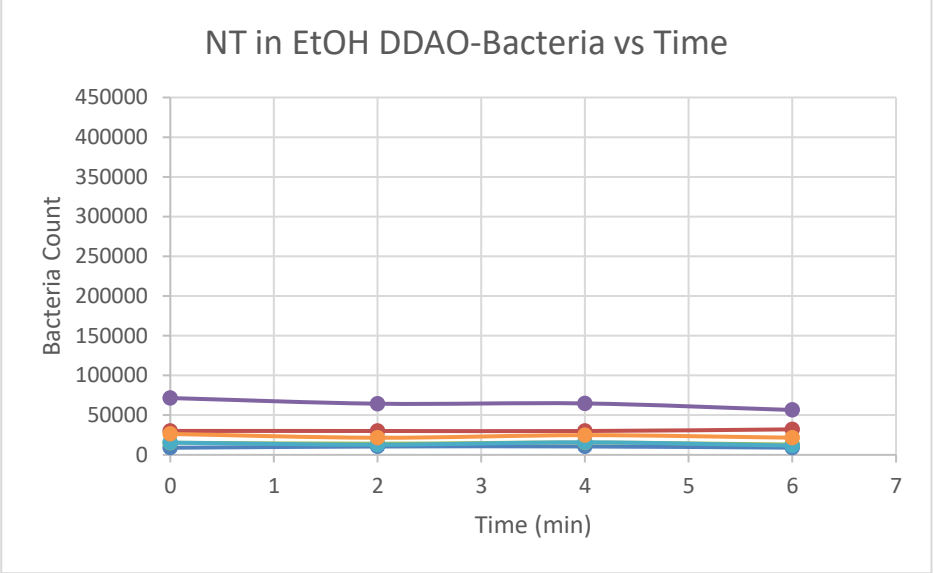
NT in EtOH DDAO-Bacteria vs Time
Bacteria Count
450000
400000
350000
300000
250000
200000
150000
100000
50000
0
0
1
2
3
4
5
6
7
Time (min)

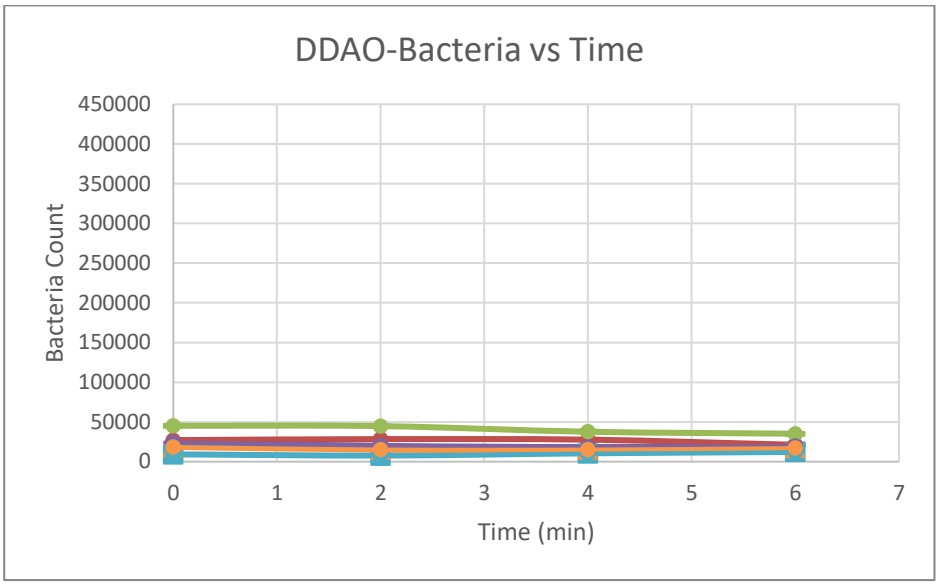
DDAO-Bacteria vs Time
Bacteria Count
450000
400000
350000
300000
250000
200000
150000
100000
50000
0
0
1
2
3
4
5
6
7
Time (min)

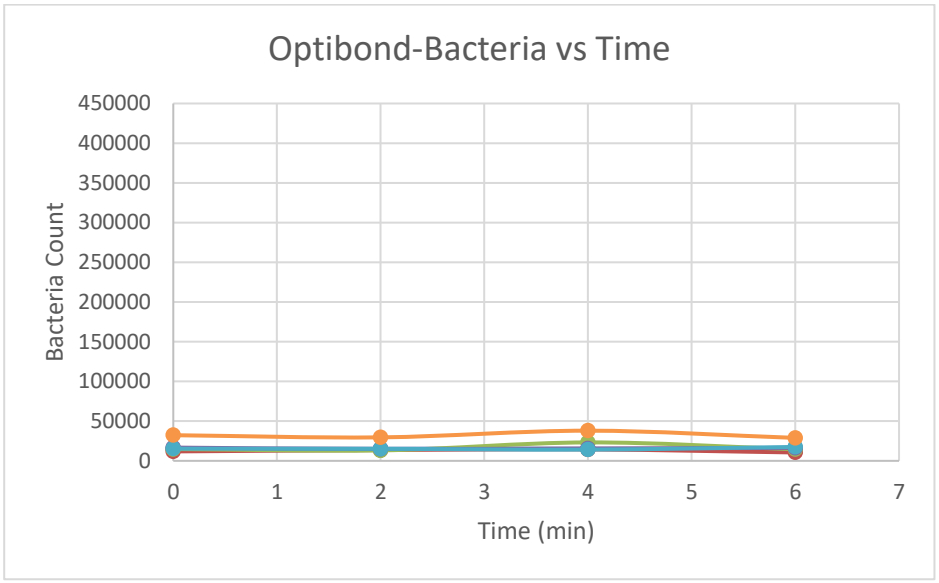
Optibond-Bacteria vs Time
Bacteria Count
450000
400000
350000
300000
250000
200000
150000
100000
50000
0
0
1
2
3
4
5
6
7
Time (min)

Week 2:

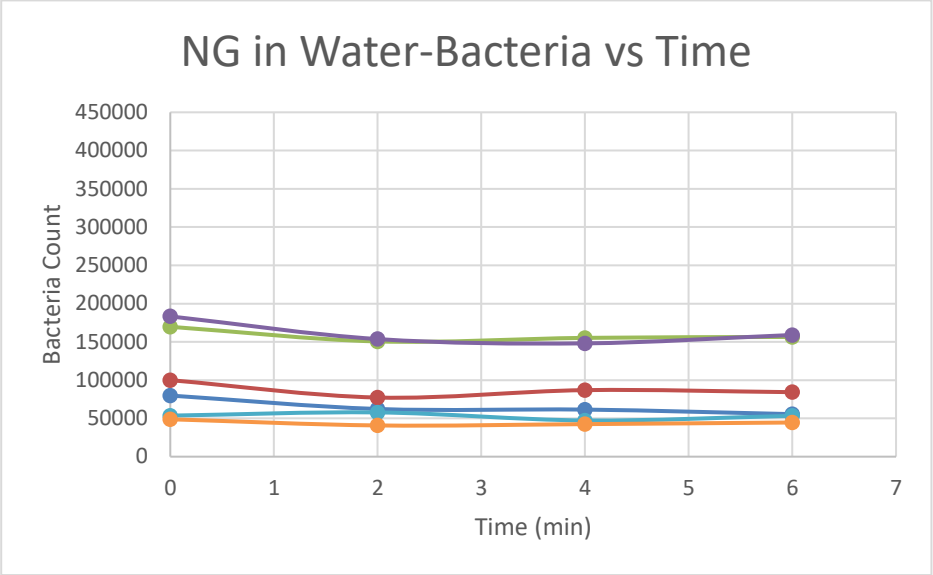
NG in Water-Bacteria vs Time
Bacteria Count
450000
400000
350000
300000
250000
200000
150000
100000
50000
0
0
1
2
3
4
5
6
7
Time (min)

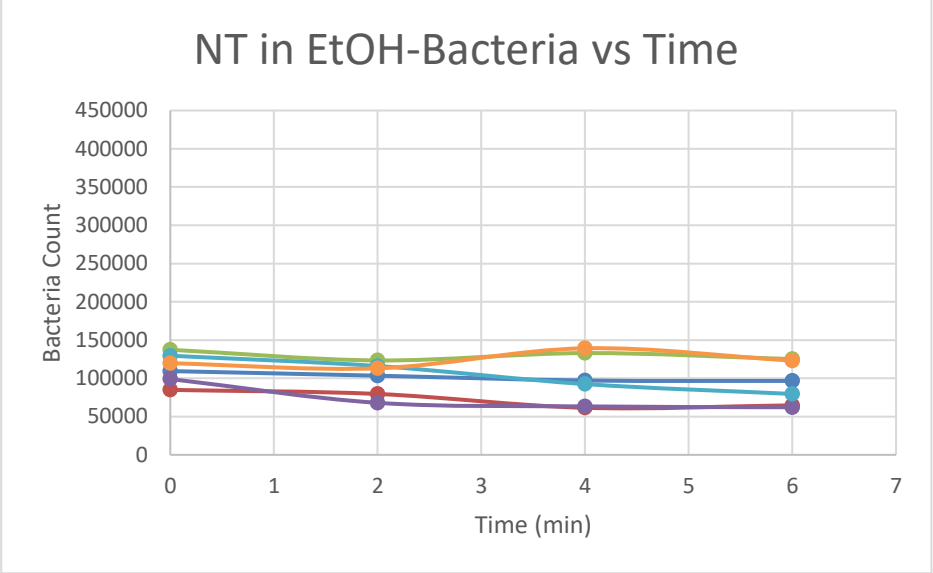
NT in EtOH-Bacteria vs Time
Bacteria Count
450000
400000
350000
300000
250000
200000
150000
100000
50000
0
0
1
2
3
4
5
6
7
Time (min)

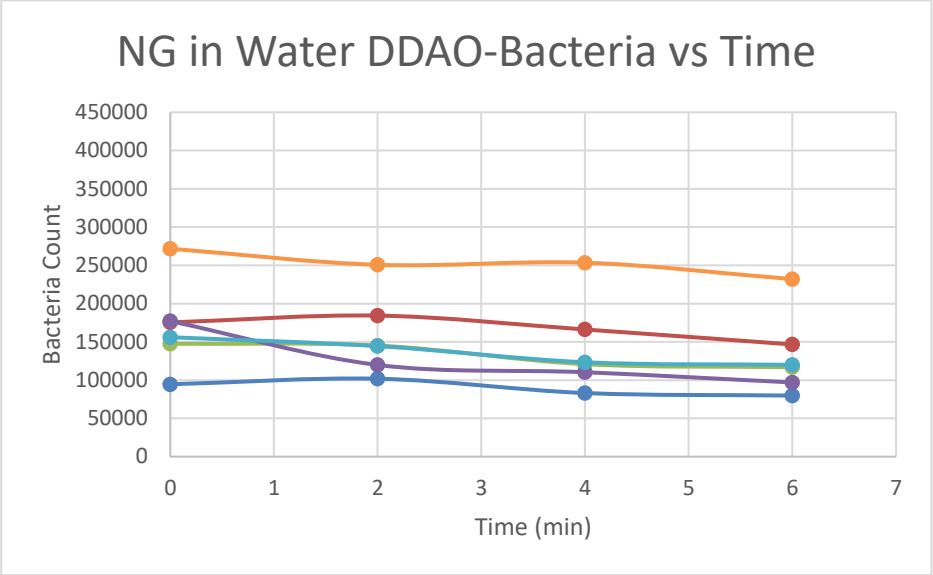
NG in Water DDAO-Bacteria vs Time
Bacteria Count
450000
400000
350000
300000
250000
200000
150000
100000
50000
0
0
1
2
3
4
5
6
7
Time (min)

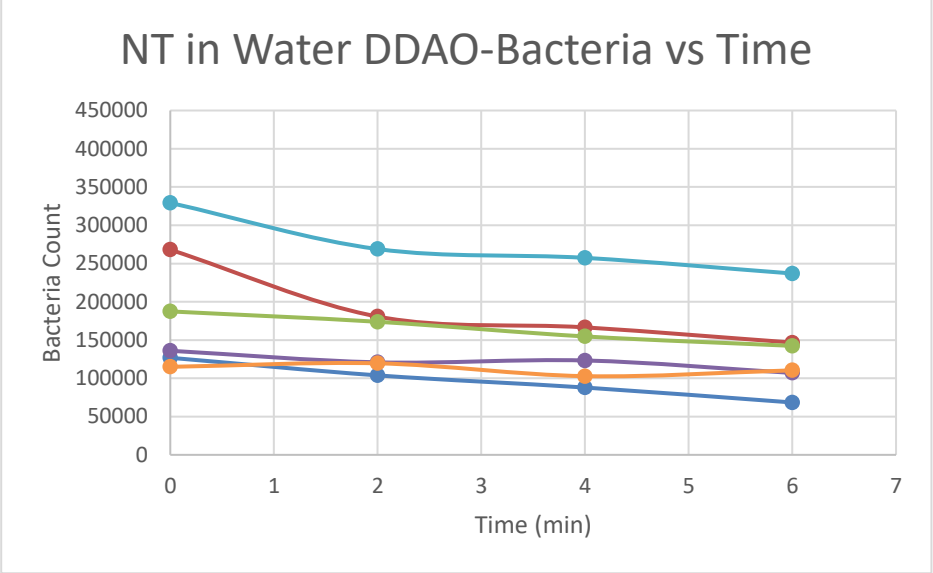
NT in Water DDAO-Bacteria vs Time
Bacteria Count
450000
400000
350000
300000
250000
200000
150000
100000
50000
0
0
1
2
3
4
5
6
7
Time (min)

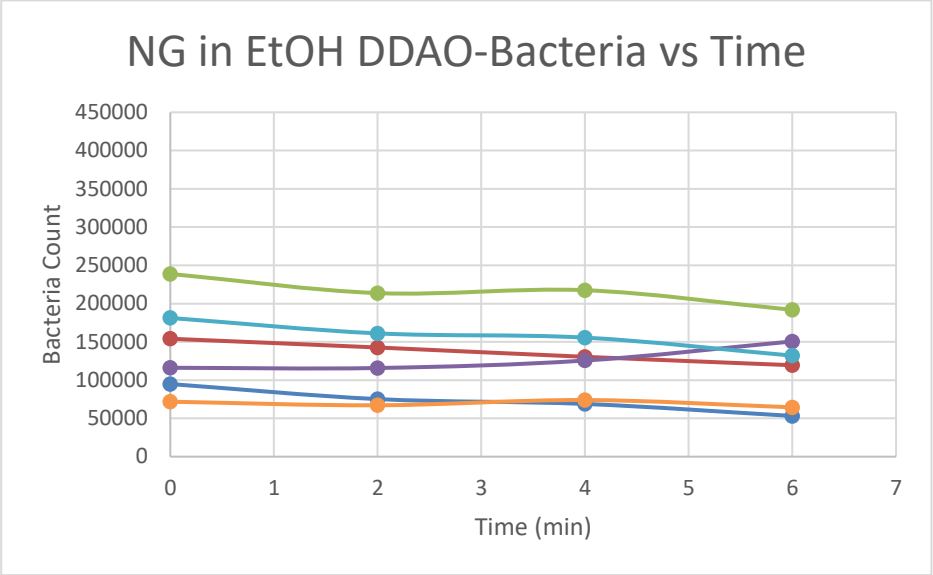
NG in EtOH DDAO-Bacteria vs Time
Bacteria Count
450000
400000
350000
300000
250000
200000
150000
100000
50000
0
0
1
2
3
4
5
6
7
Time (min)

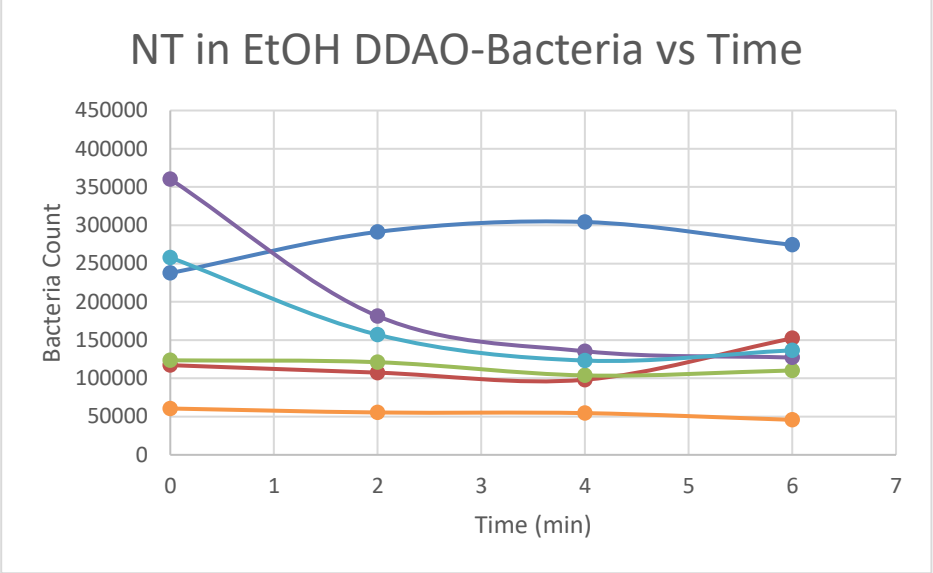
NT in EtOH DDAO-Bacteria vs Time
Bacteria Count
450000
400000
350000
300000
250000
200000
150000
100000
50000
0
0
1
2
3
4
5
6
7
Time (min)

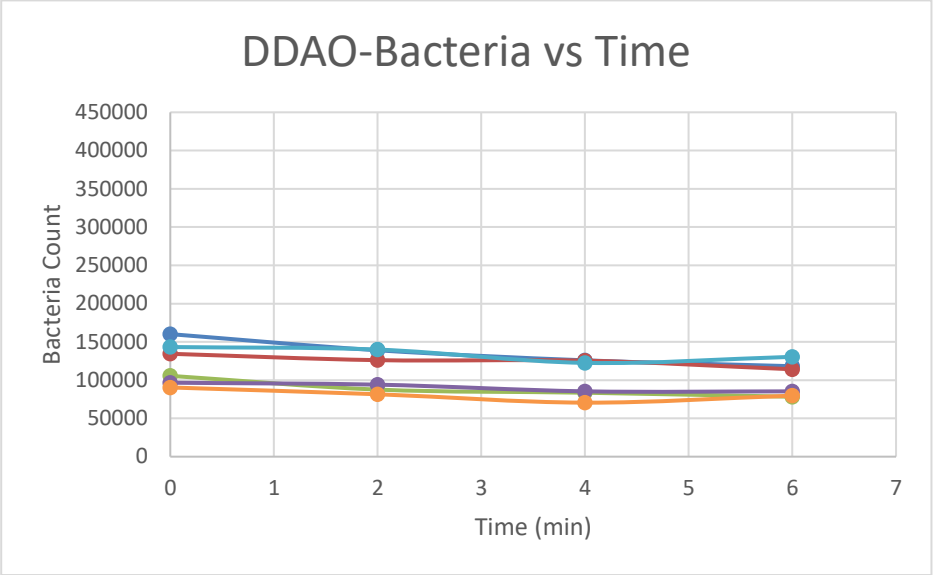
DDAO-Bacteria vs Time
Bacteria Count
450000
400000
350000
300000
250000
200000
150000
100000
50000
0
0
1
2
3
4
5
6
7
Time (min)

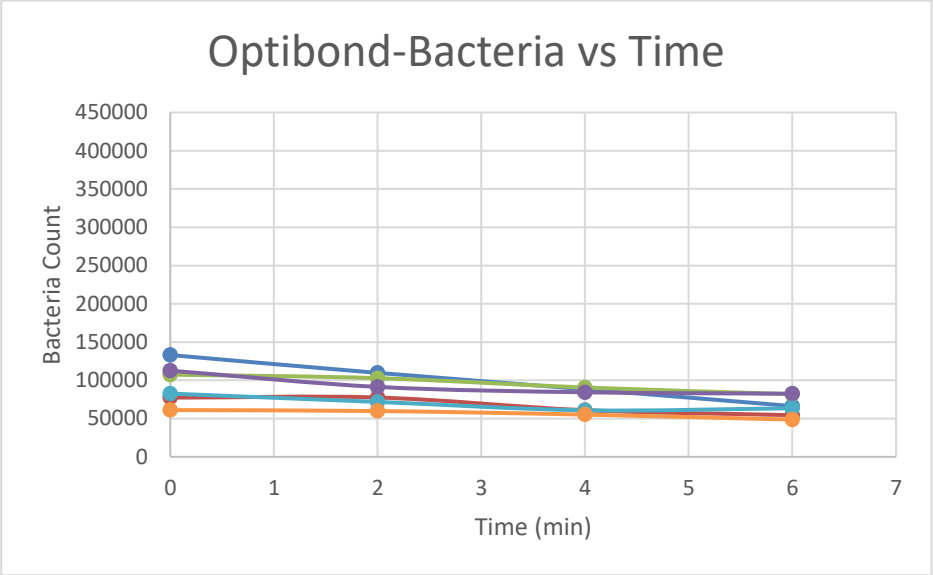
Optibond-Bacteria vs Time
Bacteria Count
450000
400000
350000
300000
250000
200000
150000
100000
50000
0
0
1
2
3
4
5
6
7
Time (min)

Week 3:

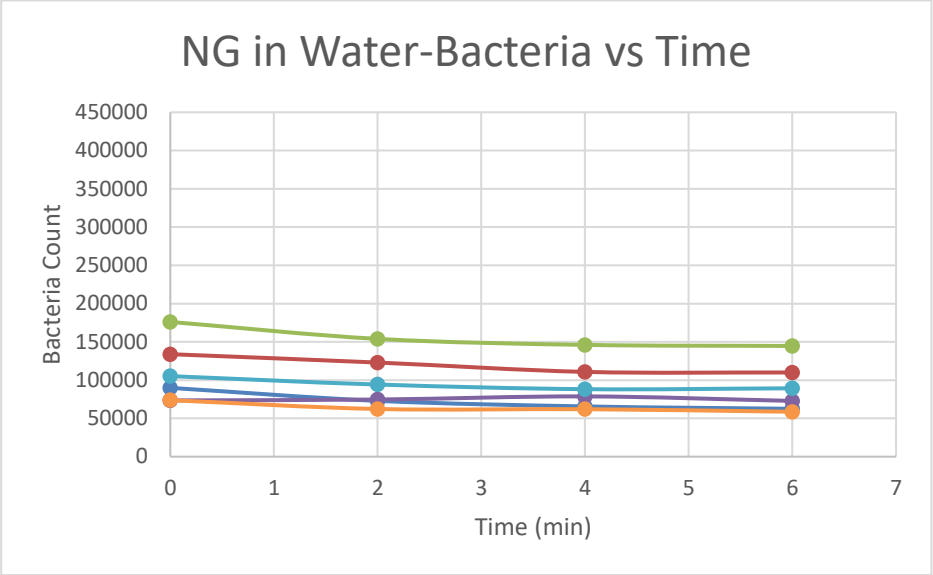
NG in Water-Bacteria vs Time
Bacteria Count
450000
400000
350000
300000
250000
200000
150000
100000
50000
0
0
1
2
3
4
5
6
7
Time (min)

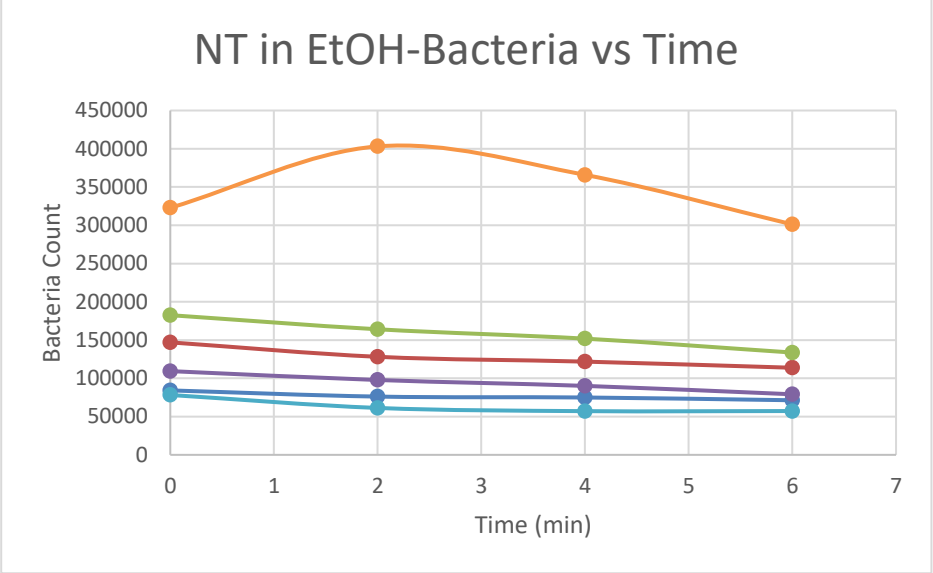
NT in EtOH-Bacteria vs Time
Bacteria Count
450000
400000
350000
300000
250000
200000
150000
100000
50000
0
0
1
2
3
4
5
6
7
Time (min)

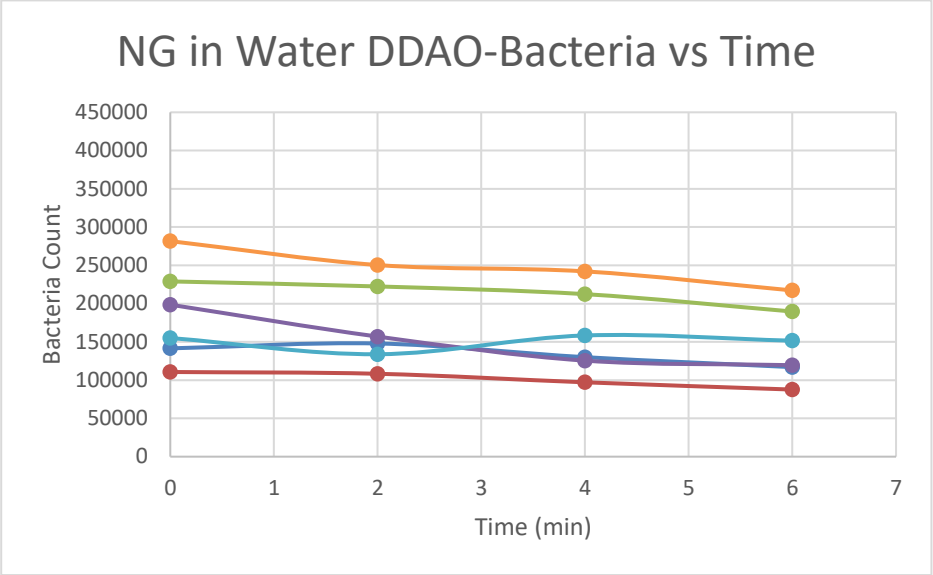
NG in Water DDAO-Bacteria vs Time
Bacteria Count
450000
400000
350000
300000
250000
200000
150000
100000
50000
0
0
1
2
3
4
5
6
7
Time (min)

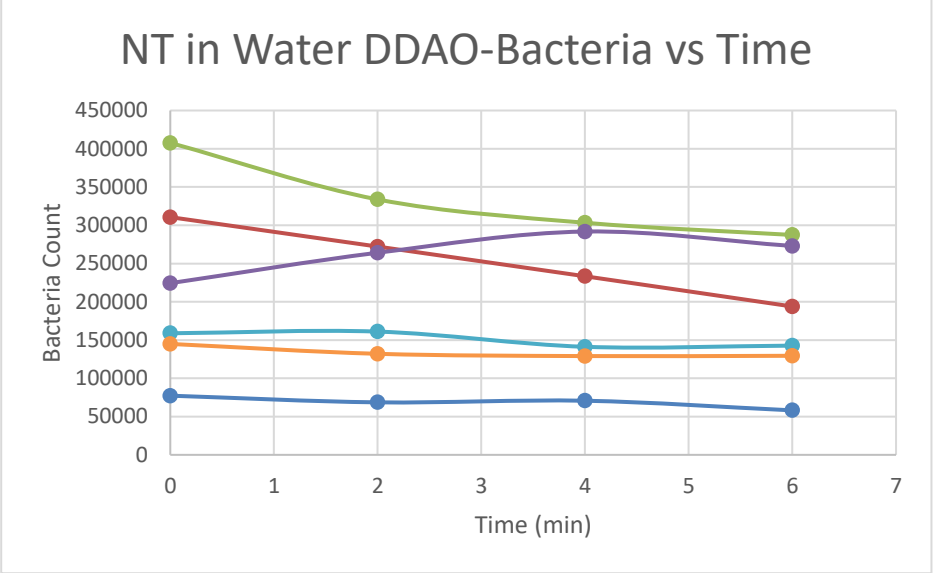
NT in Water DDAO-Bacteria vs Time
Bacteria Count
450000
400000
350000
300000
250000
200000
150000
100000
50000
0
0
1
2
3
4
5
6
7
Time (min)

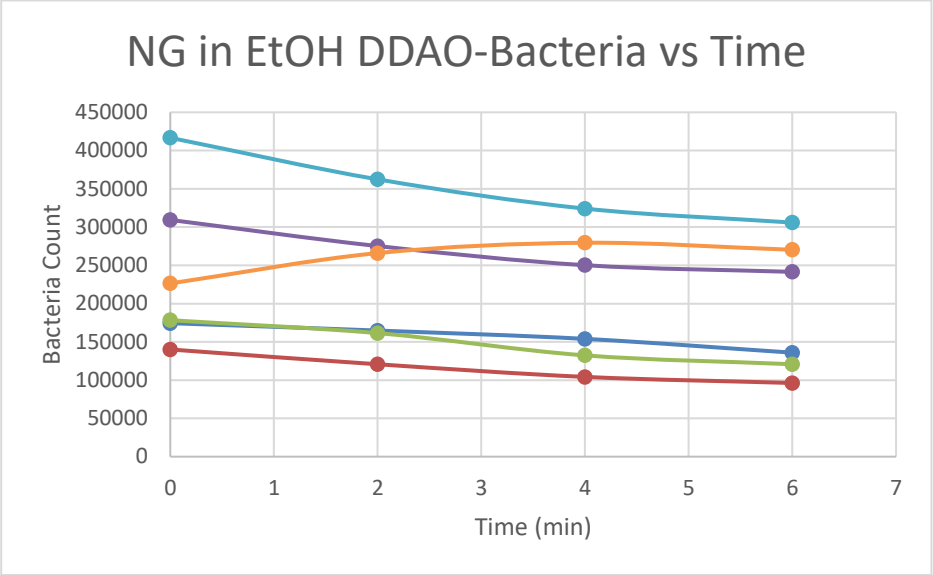
NG in EtOH DDAO-Bacteria vs Time
Bacteria Count
450000
400000
350000
300000
250000
200000
150000
100000
50000
0
0
1
2
3
4
5
6
7
Time (min)

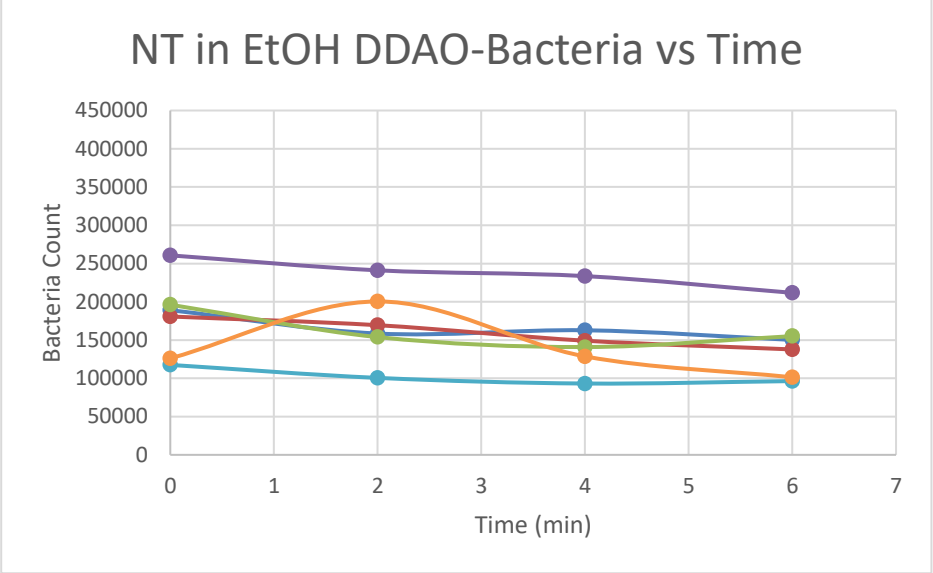
NT in EtOH DDAO-Bacteria vs Time
Bacteria Count
450000
400000
350000
300000
250000
200000
150000
100000
50000
0
0
1
2
3
4
5
6
7
Time (min)

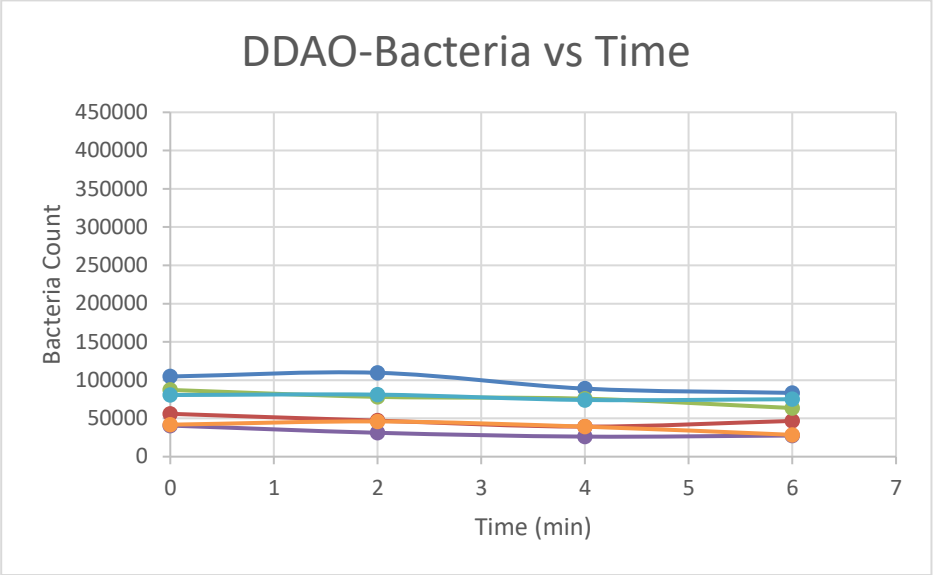
DDAO-Bacteria vs Time
Bacteria Count
450000
400000
350000
300000
250000
200000
150000
100000
50000
0
0
1
2
3
4
5
6
7
Time (min)

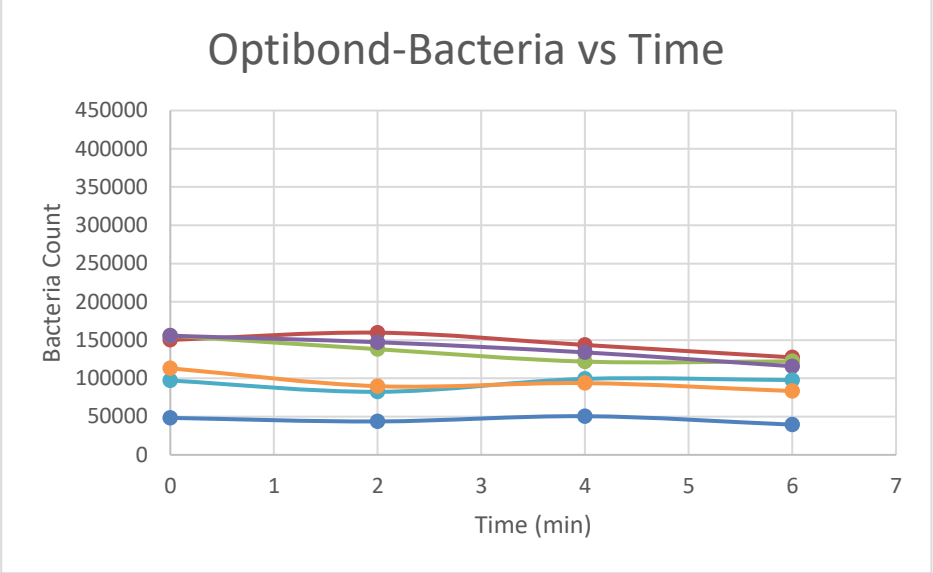
Optibond-Bacteria vs Time
Bacteria Count
450000
400000
350000
300000
250000
200000
150000
100000
50000
0
0
1
2
3
4
5
6
7
Time (min)